The Role of Cardiac Fibroblast Talins on Regulating Fibrosis and Hypertrophy Following Pressure Overload of the Heart

By

Natalie A. Noll

Dissertation

Submitted to the Faculty of the

Graduate School of Vanderbilt University

in partial fulfillment of the requirements

for the degree of

DOCTOR OF PHILOSOPHY

In

Biomedical Engineering

March 31, 2022

Approved by:

W. David Merryman, Ph.D.

Cynthia Reinhart-King, Ph.D.

Franz Baudenbacher, Ph.D.

Roy Zent, M.D, Ph.D.

Hind Lal, Ph.D.

ACKNOWLEDGEMENTS

This work was only made possible with the support and help of many mentors, coworkers, friends, and family. I want to acknowledge my mentor Dave Merryman, and my colleagues, dissertation committee, and co-authors on the two manuscripts that have been adapted for this dissertation, as well as my funding sources: the NIH and Foundation Leducq.

I want to especially acknowledge my lab mates who I have had the privilege of overlapping with. There are many highs in science, but also many lows, and all of you were there to experience mine firsthand. Thank you for brainstorming with me, editing multiple manuscripts, helping me see the bright side of failures, celebrating my accomplishments, and helping me to adapt to working two years in lab during a pandemic. You made every day in lab better: David Armstrong, Matt Bersi, Nathen Bloodworth, Erin Booton, Meghan Bowler, Cyndi Clark, Tessa Huffstater, Cami Johnson, Ethan Joll, Olu Ogungbesan, Caleb Snider, Chrisi Scott, Michael Raddatz, Lance Riley, Mark Vander Roest, Allison Schroer, and Michael Valentine.

Through this journey beach volleyball has provided with me a place for mental recharge and rejuvenation, and the people that I have met through volleyball have become my second family. Thank you all for supporting me and becoming forever friends.

Chris, your support these last two years has been incredible. My stress disappears when we are together. Thank you for being my volleyball partner, but also my partner in life.

Lastly, but most importantly I want to thank my parents and sister – Nicola, Tom, and Stephanie, as well as my entire extended family. Thank you for always being there for me and supporting me from near and afar. I know you are always there for me, and your support means the world.

TABLE OF CONTENTS

LIST OF TABLES

Table **Page**

LIST OF FIGURES

Figures **Page**

LIST OF ABBREVIATIONS

Abbreviations and Key Terms	Definition
ACC	American Heart Association
AFM	Atomic force microscopy
AHA	American Heart Association
AngII	Angiotensin II
CF	Cardiac fibroblast
CKD	Chronic kidney disease
CO	Cardiac output
DCM	Dilated cardiomyopathy
DL/BW	Dry lung / body weight
DOCA	Deoxycorticosterone acetate
DOX	Doxorubicin
ECM	Extracellular matrix
EF	Ejection fraction
F	Blood flow
Gal-3	Galectin-3
GEO	Gene Expression Omnibus
HF	Heart failure
HFpEF	Heart failure with preserved ejection fraction
HFrEF	Heart failure with reduced ejection fraction
HT	Hypertension
IL-1β	Interleukin-1β
IL-6	Interleukin -6
IR	Ischemia reperfusion
ISO	Isoproterenol
IVS	Interventricular septum wall thickness
LAD	Ligation of the left anterior descending artery
LV	American College of Cardiology
LVAW	Left ventricular anterior wall thickness
LVOT VTI	Left ventricular outflow track time integral
LVPW	Left ventricle posterior wall thickness
MI	Myocardial infarction
MMP	Matrix metalloproteinase
MTJ	Myotendinous junction
NPPA	Natriuretic peptide A
NPPB	Brain natriuretic peptide
PAB	Pulmonary aortic banding
PE	Phenylephrine
PH	Pulmonary Hypertension

POSTN	Periostin
PSR	Picrosirius red
qPCR	Quantitative polymerase chain reaction
R	Resistance of the vasculature
ROS	Reactive oxygen species
SBP	Systolic blood pressure
Scr	Scramble
STZ	Streptozotocin
T1D	Type 1 Diabetes
T2D	Type 2 Diabetes
TAC	Transverse aortic constriction
TCF21	Transcription factor 21
TGF-β	Transforming growth factor-β
TIMP	Tissue inhibitor of metalloproteinase
Tln1	Talin 1
Tln2	Talin 2
TLR2	DOX-receptor 2
TNF-α	Tumor necrosis factor-α
TNF-β	Tumor necrosis factor-β
TPR	Total peripheral resistance
VEGEF	Vascular endothelial growth factor A
VW/BW	Ventricle / body weight
WGA	Wheat germ agglutinin
αSMA	α-smooth muscle actin

Dissertation Overview

My doctoral work has investigated the cell-specific contributions of the two talin proteins - Tln1 and Tln2 - in cardiac fibroblasts and myofibroblasts during pressure overload injury in the heart. The first focus of this research was to explore the effect that myofibroblast Tln1 had during transverse aortic constriction. The second aim of my work was to generate a Tln2 null, Tln1-cardiac fibroblast specific genetically modified mouse and then find and validate a dosing strategy that reproducibly resulted in interstitial fibrosis during pressure overload injury to the heart. Lastly, my work applied the model to study cardiac fibroblast remodeling post hypertension injury in the absence of Tln2 and loss of Tln1 in cardiac fibroblasts and the resulting cardiac remodeling that occurs.

In this dissertation, I provide a thorough background on heart failure, hypertension, and the roles of cardiac fibroblasts and cardiomyocytes to response to prolonged pressure overload of the heart. Next, I justify targeting Tln1 and Tln2 in cardiac fibroblasts in the context of hypertension disease. Following this, I summarize the known mouse models for inducing hypertension and pressure overload experimentally. Subsequentially, I present my research into the effects of cardiomyocyte Tln1 using the experimental model of transverse aortic constriction *in vivo* and siRNA knockdown *in vitro*. Following this, I describe the generation and creation of a novel genetic mouse to explore cardiac fibroblasts specific Tln1 and Tln2 contribution to fibrotic remodeling and cardiac hypertrophy in response to pressure overload injury. I then use this novel mouse to research the effect of cardiac fibroblast Tln1 and Tln2 loss following angiotensin II induced pressure overload of the heart. Echocardiography, RNA sequencing and *in vitro* assays were implemented to characterize the phenotypic alterations due to loss of Tln1 and Tln2 in cardiac fibroblasts. Finally, I discuss the impact of this work and potential future directions the research could be taken.

Chapter 1

Cardiovascular Disease and Tissue Response to Hypertension

Text for Chapter 1 was adapted from **Noll NA**, Lal H, Merryman WD. *Mouse Models of Heart Failure with Preserved or Reduced Ejection Fraction*. The American Journal of Pathology, Vol. 190, No. 8, August 2020.

1.1 Heart failure disease burden

Heart failure (**HF**) is the leading cause of death worldwide. There are approximately 6.5 million Americans living with HF with an incidence in 10 in 10,000 people over the age of 65.[1] Recently, morbidity attributed to HF has dropped to one in nine deaths due to improvements in strategies focused on treating the conditions proceeding and leading to HF, including hypertension, myocardial infarction (**MI**) and atherosclerosis.[2] However, even with improvements in treatment, mortality associated with HF is still high, with 50% of patients diagnosed with HF dying within five years of diagnosis.[3] Current predictions show that by 2030, 8 million American adults will be diagnosed with HF.[3]

Two-thirds of all HF cases can be attributed to one of four underlying conditions: ischemic heart disease, chronic obstructive pulmonary disease, hypertensive heart disease, or rhematic heart disease.[4] Of these, hypertension remains the major preventable cause of cardiovascular disease through pharmacological intervention and life style changes.[5] This is done by treating the underlying symptoms, namely systolic blood pressure (**SBP**). However, these treatments do not address the chemical and cellular changes that are occurring in the heart leading to HF. Therefore, there is a need to identify the cellular processes underlying the conditions leading to HF so that new therapeutic strategies can be developed.

1.2 Heart failure classifications

The American Heart Association (**AHA**) defines HF as a complex clinical syndrome that results from any structural or functional impairment of ventricular filling or ejection of blood.[6] HF is classified based on ejection fraction (**EF**), and the progression of the disease based on cardiac deterioration. The American College of Cardiology (**ACC**)/AHA defines HF in four stages. These stages range from stage A, where there is a high risk of HF but no symptoms or structural damage to the heart, to stage D, where patients with refractory HF require advanced intervention (**Table 1**).[7–9] Left-sided HF is associated with an increased risk of sudden death,[10] and is subdivided based on left ventricular (**LV**) EF: HF with preserved ejection fraction (**HFpEF**; LVEF ≥ 50%), HF with mid-range ejection fraction (**HFmrEF**; LVEF 40-49%), and HF with reduced ejection fraction (**HFrEF**: LVEF <40).[11] Medical advances have developed specific treatments for HFrEF by acting on the neuro-hormonal axis, but effective drugs for treatment of HFpEF are absent.[12] This has led to an increase in HFpEF prevalence, and account for more than 50% of all HF cases in the United States.[13]

Stage	Discription	Additonal Treatment
A	High risk with no symptoms	Treat underlying conditions: hypertension, diabetes, dyslipidemia
B	Structural heart disease, no symptoms	ACE inhibitors or ARBs with beta-blockers in selected patients
C	Structural disease, symptomatic	Dietary sodium restrition, diuretics, revascularization, mintral-valve surgery, aldosertone agonist
D	Refractory systoms with special interventior	VAD, transplantation

Table 1: Stages of Heart Failure and Treatment Options for Systolic Heart Failure. Adapted from Jessup et al.[7,8]

HFpEF is clinically defined as HF with normal EF and diastolic dysfunction, the inability of the ventricles to relax properly.[14] HFpEF is usually the result of chronic diseases such as hypertension, diabetes mellitus, atrial fibrillation, aging, obesity, and/or renal dysfunction (**Figure 1**).[15] Of these, hypertension is the most predominant underlying condition with a prevalence in 60-80% of all HFpEF cases.[16] These chronic diseases gradually diminish the normal relaxation ability of the LV as the ventricular walls become stiffer from increasing interstitial fibrosis. As a result, the heart can no longer fill properly with blood during the resting period between each beat, which eventually leads to diastolic failure. Cardiomyocytes increase their thickness, by adding sarcomeres, the contractile unit of the cell, in parallel, resulting in cardiomyocyte hypertrophy and concentric hypertrophy of the heart. HFpEF occurs more often in women (79% vs 49% of all HFpEF cases) and is more prominent in older populations.[14] HFpEF manifests clinically as exercise intolerance, dyspnea, edema, pulmonary hypertension and pulmonary edema, all of which are symptoms associated with cardiac hypertrophy, increased fibrosis, and decreased capillary content. Additional acute insults to the heart, or chronic high blood pressure can cause a transition from HFpEF to HFrEF during increased cardiomyocyte injury.

In contrast with the reduced relaxation capacity of HFpEF, HFrEF occurs when the ventricles lose their ability to contract normally. A wide range of cardiac conditions can cause HFrEF, including coronary artery disease, MI, and cardiomyopathies (**Figure 1**).[15] These diseases result in apoptosis of cardiomyocytes which causes an imbalance in heart wall structure, causing eccentric remodeling with left ventricular dilation, but normal wall thickness.[17–21] These adaptations initially allows the heart to normalize left ventricle (LV) wall stress and maintain cardiac output and EF. However, as remodeling continues, stiffening of the ventricular walls diminishes the cardiomyocyte's ability to contact with enough force to adequately eject blood into the systemic circulation. This eventually leads to systolic failure. Patients with HFrEF have higher

levels of circulating brain natriuretic peptide (**NPPB**), a common biomarker for HF, and a higher mortality rate than those with HFpEF.[22]

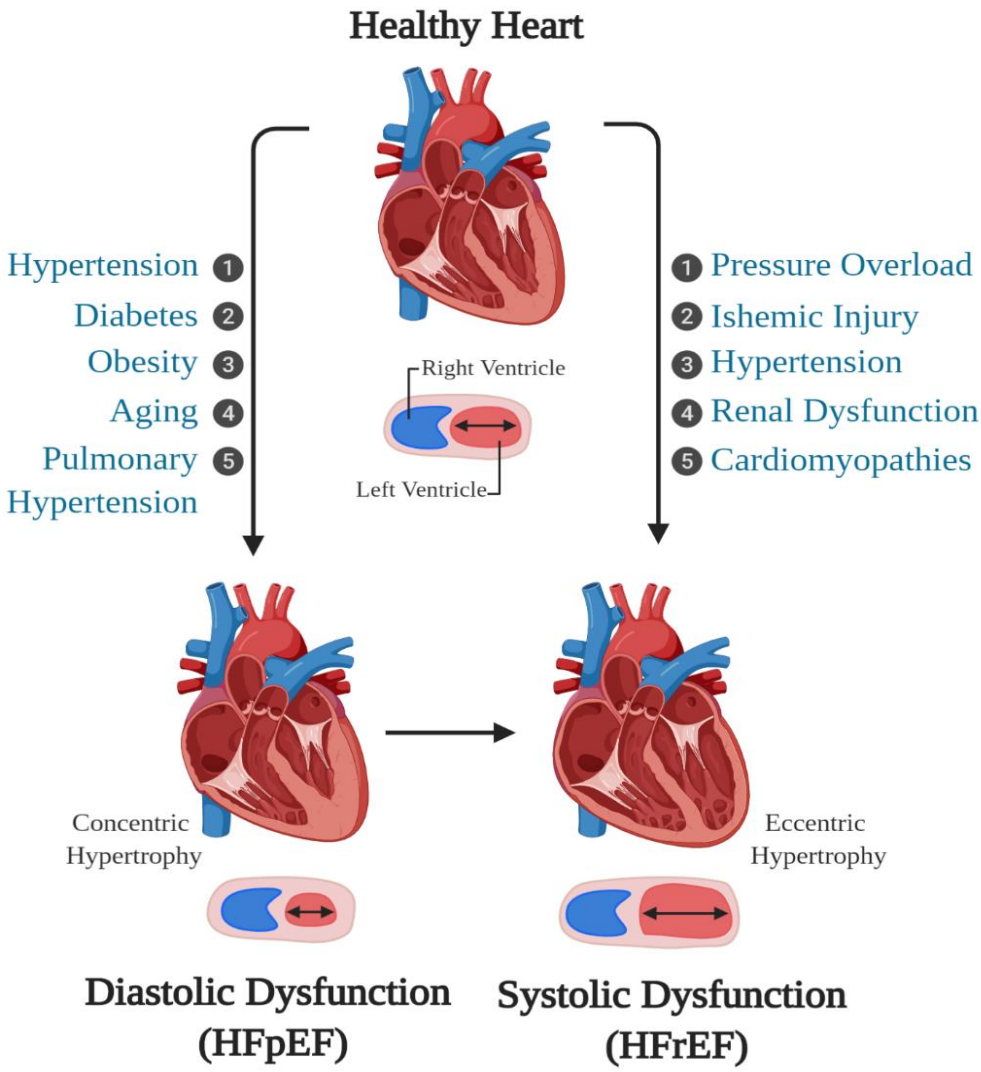

Figure 1: Disease states and presenting phenotypes of HFpEF and HFrEF. Disease states and their resulting left ventricular remodeling leading to the development of heart failure with preserved ejection fraction (HFpEF) and heart failure with reduced ejection fraction (HFrEF). Created with BioRender.com.

1.3 Hypertension

Hypertension (**HT**) is one of the main underlying conditions that leads to HFpEF and is the most important risk factor for the development of HFrEF in the United States.[4,23,24] In the Framingham Heart Study, 91% of all patients developed hypertension that predated their newly diagnosed HF.[16] HT is characterized by an increase in SBP which causes increased ventricular pressure in the heart. 2017 guidelines by the ACC/AHA define HT as blood pressure greater than 130/180 mmHg.[25] Currently, there are 70 million adults in America with HT, only 52% of which have their blood pressure properly managed.[26] Studies show that that a SBP reduction as low as 5mmHg can reduce the risk of HF by 24% in early onset HT, underscoring the importance of the development of therapies that target hypertension and SBP.[27]

1.3.1 Systolic blood pressure

Blood pressure is the pressure or tension that is exerted by the blood as it circulates the arterial vessels and is the result of cardiac output (**CO**) of the heart and the total peripheral resistance (**TPR**) of the systemic circulation (**Equation 1**).[28] Blood flow (**F**) through the heart is maintained by the change in perfusion pressure (atrial – venous pressure) and the amount of resistance (**R**) in the vasculature (**Equation 2**).[29] Under normal conditions, perfusion pressure and vascular resistance do not change. HT is caused by, but not limited to, malfunction of the humoral system, neuronal and autoregulatory systems.[30] Under pathological conditions such as HT and during aging, narrowing of the vasculature causes an increase in vascular resistance. The heart initially responds through autoregulation. Autoregulation is the ability of the heart to maintain blood flow despite a change in perfusion pressure (P_a-P_v).[29] The heart does this by increasing the flow of blood by dilating the vasculature to decrease resistance. This allows for the maintaining of homeostatic SBP. Under continual pathological insults, such as plaque buildup in the arteries, and a reduced coronary endothelium-dependent dilation capacity in HFpEF, vascular dilation alone cannot adequately reduce the vascular resistance, resulting in an increase in blood

pressure.[31–37] This leads to a sequential increase in ventricular heart pressure, and ventricular wall stress.

$$BP = CO\ x\ TRP \qquad \textbf{Equation (1)}$$

$$F = \frac{(P_a - P_v)}{R} \qquad \textbf{Equation (2)}$$

1.3.2 Cardiac fibroblasts

The adult heart is comprised of approximately 30% cardiomyocytes with the remaining 70% non-myocyte cells being primarily cardiac fibroblast (**CFs**).[38] CFs are arranged in sheets that run in parallel with muscle fibers and they help maintain continuity of cell signaling between cardiomyocytes.[39] Genetic lineage tracing has shown that *Tcf21* is the best marker for CFs as it is expressed most widely expressed marker of all fibroblast-like cells in the heart, and is expressed by all activated cardiomyocytes derived from CFs.[40]

CFs are recognized chiefly as regulators of the extracellular matrix (**ECM**) and are involved in general maintenance of myocardial structure.[41] Collagen is the major stress-bearing element within the ECM and forms a 3D network around bundles of myocytes to generate a stress-tolerant network.[42] In the healthy heart, ~85% of the ECM is composed of thicker collagen I fibers, witch conifer tensile strength, and ~11% of collagen type III fibers that maintain the elasticity of ECM.[43] Additionally, the ECM acts as an insulator for myocardial signaling. Electrical signals are passed between CFs and cardiomyocytes through gap junctions. *In vitro* analysis of single fibroblasts

have shown them to be capable of synchronizing contractions between myocytes, illustrating the role that CFs play in maintaining total heart contractility.[44]

Pathological conditions such as systemic inflammation, hypoxia, cardiomyocyte death, mechanical stress, and activation by pro-fibrotic cytokines can lead to the phenotypic shift of quiescent CFs to active myofibroblasts. Myofibroblasts proliferate and migrate to the site of injury, where they secrete and compact ECM components.[45,46] This migration is cytokine-induced and requires the co-coordinated activity of matrix metalloproteinases (**MMPs**) and tissue inhibitor of metalloproteinase (**TIMPs**) to move through the ECM network in the heart (**Figure 2**).[47] CFs express a limited subset of MMPs; collagenases (MMP-1, MMP-13), gelatinases (MMP-2, MMP-9), and stromelysin (MMP-3).[42] Myofibroblasts also differ from inactivated CFs by having a more contractile phenotype, marked by the expression of alpha-smooth muscle actin (**α-SMA**) (**Figure 2**). This allows myofibroblasts to compact and arrange ECM components such as collagen types I and III, and fibronectin. The secretion and compaction of ECM components leads to interstitial and perivascular fibrosis of the ventricular walls, allowing for short-term adaptation to tissue injury.[48–52]

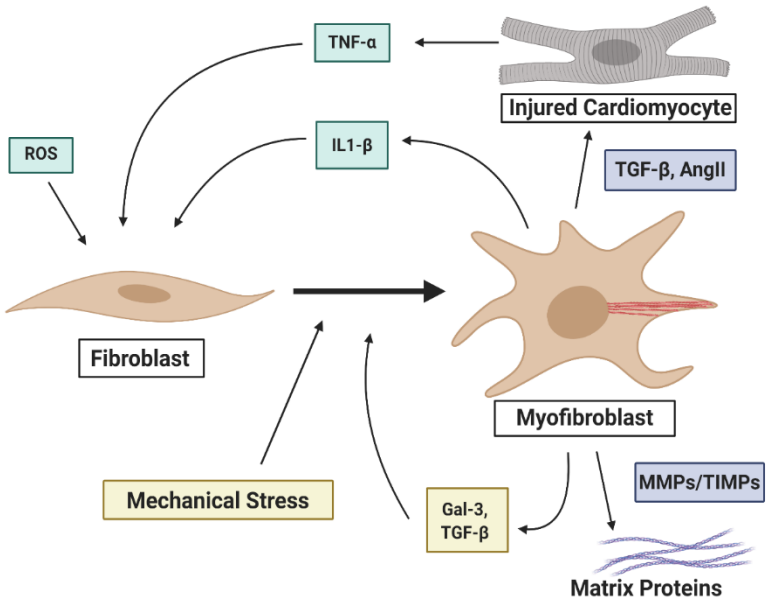

Figure 2: Cardiac fibroblasts to myofibroblast activation. Fibroblast to myofibroblast transition in the heart in response to cardiomyocyte injury, proinflammatory cytokines, and systemic inflammation through reactive oxygen species (ROS). Ang II, angiotensin II; Gal-3, galectin-3; MMP, matrix metalloproteinase; TGF-β, transforming growth factor- β; TIMP, tissue inhibitor of metalloproteinase; TNF-α, tumor necrosis factor-α. Created with Bio-Render.com.

While necessary for initial survival, continued CF remodeling of the heart can lead to negative effects. Chronic pressure overload of the heart increases ventricular wall stiffness, and secretion of pro-fibrotic signaling factors resulting in a positive feedback loop of further myofibroblast activation (**Figure 2**). Unlike myofibroblasts in other regions which undergo apoptosis after healing is complete, cardiac myofibroblasts can persist in fibrotic areas, such as the scar post-MI.[53] Clinical studies have shown that in the failing heart TIMP activity is decreased, while MMP activity is increased, pointing to an imbalance in the hearts ability to degrade unnecessary collagens.[54–56] Angiotensin II (**AngII**), which is secreted by CFs, has been shown to induce collagen synthesis, as well as decrease TIMP-1 and TIMP-2 in humans.[57] AngII stimulation causes the increased expression of TGF-β, resulting in collagen I and III secretion, and further

induction of the CF to myofibroblast transition.[58] Additionally, myofibroblasts produce cytokines (TNF-α, IL-1B, IL-6, TNF-β), vasoactive peptides, and growth factors (AngII, TN-1, ANP, BNP, VEGEF), which can increase collagen synthesis in CFs, while also inducing cardiomyocyte hypertrophy (**Figure 2**). The pathological responses of myofibroblasts results in a stiffer, non-compliant myocardium that can lead to impaired cardiomyocyte contraction and hypertrophy (**Figure 1**).

During HFrEF, cardiac fibrosis occurs primarily due to the loss of cardiomyocytes, where myofibroblasts lay down ECM to fill the empty gaps left by cardiomyocytes death. This fibrosis leads to the impairment of cardiomyocyte contraction transduction resulting in uncoordinated contraction of cardiomyocyte bundles.[59] Further disruption of the interactions between laminin, which connect cardiomyocytes and capillaries, causes a further reduction in cardiomyocyte mass.[60] During HFpEF, excessive collagen deposition and a reduction in collagen III results in a stiffer, less compliant ventricular wall.[61,62]

1.3.3 Cardiac myocytes

Cardiomyocyte remodeling in HFpEF and HFrEF are driven by the amount of damage that cardiomyocytes endure during the initial injury of the heart. During HFrEF, remodeling is driven by cardiomyocyte damage and death, leading to an imbalance in the heart wall structure.[17–21] This death can be driven by ischemia, an inappropriate inflammatory response, and pressure overload.[63–66] Increasing levels of circulating Troponin-T leads to a reduction in cardiomyocyte mass, causing cardiomyocytes to become thinner and more elongated.[17–21] This results in eccentric remodeling of the heart, with left ventricular dilation, but normal wall thickness (**Figure 1**). Increased stiffness of the heart walls due to interstitial fibrosis results in impaired cardiomyocyte contraction.[59] This results in a decrease in SV and a decrease in EF as cardiomyocytes are unable to push blood out of the ventricles and into the systemic circulation as the same rate.

Conversely, under chronic injury to the heart, such as increase systolic blood pressure during hypertension, the heart undergoes HFpEF first. As the LV walls become stiffer from increasing interstitial fibrosis, cardiomyocytes lose their ability to relax properly. To normalize their ability to contract cardiomyocytes add sarcomeres in parallel to increase their contractility, which also results in increased cardiomyocyte thickness.[67,68] This results in concentric hypertrophy, where the heart wall thickens and ventricular chamber volume decreases (**Figure 1**). As concentric remodeling continues, the heart can no longer fill properly due to the decrease ventricular chamber volume and altered cardiomyocyte relaxation, resulting in diastolic heart failure.

1.4 Therapeutic shortcomings of hypertension

Two-thirds of all HF cases can be attributed to one of four underlying conditions: ischemic heart disease, chronic obstructive pulmonary disease, hypertensive heart disease, or rhematic heart disease.[4] Of these, HT remains the major preventable cause of cardiovascular disease.[5] Treatment of adults with HT has centered around lowering blood pressure to less than 140/90 mmHg. However, new evidence from the Systolic Blood Pressure Intervention Trail suggests that lowering SBP to less than 130 mmHg may be vital for patients who are high-risk, including those with a history of cardiovascular disease and chronic kidney disease.[69] Life style changes, in combination with pharmacotherapy are the most commonly used method to treat hypertension. The most modifiable lifestyle changes are obesity, high sodium intake, insufficient physical activity, and excessive alcohol consumption. For patients eating a typical American diet, reduction to intake of 2400mg of sodium per day shows benefits in reduction of blood pressure across a wide range of patients.[70] This benefit is increased with a reduction of sodium intake to 1500mg and 1000mg per day.

Therapeutics for high blood pressure fall into 3 categories: 1) Thiazide-type diuretics 2) calcium channel blockers (**CCBs**) 3) angiotensin converting enzyme (**ACE**) inhibitors / angiotensin II receptor blockers (**ARBs**).[71] For stage 1 hypertension (SBP between 140-159 mmHg), each of the first 3 classes are similarly effective in lowering BP in 30-50% of the general adult population.[72,73] However, initial monotherapy is unlikely to lower BP to the goal in patients whose BPs are greater than 20/10 mmHg of their goal BP. When this occurs, in stage 2 hypertension (SBP ≥ 160 mmHg), and in many cases of stage 1 hypertension, combination therapy using 2 drugs is needed.[72,73]

While the right combination of pharmacotherapy and lifestyle modifications can decrease blood pressure, there are currently no treatments for the underlying interstitial fibrosis,

cardiomyocyte hypertrophy, and additionally cellular changes that occurred during injury. Additionally, lifestyle modifications may not be able to be made due to economic status, underlying risk factors, and living environment. Therefore, there is a need to identify the cellular process underlying the conditions leading to HT so that new therapeutic strategies can be developed to treat the cause of HT, and not the underlying symptom of increased blood pressure.

Chapter 2

Integrin Adhesions & Talin

2.1 Mechanotransduction between cells and the extracellular matrix

Mechanotransduction is the ability of cells to sense and transduce physical forces into biomechanical signals and a cellular response.[74] In the heart, resident cardiomyocytes and cardiac fibroblasts (**CFs**) are subjected to physical forces during normal cardiac function such as membrane stretch, gain and loss of adhesion, and compression[75]. Mechanotransduction is vitally important in the heart, as this process drives cardiomyocyte hypertrophy, CF migration, and deposition of collagen in response to increased stiffness and stress on ventricular and atrial walls during acute and prolonged injury.

Integrin adhesion complexes allow cells to transduce forces between the extracellular environment and their cellular body. Integrin adhesion complexes require 4 components for their formation: an extracellular matrix (**ECM**) ligand, a transmembrane integrin heterodimer, a mechanosensitive protein (e.g., talin), and filamentous actin.[76] Integrin adhesion complexes form a variety of adhesions from small, transient nascent adhesions, to larger, more stable focal adhesions that develop under high mechanical loads. Integrin adhesions can also form structures such as protostomes and invadopodium that mediate matrix degradation and remodeling, as well as fibrillar adhesions that mediate ECM assembly.[77–79]

Integrin adhesions function in a bidirectional manner, resulting in ‘outside-in’ and ‘inside-out’ signaling.[80–82] Outside-in signaling is a result of integrins binding the ECM leading to intracellular signaling events that can influence a wide-range of cellular activities including

migration, proliferation, gene expression, survival, and alterations in cellular morphology. Inside-out signaling occurs when non-integrin cellular receptors modify integrin activation. This signaling results in a change in integrin binding affinity and clustering on the cellular membrane, which has been associated with chemical and mechanical signaling in cardiomyocytes and CFs.

2.1.1 Integrins

Integrins are heterodimeric transmembrane receptors that are comprised of an α and β subunit.[83,84] Integrins binding to the ECM occurs in the extracellular domain of the integrin and is modulated by binding of proteins to its intracellular portion.[85] Integrin activation occurs when talin, a cytoskeletal linker molecule, binds the intracellular β subunit of the integrin, resulting in a change in integrin affinity for the ligand.[86,87] While integrins can be activated by numerous proteins, talin is the cytoskeletal link common to all integrin adhesions.[76]

Integrin expression is unique to each cell type and can change based on developmental stage and pathological state. In adult cardiomyocytes, α1β1, α5β1, and α7β1 are the most highly expressed integrin heterodimers, and are the binding receptors for collagen, fibronectin, and laminin, respectively.[88] The β1 integrin subunit is unique as it has two differently spliced isoform, β1A and β1D.[88–90] The β1A isoform is expressed embryonically, while the β1D isoform is expressed in adult cells, providing them with distinct, isoform-specific interactive properties with the ECM and signaling molecules.[91] Knockout studies have shown that integrin function in cardiomyocytes is vital for preservation of normal heart function.[92]

In CFs there is redundancy in ECM binding partners, as CFs express α5β1 integrins which bind both fibronectin and osteopontin. Additionally, CFs express αvβ1, αvβ3 and αvβ5, which bind vitronectin, as well as fibronectin and osteopontin.[89,93,94] Post-myocardial infarction, myofibroblasts migrating to the site of injury had an upregulation of β1 integrins.[95,96] This upregulation of β1 integrins and integrin localization on the cellular membrane of CFs was also

seen in a rat model of AngII-induced hypertension, as well as in *in vivo* stimulation of CFs with AngII.[97–99] These data show that increased integrin activation and modulation in vital in the response to injury in the heart.

2.1.2 Talin

The mechanotransdution of signals across integrin adhesions are facilitated by mechano-effector proteins which bind integrins to the F-actin cytoskeleton of the cell. Talin is a key mechano-effector protein for integrin-mediated adhesion to the ECM.[100,101] Talin is a large 270kDa cytosolic protein composed of an N-terminal FERM head domain, a flexible neck region, and a C-terminal rod domain (**Figure 3**).

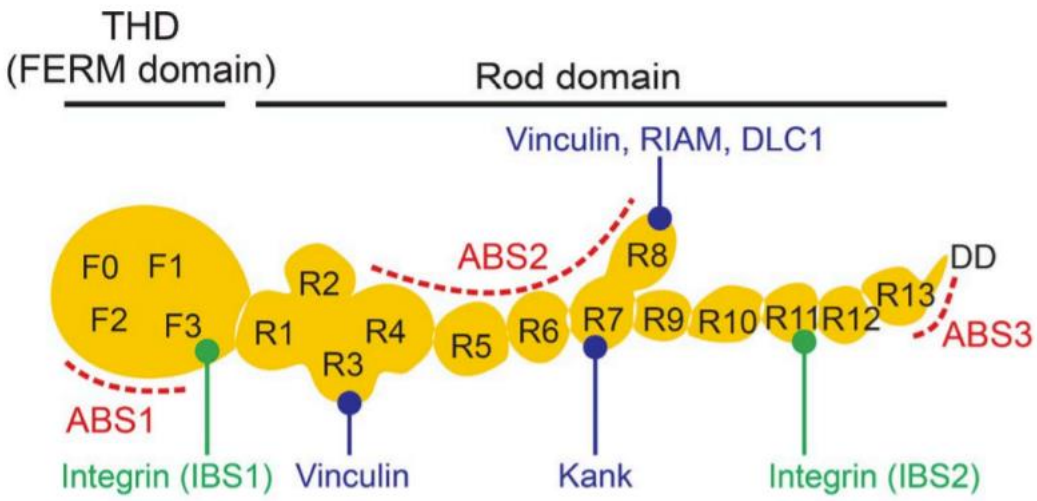

Figure 3: The talin protein. Talin-based molecular clutch mediates Mechanotransduction. Domain organization of talin. The N-terminal talin head FERM domain that consists of F0,F1,F2 and F3 subunits containing an integrin tail-binding site (IBS1). The talin rod domain contains 13 helix bundles (R1-13) which contain a second IBS (IBS2) and two actin binding sites (ABS2, ABS3) as well as two critical vinculin binding sites (VBS) in the R3 and R8 domains. The other VBS are not pictured. Reprinted with permission from © 2016 Sun et al. Originally published in J Cell Biol.

In the cytoplasm, talin adopts a closed, autoinhibited conformation.[102–104] Upon activation, talin migrates to the cell membrane, where it activates integrins via its FERM domain by binding the cytoplasmic β-tail of integrins on talins IBS1 site (**Figure 3**). This results in a conformational change of the integrin receptor where binding of talin to the integrin β-tail disrupts the autoinhibitory association between the integrins α- and β-tails, causing an increase in affinity for ECM ligands (**Figure 4**).[105–107] This triggers a series of intracellular events such as cell motility and ECM adhesion. Deletion of talin resulted in cells that were unable to migrate or proliferate as well as diminishing the structural integrity of FAs.[108] Studies in in *C. elegans*, *Drosophila*, and mice have demonstrated that talin is essential for integrin adhesion.[109–111] The fact that talin is necessary for integrin activation is evolutionarily conserved suggests that talins are critical mediators of cell-environmental interactions. Thus, understanding their functions during environmental change is essential.

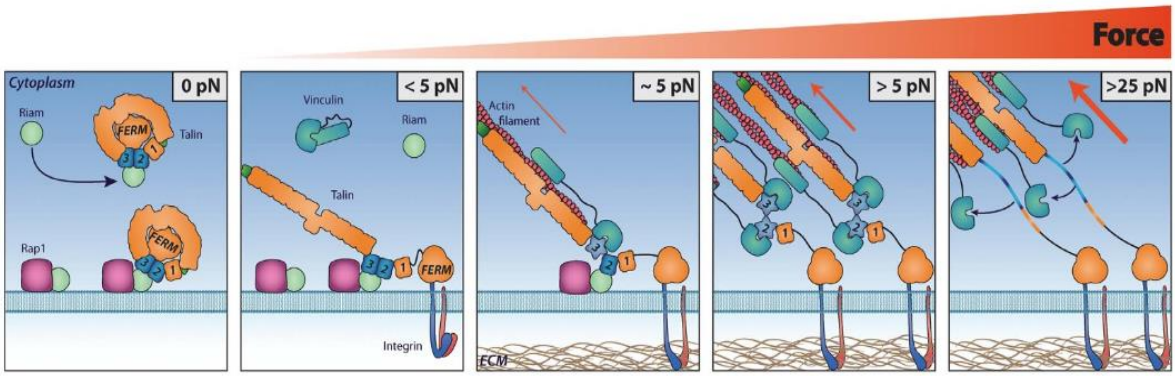

Figure 4: Talin activation and the formation of focal adhesion complexes under increasing applied force. Talin changes binding partners in response to force induced conformational changes. Force plays a key role in driving the formation of FA.0–5pN: RIAM recruits autoinhibited talin to the plasma membrane in a Rap1 via synergistic binding of RIAM to the R2–R3domains of talin. At the membrane talin autoinhibition is relieved. Talin can then activate integrins.,5pN: Only when talin has engaged the integrins and also captured the retrograde flow of actin is force exerted on talin. At,5 pN, the force of a single actomyosin contraction, the R3 domain is destabilized, and this reduces RIAM binding whilst exposing the high affinity VBS which then bind vinculin strengthening the adhesion. 5pN: With more vinculin cross-linking the adhesion can withstand greater force exposing further VBS. 25pN: At sufficiently high forces vinculin is displaced, resulting in unfolding of the VBS to a random coil. Reprinted with permission from 2014 Yao et al. Originally published in Scientific Reports.

The rod domain of talin consists of 13 α-helical bundles (R1-R13) that connect to F-actin directly through two actin-binding sites (ABS2 and ABS3), and indirectly through vinculin, and other adapter molecules such as RIAM, DLC1, and Kank (**Figure 3**).[112] These connections between ECM, integrin, talin, and actin allow for the transmission of cell generated contractile forces and forces derived from externally applied strains.

When talin is under force, the α-helical bundles in the talin rod domain unfold. This allows for new binding sites to be exposed and disrupts the binding of proteins to the folded state. For example, RIAM binds to the R3 folded domain. However, under force unfolding of R3, vinculin is recruited and binds to the unfolded R3 domain (**Figure 4**).[113,114] Vinculin also binds actin, causing increased stability of talin in its unfolded state under higher forces. Each talin α-helical bundle

operates as a mechanical switch and opens under different levels of tension. This allows for complex, time-dependent responses to tension exerted across the integrin-actin complex.

Vinculin is the best characterized cytoskeletal linkage protein to talin and can bind to 11 vinculin binding sites throughout the talin rod.[115] Binding of vinculin to talin stabilizes the rod domain in its open state, even after tension is reduced (**Figure 4**).[116] This results in the force necessary for talin refolding to be lower than the force needed for unfolding, allowing for stabilization of talin in the unfolded state.[117] Vinculin also creates an additional links to F-actin which allows for higher force transmission and increased stabilization of the unfolded talin rod domain.[118]

Due to mechno-effector proteins playing a key role in the transmission of forces between the ECM and the cells actin cytoskeleton, researchers have tried to parse talins specific contributions to mechanotransdution in cells that are under force during normal and pathological conditions.

2.2 Talin in the body

In vertebrates there are two talin genes, *Tln1* and *Tln2*, which encode very similar proteins (74% amino acid sequence identity). Tln1 is ubiquitously expressed in adults, while Tln2 expression is dominant in the heart, brain, and skeletal muscle.[52] While Tln1 and Tln2 play the same role in cells, Tln2 has a stronger affinity for F-actin through its co-localization with β1D integrins.[119,120] This allows Tln2 to make stronger bonds.[121] As such, cells that are under constant forces, such as cardiomyocytes, have higher expression of Tln2 than Tln1, which leads to the unequal expression of Tln2 throughout different cell types. During development, Tln2 knockout mice develop normally, and only incur a mild skeletal myopathy at 3 months of age due to a defect in their myotendinous junctions (**MTJs**) in skeletal muscle.[122] Tln1 knockout mice, however, are embryonically lethal at E8.5-9 due to gastrulation defects.[111] This indicates that Tln1 is an essential protein for development, and Tln2 cannot completely compensate for loss of Tln1.

In adult cells, Tln1 and Tln2 switching has shown that talins can partially compensate for each other when one is removed. This was demonstrated in mouse skeletal muscle tissue where knockdown of Tln2 *in vivo* resulted in successful assembly of integrin complexes at costameres and MTJs.[123] However, with aging, defect in MTJs occurred. Likewise, when only Tln1 was knockdown in mouse muscle cells, successful assembly of integrin complexes at costamere and MTJs was seen, with MTJ defects occurring over time.[124] This shows that while talins can partially offset each other, they cannot completely compensate. When Tln1 and Tln2 were both removed from skeletal muscle, mice died shortly after birth, illustrating that talins are required for intact integrin function during muscle development and growth.[123] Interestingly, these mice had a phenotype similar to β1-integrin KO mice, suggesting that removal of talin from skeletal muscle also inhibited integrin functions. This is consistent with findings *in vitro* that knockdown of Tln1 and Tln2 in mouse fibroblasts resulted in cells unable to form integrin adhesions,[125] and in *Drosophila* where all of the adhesive functions of βPS (orthologous to β1) required talin to form.[110]

2.3 Talin in the heart

In the heart, talin has been primarily studied in cardiomyocytes, with a focus on talins role in cardiac hypertrophy. During development, both Tln1 and Tln2 are highly expressed in embryonic cardiomyocytes. However, Tln2 becomes the dominant form of adult cardiomyocytes with minimal expression of Tln1.[126] In the adult mouse heart, Tln2 is localized to myocyte costameres, where Tln2 colocalizes with β1D integrins, allowing cardiomyocytes to support the high and constant forces that they must endure. This expression level is similar to human hearts, with a slightly higher Tln1 expression in human cardiac muscle.[126]

Under basal conditions, Tln2-null (**Tln2$^{-/-}$**) mice have normal cardiac structure and function up to 12 months of age.[127] In these mice, a decrease in β1D integrins coincided with a two-fold increase of Tln1 in the costameres of cardiomyocytes, illustrating that Tln1 can functionally replace Tln2 in cardiomyocytes under basal conditions. This was also observed in a mouse model of cardiomyocyte-specific deletion of Tln1 (**Tln1$^{CM-/-}$**). Tln1$^{CM-/-}$ mice had normal basal cardiac structure and function,[126] suggesting that Tln1 and Tln2 function in similar roles in cardiomyocytes, and this is protectively redundant under basal conditions. However, during disease, loss of cardiomyocyte Tln1 is beneficial, and blunts cardiac hypertrophy and interstitial fibrosis in response to prolonged pressure overload of the heart, suggesting that during disease, Tln1 and Tln2 play different roles in cardiomyocyte response to injury.

Under pressure overload of the mouse heart, Tln1 protein levels were increased in WT mice 4-weeks post-transverse aortic constriction (**TAC**) in cardiomyocytes and whole heart tissue, with no change in Tln2 expression.[126] This is consistent with protein levels of Tln1 and Tln2 taken from patients with end-stage, non-ischemic dilated cardiomyopathy (**DCM**) and suggests that Tln1 upregulation plays a key role in cardiomyocyte response to injury.[126] When TAC was performed on the Tln1$^{CM-/-}$ mice, ablation of Tln1 in cardiomyocytes resulted in a blunted response to TAC;

with a decrease in HW/BW ratio, cardiomyocyte area, and a reduction in fibrosis.[128] This showed that cardiomyocyte Tln1 alters acute biomechanical signaling and offers an apparent beneficial response to cardiac remodeling after pressure overload of the heart. When the $Tln1^{CM-/-}$ mouse was crossed with the global Tln2 null mouse (**$Tln2^{-/-}$; $Tln1^{CM-/-}$**), rapid cardiac dysfunction occurred. $Tln2^{-/-}$;$Tln1^{CM-/-}$ mice developed dilated cardiomyopathy with defects in integrin adhesion complexes and abnormal costameres that resulted in death by 25 weeks of age, illustrating that cardiomyocytes need a form of talin to respond to pressure-overload injury of the heart (**Figure 5**).[127] While deletion of talins in cardiomyocytes has been evaluated, the effect of talin deletion in CFs in unknow.

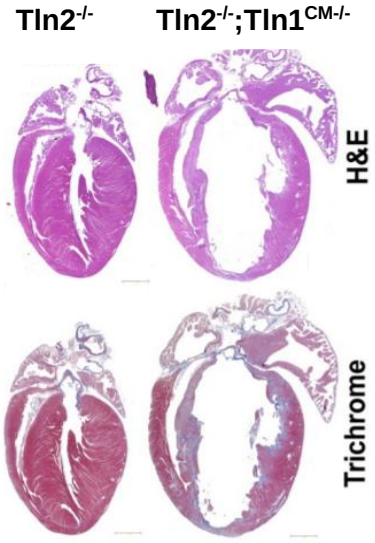

Figure 5: Loss of Tln1 and Tln2 in cardiomyocytes leads to dilated cardiomyopathy. Histological (H&E and trichrome staining) analysis showed cardiac dilation with fibrosis in 8-week-old male mice that were Tln2-null, with Tln1 knockdown in cardiomyocytes as compared to Tln2 null mice. Reprinted with permission from Manso, et al. Originally published in PNAS.

Chapter 3

Mouse Models of Pressure Overload Injury to the Heart

Text for Chapter 3 was adapted from **Noll NA**, Lal H, Merryman WD. *Mouse Models of Heart Failure with Preserved or Reduced Ejection Fraction*. The American Journal of Pathology, Vol. 190, No. 8, August 2020.

3.1 Introduction

Mouse models of heart failure (**HF**) have been utilized to improve our understanding of the various aspects and etiologies of HF towards the goal of developing novel treatment strategies. Mice are the most commonly used animal models in HF research, as they share the majority of their genes with humans, and approximately 85% of the protein-coding regions to the human genome.[129] Additionally, mice provide unique experimental advantages, such as the ability to impose genetic alterations, short breeding cycles, and relatively low housing costs. Numerous murine models of HF have been developed through a combination of genetic modifications, administration of pharmacological compounds, and/or surgical approaches to recapitulate human disease.[129,130] Mouse models allow for the study of specific risk factors of and treatment strategies for HF without some of the confounding effects of comorbidities seen in other animal models. Over the last decade, a large increase in mouse models of HF has increased our knowledge of both HF with preserved ejection fraction (**HFpEF**) and HF with reduced ejection fraction (**HFrEF**), many of which are highlighted in this chapter and summarized in **Table 2**.

3.2 Mouse models of HFpEF

There are many different models of HFpEF. These models strive to recapitulate the chronic disease progression and risk factors associated with the development of HFpEF, including hypertension, obesity, diabetes, and gaining. Some of these models, if permitted to run long enough, may also lead to the development of HFrEF.

3.2.1 Hypertension

Hypertension is one of the main underlying conditions that leads to HFrEF in humans.[4,23] Hypertension, which causes broad changes in inflammation and metabolism, can cause myocardial stiffness and diastolic dysfunction.[131] This is additionally exacerbated when hypertension results in increased pressure in the left ventricle (**LV**), resulting in the expansion of fibroblasts, hypertrophy of vascular smooth muscle cells, and pathological deposition of interstitial collagen. This leads to increased myocardial wall stress, which causes LV hypertrophy in an attempt to compensate for the increased pressure.[132] The most commonly used mouse model to study hypertension-induced HFpEF is the administration of deoxycorticosterone acetate (**DOCA**) while providing high-salt (1% NaCl) drinking water. This model causes increased sodium and water reabsorption in the kidneys, leading to high blood pressure through a decrease in the renin-to-aldosterone ratio. This model has also been shown to be mouse strain-dependent, as C57BL/6 mice are less susceptible to renal damage and hypertension than the 129/Sv strain[133]. Additionally, renal impairment is more severe in males than in females[134]. The DOCA model results in cardiac hypertrophy, ventricular fibrosis, upregulation of the hypertrophy markers atrial and brain natriuretic peptides (**NPPA, NPPB**), and infiltration of inflammatory cells into the cardiac tissue[134].

Angiotensin II (**Ang II**) administration has also been used to induce hypertension and chronic kidney disease in mice. Sustained elevation of Ang II levels in the circulation results in

Ang II-mediated vasoconstriction, hypertension, aldosterone secretion, TGF-β-mediated fibrosis, and inflammation - all of which contribute to the development of cardiac hypertrophy. This model has contributed to many cardiovascular discoveries, including that sildenafil, an inhibitor of PDE5A, improves LV performance, reduces adverse remodeling, and diminishes infiltration of inflammatory cells during Ang II-induced HFpEF.[135] Additionally, the Ang II model has been combined with the DOCA salt and uninephrectomized models in an attempt to overcome the resistance of C57BL/6 mice to chronic kidney disease (**CKD**) and hypertension development[136,137].

3.2.2 Pulmonary hypertension

Diastolic dysfunction, as experienced in HFpEF, is the most frequent cause of pulmonary hypertension (**PH**).[138] PH is commonly found in deteriorating HFpEF, and is therefore closely associated with worse outcomes and mortality in patients with HFpEF.[139] During HFpEF, chronically elevated filling pressure in the LV causes backward pressure in the pulmonary arteries, resulting in vascular remodeling and increased pulmonary arterial pressure, pulmonary vascular resistance, and right ventricular hypertrophy that are associated with PH.[140] PH exacerbates the LV diastolic dysfunction that is already occurring in the heart.[141] As a result, mouse models of PH were developed to study how PH leads to increased diastolic dysfunction. AKR/J, NON/shiLtJ, and WSB/EiJ mice, when placed on a high-fat diet for 20 weeks, develop elevated right ventricular systolic pressure and LV end-diastolic pressure while having a preserved EF.[142] These findings illustrate that these mice develop biventricular hypertrophy, HFpEF, and PH.

3.2.3 Type 2 diabetes

Cardiovascular complications are the leading cause of diabetes-related morbidity and mortality.[143] Diabetes mellitus, or Type 2 diabetes (**T2D**), is non-insulin-dependent and results from a combination of insulin resistance and β-cell secretory defects.[144] Complications associated

with T2D include increased coronary heart disease and accelerated atherosclerosis due to associated risk factors of hypertension, obesity, and dyslipidemia[145]. Db/db and ob/ob mice are the most commonly used T2D that are based on leptin-receptor deficiency or lack of functional leptin, respectively.[146] In both mouse models, circulating leptin is taken up in the hypothalamus, causing an increase in appetite, body weight, and decreased energy expenditure. This results in both models having severe, early onset obesity at four-weeks of age and the development of hyperinsulinemia and T2D by 15 weeks.[147] Cardiac hypertrophy, increased LV mass and diastolic dysfunction occur in these mice as myocardial oxygen consumption is increased, resulting in decreased cardiac efficiency.[146,148,149] Ob/ob mice experience contractile dysfunction; however, db/db cardiomyopathies are more pronounced.[150] The major disadvantage of the db/db and ob/ob mouse models is that while there is a robust phenotype of T2D, there are potentially confounding side effects from altered leptin signaling. In db/db mice, there is no altered tyrosine kinase signaling changes in cardiomyocytes, a variation from decreased signaling seen in human muscle tissue.[151] In ob/ob mice, the innate and acquired immune response is repressed, potentially resulting in an altered response to acute and chronic injury to the heart.[152]

3.2.4 Type 1 diabetes

Type 1 diabetes (**T1D**) is defined by the National Institute of Diabetes, Digestive and Kidney Disease as an autoimmune disease in which the immune system attacks and destroys insulin-producing pancreatic β-cells, resulting in an absolute insulin deficiency.[153] The autosomal dominant mutant *INS*-gene is one known human genetic cause of T1D and serves as a reproducible model of T1D in mice.[154] The *Akita* mouse ($Ins2^{Akita+/-}$) is heterozygous for the *Ins2* gene mutation, wherein all males develop T1D after weaning age. At 5-6 weeks of age, the *Akita* mice develop hyperglycemia (which is similar to humans who develop T1D between 15 and 25 years of age).[155] At 12 weeks, these mice have an increase in the circulating HF markers NPPA

and NPPB with diastolic dysfunction and a decrease in the radial strain occurring between 3 and 6 months.[155,156]

To look at the acute onset of T1D in mice, Streptozotocin (**STZ**), which directly kills pancreatic β-cells, is administered, inducing chronic T1D. High doses of STZ can cause toxicity outside of the pancreas, so a low continuous dose of STZ is recommended. The STZ mouse model results in hyperglycemia seven to 14 days after the first injection.[157] STZ induces early diastolic and vascular dysfunction, which is progressively exacerbated by the development of diabetes, leading to systolic dysfunction and HFpEF, accompanied by abnormal patterns of mitral valve inflow and pulmonary venous flow.[158,159] While the STZ model of T1D produces a robust imitation of the disease, it does not capture the autoimmune aspect of the development of T1D in humans.

Acute onset of T1D can also be studied without the use of toxins by using OVE26 mice. OVE26 mice overexpress calmodulin in pancreatic β-cells, resulting in mice with diabetic nephropathy and severe early onset of T1D during the first week of life. OVE26 mice can live for one year with no insulin treatment and will maintain near-normal body weight.[160] These mice spontaneously develop diastolic dysfunction with an increase in end-systolic interventricular septum thickness and end-systolic left ventricular posterior wall thickness. When treated with Ang II, OVE26 mice have exacerbated cardiac hypertrophy, with an increase in LV mass and NPPA expression.[161]

3.2.5 Obesity

Obesity is a complex chronic disease resulting from the accumulation of several physiological changes over a long period of time and is associated with many other risk factors in the development of HF (e.g. hypertension, diabetes, and psychosocial stress). In the lab, diet-induced obesity in mice has been developed as the standard practice to probe the pathologic

contributions of an imbalance of food intake, basal metabolism, and energy expenditure.[162] C57BL/6J mice on a high-fat diet closely parallel patterns of progression and metabolic irregularities found in human obesity. After two weeks, C57BL/6 mice have decreased rates of glucose oxidation and glycolysis, which further develops into obesity and T2D.[163] At 20 weeks, a 20 to 30% increase in body weight occurs alongside cardiac dysfunction, elevated filling pressures, myocardial fibrosis, and exercise intolerance.[164] This model was used to discover the importance of Akt and mTOR signaling in obesity.[165] Physiosocial stress is recognized as an independent risk factor for cardiovascular disease, and when it is added to a high-fat diet model of obesity, cardiac dysfunction will occur.[166] This model results in prominent interstitial fibrosis, apoptosis of CMs, remodeling of the larger coronary branches, and augmented oxidative stress in the LV.[166]

3.2.6 Aging

HF is disproportionately distributed among the elderly, as over half of all patients hospitalized with HF are over the age of 75, with 50% presenting with diastolic dysfunction.[167] The senescence-accelerated prone (**SAM**) mouse, derived from inbreeding AKR/J mice, recapitulates many common geriatric disorders evident in elderly human populations.[168] The SAM model is comprised of both a senescence-prone (**SAMP**) and senescence-resistant (**SAMPR**) control strain. The SAM strains are the best-studied strains regarding HFpEF, as they result in age-dependent diastolic dysfunction in the absence of systolic dysfunction. Additionally, there is an increase in pathological fibrosis and the production of the pro-fibrotic cytokines TGF-β and connective tissue growth factor.[169]

3.3 Advantages and disadvantages of HFpEF models

HFpEF results from systemic underlying conditions that cause diastolic dysfunction to develop overtime with the progression of the principle disease. To study HFpEF, mouse models aim to accurately recapitulate the risk factors of HFpEF, which include hypertension, obesity, diabetes, and aging. In hypertension-induced HFpEF mouse models, DOCA and Ang II administration both cause systemic changes to the cardiovascular system with increased blood pressure through the renin-aldosterone pathways. This makes DOCA and Ang II advantageous models for looking at HFpEF progression due to there being no direct insult on the heart. However, both DOCA and Ang II have effects on the kidneys, leading to CKD, which could cause additional changes to the heart outside the scope of just hypertension.

These potential off-target effects are additionally seen in the T2D models of db/db and ob/ob mice. Altered leptin signaling in these mice is also seen in addition to changes in tyrosine kinase and immune signaling, respectively, to humans with T2D.[150,152] Additionally, in both the ob/ob and db/db models of T2D there is a reverse lipid profile as compared to humans, high HDL, low LDL, which results in high clearance of lipoprotein which keeps atherosclerosis from developing spontaneously, as seen in humans with T2D.[170] Altered signaling in other tissues/organs is not an issue in T1D-induced HFpEF mouse models, as the pancreatic β-cells in the *Akita*, STZ, and OVE26 mice are destroyed. The advantages of using the *Akita* mice and OVE26 mice are that they develop T1D due to genetic mutations. The *Akita* mouse develops T1D at 5-6 weeks of age, which is equivalent to humans who developed T1D between 15 and 25 years of age and will survive with insulin treatment until HFpEF occurs. OVE26 mice develop T1D after the first week of life, making it a good model of childhood T1D. Additionally, they can be aged for a year without insulin treatment, allowing them to be a model of T1D-induced HFpEF with untreated T1D. The advantage of using STZ toxin to induce the onset of T1D and HFpEF is that it can be given when the mice are at a specific age, allowing researchers to study T1D-induced

HFpEF when T1D occurs at multiple ages. However, too high a dose of STZ has off-target effects and can cause toxicity outside of the pancreas due to STZ being a potent alkylating agent. These effects include direct and indirect immunosuppressive effect through toxicity on lymphocytes and B cells, as well as toxicity to the kidney, liver and brain.[171]

Obesity and aging models of HFpEF develop diastolic dysfunction over time without directly causing the initiation of any of the other precursors of HFpEF. This is advantageous because there is no direct insult to the mouse's system through the ablation of a particular cellular population or injecting a toxin systemically. However, this means the mice could develop multiple risk factors for HFpEF, such as hypertension and diabetes, and the individual contribution of each risk factor to HFpEF may be hard to parse out, as each animal may not develop the same underlying conditions.

Additional spontaneously developed insults, such as myocardial infarction, in all models of HFpEF can cause further cardiovascular remodeling. In such instances, this can drive extracellular matrix deposition, LV wall thinning, and additional hypertrophy, resulting in systolic dysfunction and HFrEF (**Figure 1**). Therefore, it is suggested that echocardiographic analysis of all mice should be performed during HFpEF studies to monitor diastolic dysfunction and any potential systolic dysfunction occurring.

A key limitation of all the above preclinical HFpEF models is that they largely reflect a temporary stage of ejection fraction maintenance during the initial trajectory of the disease and ultimately leads to the HFrEF phenotype. A transition from HFpEF to HFrEF is not typical of all human etiologies. Thus, these animal models of HFpEF fail to accurately recapitulate all the HFpEF phenotypes observed in humans. Overall, the attempts to developing novel and relevant animal models of HFpEF have been disappointing. This has seriously hampered our mechanistic understanding of the fundamental biology of HFpEF. In humans, HFrEF cardiomyocytes are

characterized as a systolic deficit, compromised contractile potential, with depleted Ca^{2+} reserves, whereas these characteristics are not featured in the HFpEF cardiomyocytes. Unfortunately, the current preclinical models of HFpEF have not yet facilitated the discovery of fundamentally different biology of cardiomyocytes or other cell types in the heart specific to HFpEF. The emergence of patient-specific HiPSC-derived cardiomyocyte and fibroblast model system have brought new hope. Functional studies with HFpEF patient-derived HiPSC-induced cardiomyocytes or bioengineered microtissues from them have the potential to revolutionize the fundamental research of HFpEF biology, including bioengineered tissue patches from HFpEF patients can display a phenotype of relaxation defects, diastolic dysfunction, with maintained contractility.[172,173] However, as of now, the field of HiPSC-derived cardiomyocyte biology is facing challenges of relatively immature cardiomyocytes, and difficulty in maintaining a differentiated phenotype for long-term studies. Therefore, even though this model system has enormous potential, only time will tell if it can accurately mimic the HFpEF phenotype.

3.4 Mouse models of HFrEF

The following sections discuss mouse models that routinely result in HFrEF (**Table 2**). Some of these models initially cause HFpEF, with the eventual development of systolic dysfunction indicative of HFrEF.

3.4.1 Left ventricular pressure overload

Hypertension is the single most important risk factor for the development of HFrEF in the United States.[24] To study HFrEF induced by chronic pressure overload of the LV, various surgical approaches have been developed to mimic the adaptations associated with hypertension in patients. Rockman et al. first described the transverse aortic constriction (**TAC**) method, and this is currently the most prevalent method of studying LV pressure overload-induced HF.[174] TAC causes an increase in LV afterload, resulting in concentric hypertrophy, interstitial fibrosis, and increasing LV stiffness, eventually leading to systolic failure.[24,174,175] The severity of the TAC procedure is assessed by measurement of pulsed wave Doppler images of the aortic arch and comparing these to sham animals.[176] The TAC model has allowed for the discovery of many underlying causes of HF, including that *NOS3*$^{-/-}$ augments LV remodeling.[177] However, the TAC procedure is not without its drawbacks, as it is highly operator-dependent, has poor reproducibility, and is technically demanding, which can lead to variable degrees of aortic constriction. The hypertrophic response to TAC and the progression to HF depend on the sex, weight, age, and genetic background of the mice. This is exemplified by C57BL/6J mice developing HFrEF, with a similar expression pattern to human dilated cardiomyopathy, more readily post-TAC than 129/Sv mice.[176] Additionally, the range of mortality of TAC varies between studies as much as 6 to 45% when a large TAC is induced.[176,178,179]

More recently, a modified TAC technique, the double loop-clip technique, was developed to decrease variability during the surgical procedure. Merino et al. measured the mid-aortic arch's

luminal diameter during pre-surgery echocardiography to calculate the inter-knot span of the suture for the modified double loop-clip technique. This allowed for the customization of the constriction to the mouse somatometry.[180] This new procedure results in a far more accurate, reproducible stenosis that decreases mouse mortality and increases the homogeneity of structural and molecular features post-aortic constriction.[180]

3.4.2 Ischemic injury

Coronary artery ligation is the most common mouse model used to mimic myocardial infarction (**MI**).[181] Ligation of the left anterior descending (**LAD**) artery results in HF, with HFrEF developing by 6 weeks post-infarction. Myocyte death and ECM deposition leading to a collagenous scar can be assessed by Evans blue and TTC (2,3/5-triphenyltetrzolium chloride) double staining, where the typical infarct area is between 50 and 60% of the total LV wall area.[175,182] This results in thinning and dilation of the infarcted area, causing reactive hypertrophy and fibrosis in the non-affected myocardium and eventual LV dilation and impaired systolic function.[183,184] Additionally, PH develops in these mice, with severity proportional to the size of the infarct.[185] While coronary artery ligation is a reliable model to induce tissue damage that leads to HFrEF, it does not reflect the development of HF in patients, as the underlying factors that cause MI in humans - coronary artery disease, atherosclerosis, thrombus formation and hypertension - do not exist in this model.

Ischemia/reperfusion (**IR**) injury during MI is a major cause of morbidity and mortality of patients with HF.[186] IR injury in the heart results in cardiac remodeling and fibrosis, resulting in HFrEF. In mice, IR injury is simulated by temporarily occluding the LAD to produce transient ischemia to the LV.[187] This procedure results in a smaller injury than is achieved by coronary artery ligation.[188] Furthermore, the IR mouse model closely parallels the clinical scenario where reperfusion of the occluded vessel occurs during coronary angiography after an acute MI.

3.4.3 Other surgical models

Increasing clinical evidence has shown that ischemic heart disease and accompanying hypertension result in additional risk factors for developing HFrEF.[167] Previously studied in dogs and rats, a mouse model has been developed where a moderate TAC is performed on mice followed by a small MI (myocardial injury is less than 25% of infarct size).[189] In this model, LV remodeling post-MI is exaggerated due to increased wall stresses from the induced hypertension. This leads to progressive LV dilation, interstitial fibrosis, and an increase in LV mass 28 days following the procedures. This model more accurately models the comorbidities of arterial hypertension and ischemic heart disease than TAC or MI alone.

Pulmonary aortic banding (**PAB**) in mice mimics PH and pulmonary stenosis in humans and is used as a model of right ventricular hypertrophy and HF in mice.[174] PAB results in concentric hypertrophy, increased heart weight, and myocardial fibrosis 8 weeks post-injury.[190] The severity of the PAB correlates with the progression of cardiac dysfunction and mortality.[191]

Chronic kidney disease (**CKD**) is often a common underlying cause of HFrEF due to increased hypertension and other cardiopulmonary dysregulation associated with impaired kidney function. In a study of the Acute Decompensated Heart Failure National Registry, 60% of the patients studied had CKD.[192] Considering this data, CKD mouse models are being used to study the effects of CKD on myocardial dysfunction during HF. Common models of CKD, such as AngII administration, salt loading, and uninephrectomy result in HFrEF with systolic dysfunction, pulmonary congestion, cardiomyocyte hypertrophy, and an increase in fibrosis 6 weeks post-injury.[193]

3.4.4 Pharmacological models of HFrEF

Toxin-induced HF models have been increasingly used to study the underlying causes of HFrEF, including chemotoxicity, hypertension, renal injury, and liver injury.[194–196] These models

aim to induce a systemic injury to the mouse instead of specifically targeting the cardiovascular system. This section will summarize the mechanisms of action, cardiovascular effects, and disadvantages associated with several commonly used toxin-induced models of HF.

Chronic adrenergic stimulation is a hallmark of chronic HF.[197] In order to isolate this stimulation, isoproterenol (**ISO**), a nonselective β-adrenergic agonist, is administered to mice using an implanted osmotic pump or continuous injections. Echocardiography illustrates cardiac hypertrophy, dilation, and ventricular dysfunction develop after 3 weeks of continuous ISO administration.[194] ISO additionally causes cardiomyocyte apoptosis, leading to a decreased ability of the ventricle to contract.[194] Mice of different genetic backgrounds have varying increases in LV mass, hypertrophy, and dilation, as well as variable decreases in ejection fraction, suggesting that dosing of ISO must be matched to the genetic background of the mice being used.[198]

Phenylephrine is an α-adrenergic agonist that causes vasoconstriction, resulting in an increase in afterload and a decrease in ventricular function. When given in mouse models, phenylephrine causes myocardial hypertrophy of the LV, increased LV weight, systolic dysfunction, and increased expression of HF markers NPPA and NPPB.[199] When Ang II, another potent vasoconstrictive hormone, is given as a subcutaneous infusion over 14 days, mice develop hypertension, vascular inflammation, and fibrosis.[200] Phenylephrine and Ang II have also been given in conjunction to increase total vasoconstriction in the cardiovascular system and exacerbate HFrEF. The main drawback of adrenergic and Ang II-induced HFrEF is that they only recapitulate one component of the disease.

Alcohol is one of the most abused substances in the United States. While its effects on liver injury have been studied in-depth, there is a smaller amount of research looking at the secondary development of alcohol-induced cardiotoxicity. Injection of ethanol into mice has been

developed as a model of alcohol-induced cardiac disease.[201] This method results in reduced cardiac contractility, enlarged cardiomyocytes, myocyte apoptosis, and mitochondrial damage. These were also all increased with overexpression of alcohol dehydrogenase transgene in mice with a decreased LV diastolic pressure.[195]

Doxorubicin (**DOX**) is a widely used chemotherapeutic agent used as a treatment for many cancers (e.g. breast, ovary, thyroid, and bone tumors).[202] Dose-dependent DOX-induced cardiotoxicity has been noted in these patients a short time after treatment.[203] Mice differing in sex, age, or genetic background react differently to DOX administration, but all experienced some degree of cardiac injury that worsened over time, even after DOX treatment was halted.[196,204] Chronic DOX-toxicity in these mice presents with interstitial fibrosis, pervasive fibril atrophy and disorganization, collagen remodeling, and dense infiltration of macrophages and myofibroblasts most commonly observed in the atria as atrial lesions.[196] These mice additionally suffer from toxic side effects in their bone marrow and gastrointestinal systems, making this model less than ideal for the investigation of immunologic impacts on HF.

3.4.5 Genetic models

Transgenic mouse models have become the norm when investigating the impact of specific genes on cellular and molecular pathways during HF. The two most popular methods to generate whole-body gene deletions and conditional knockouts are the Cre/loxP and Flippase/FRT-mediated recombination methods. These methods combine Cre/loxP or Flippase/FRT with a specific promoter (e.g. *Postn*) that is unique to a target cardiac cell type.[40] These models have been useful in studying the various underlying causes of dilated cardiomyopathy (**DCM**), which can lead to HFrEF. DCM is the leading cause of HF and has been linked to mutations in more than 40 different genes. These mutated genes can be grouped broadly into four categories: nuclear envelope, sarcomere, cytoskeletal and other proteins.[205] This section

will discuss an example of commonly used genetic models of dilated and hypertrophic cardiomyopathy.

The LINC complex is composed of proteins that interact with the nuclear envelope that form the physical link between the cytoskeleton and the interior of the nucleus. Many diseases have been associate with mutation in LINC complex proteins, including nesprin-1 and nesprin-2, which lead to X-linked Emery-Dreifuss muscular dystrophy and cardiomyopathy. [206]Δ/ΔKASH mice are homozygous for a nesprin-1 allele but lack the KASH domain, and instead have an alternative sequence that is not homologous to any known protein domain.[207] At 52 weeks of age, Δ/ΔKASH mice exhibited longer P duration, an elongated QRS duration, and an increased atrial effective refectory period, which indicates the development of conduction defects.[208] Additionally, fractional shortening at 52 weeks is decreased, indicating HFrEF. This mimics systolic dysfunction seen in patients with DCM with conduction system defects.

Another genetic model interferes with myosin binding protein-C (**MYBPC**), a thick filament accessory protein that is present in sarcomeres. Mutations in this protein result in 20% to 30% of all mutations in familial hypertrophic cardiomyopathy.[209] *Mybpc3*$^{-/-}$ mice exhibited significant cardiac hypertrophy with interstitial fibrosis at eight weeks of age, along with systolic dysfunction. Impaired contractile function was also exhibited in these mice, as myocytes had increased Ca^{2+} sensitivity of tension.[209]

3.5 Advantages and disadvantages of HFrEF models

Mouse models of HFrEF provide several advantages and disadvantages to researchers. Surgical models, such as TAC and MI, are technically demanding, can be very hard to reproduce, and have a large degree in variability in the injury that occurs.[210] However, with new alteration to past techniques, such as the double loop-clip technique to the TAC surgery, the reproducibility of consistent injury severity is increased. Surgical models of HFrEF work by creating an acute injury to the heart either directly, as in MI and IR, or indirectly, TAC. As a result, the systemic factors associated with chronic disease leading to HFrEF are not recapitulated in these surgical models. However, these mouse models do allow for study of fibrotic and hypertrophic remodeling that are a direct response to the acute cardiac injury. These models have been used in studies such as those involving Xinji'erkang (**XJEK**), a medication used clinically to treat coronary heart disease and myocarditis, to show XJEK has a cardioprotective effect following MI in mice by reducing oxidative stress and improving endothelial dysfunction.[211]

DOX, alcohol, and Ang II, toxin-induced models of HFrEF, cause a systemic injury that leads to the development of HFrEF. These models are advantageous in that they cause the mice to develop one of the underlying conditions that lead to HF, namely hypertensive heart disease. They allow for the accurate study of disease progression and are more representative of the development of HFrEF in humans. This was demonstrated recently, where blocking toll-like receptor 2 (**TLR2**) was identified as a potential therapeutic strategy for the treatment of DOX-induced DCM. TLR2 isotype-matched IgG Ab administration resulted in reduced mortality, decreased cardiac dysfunction by 13%, and diminished cardiac fibrosis.[204] While systemic injury allows for targeting of the underlying cause of HFrEF, this introduces many variables into these studies that can result in confounding data. ISO and phenylephrine are more specific and act as adrenergic agonists, limiting some of the off-target cardiovascular injuries while still allowing for the study of HF progression.

With an increase in genetic testing and knowledge of genetic mutations that result in HF, genetic mouse models are an ideal way to study these diseases and their resulting pathologies. By creating models of known cardiomyopathies due to genetic mutations, such as nesprin-1 and MYBPC, researchers can more easily explore altered protein expression and molecular pathways to discover potential new mechanisms of action and treatment strategies. Additionally, Cre/loxP and Flippase/FRT systems can be used to study the knockout or overexpression of proteins in specific cell types. In conjunction with surgical or toxin-induced models of HFrEF, the Cre/loxP system has allowed for the study of cardiac fibroblasts and the immune system in fibrotic remodeling during HFrEF post-MI. The Cre/loxP model has been used to selectively knockout GSK-3β in CFs, resulting in CFs adopting a myofibroblast phenotype and mice developing LV dysfunction and fibrosis post-MI.[212]

While mouse models have allowed for advancement in the study of HF, they have limitations. Mice are inbred, resulting in little heterogeneity, which does not reflect the vast genetic diversity seen in humans. Additionally, most mouse studies of HF are performed in male adolescent mice. Since HF disproportionately affects the elderly, changes in the cardiovascular system due to aging are not recapitulated in these models.

3.6 Discussion

In summary, the mouse models of HFrEF are well established and characterized, however, the ideal HFpEF animal model is yet to be developed and optimized. Nonetheless, mouse models of HFpEF and HFrEF are effective tools for researchers investigating novel pathologies and therapies in HF. These models mimic various aspects of the underlying conditions that cause HFpEF and HFrEF to help decipher numerous underlying contributing mechanisms of the disease. While several limitations of these mouse models warrant the interpretation of the results of the studies performed with caution, mouse models of HFpEF and HFrEF have advanced our understanding of the pathogenesis of HF. Based on advancements in gene editing, numerous transgenic mouse models will further advance our knowledge in this area in the near future. These models in combination with surgical and toxin-induced models of HFpEF and HFrEF will continue to facilitate the identification of new targets and development of novel treatment strategies for HFpEF and HFrEF patients.

Table 2: Mouse models used to induce HFpEF or HFrEF

Type of HF Model	Model	Stimuli	Advantages	Disadvantages	Selected References
HFpEF	Hypertension	DOCA	Reliable model of hypertension	Non-specific side effects such as the development of chronic kidney disease	133,134
		AngII	Reliable model of hypertension	Non-specific side effects such as the development of chronic kidney disease	135
		DOCA + AngII + uninephrectomy	Allows for hypertension development in C57/Bl/6 mice		136,137
	Pulmonary Hypertension	High-fat-diet	Mimics right ventricular HF	Models an exasperator of HFpEF and not an initial stimulus of disease	142
	Type 2 Diabetes	db/db mouse	Reliable model of T2D	Time-dependent progression of HF phenotype, altered leptin signaling	146,148–151
		ob/ob mouse	Reliable model of T2D	Time-dependent progression of HF phenotype, altered leptin signaling	146,148–151
	Type 1 Diabetes	Akita mouse	Mimics time of T1D development in humans	Time-dependent progression of HF phenotype	155,156
		STZ	Reliable model of T1D	Toxicity to pancreas if dosed to high, does not model autoimmune aspect of the disease	157–159
		OVE26 mouse	Mimics acute onset of T1D in children	Time-dependent progression of HF phenotype	160,161
	Obesity	High-fat diet	Mimics metabolic abnormalities found in humans	HF takes 20 weeks to develop	162–165
		High-fat diet + physiological stress	Mimics metabolic abnormalities found in humans	HF takes 16 weeks to develop	166

	Aging	SAMP/SAMPR mice	Allows for studying aging-induced HFpEF on a shorter timeline	May have non-specific effects on the mouse during aging	168,169
HFrEF	LV Pressure Overload	TAC	Reliable model of hypertrophy	Technically demanding surgery	175–177,213
		TAC-double loop technique	Easier surgery where degree of hypertension is more reproducible		180
	Ischemic Injury	LAD ligation	Reliable model of ischemic injury	Does no reflect cardiovascular disease leading to MI	181–185
		IR	Smaller more consistent injury than LAD	Does no reflect cardiovascular disease leading to MI	187,188
	LV Pressure Overload + Ischemic Injury	TAC + LAD ligation	Comorbidities of pressure overload and ischemic heart disease modeled	Does no reflect cardiovascular disease leading to MI	189
	Volume Overload	PAB	RV hypertrophy		174,190,191
	Chronic Kidney Disease	AngII + salt loading + uninephrectomy	Models an underlying of HF without injury to the heart	Time dependent progression of HF phenotype	193
	Hypertension	Isoproterenol	Reliable inducer of cardiac hypertrophy	Chronic adrenergic stimulation is only one contributing factor to the development of HF	194,198
		Phenylephrine	Reliable inducer of cardiac hypertrophy	Chronic adrenergic stimulation is only one contributing factor to the development of HF	199
		AngII	Reliable inducer of cardiac hypertrophy	Non-specific side effects such as the development of chronic kidney disease	200
	Cardiotoxicity	Alcohol	Induces dilated cardiomyopathy	Non-specific side effects such as liver toxicity	195,204
		DOX	Induces dilated cardiomyopathy	Chronic toxicity of bone marrow and gastrointestinal system	196,204

	Cardiomyopathies	Δ/Δ KASH mouse	Induces cardiomyopathy	Time dependent progression of HF phenotype	207,208
		Mybpc3$^{-/-}$ mouse	Induces cardiomyopathy	Time dependent progression of HF phenotype	209

HF, heart failure; DOCA, deoxycorticosterone acetate; AngII, angiotensin II; T2D, type 2 diabetes; T1D, type 1 diabetes; STZ, Streptozotocin; TAC, transverse aortic constriction; LAD, left anterior descending artery; MI, myocardial infarction; IR, ischemia/reperfusion; PAB, pulmonary aortic banding; DOX, Doxorubicin.

Chapter 4

Loss of Tln1 in Myofibroblasts During Pressure-Overload Induced HFpEF Results in Augmented Cardiac Hypertrophy

4.1 Introduction

Adverse myocardial remodeling in response to pressure overload is a leading cause of heart failure.[4,23,24] The two principal components of myocardial remodeling in the context of pressure overload are cardiac hypertrophy and interstitial fibrosis.[48,214] These adaptations cause the heart to initially normalize LV wall stress and maintain cardiac output.[215,216] However, as remodeling continues, interstitial fibrosis causes a stiffening of the heart walls leading to impaired cardiomyocyte contraction and heart failure. Hypertension is the single most important risk factor for the development of HFrEF in the United States.[24] To study HFrEF induced by chronic pressure overload of the LV, various surgical approaches have been developed to mimic the adaptations associated with hypertension in patients. One of the most common is transverse aortic constriction (**TAC**). TAC results in increased LV afterload, resulting in concentric hypertrophy, interstitial fibrosis, increasing LV stiffness, and systolic failure.[217]

Cardiac fibrosis is a key feature of the remodeling response and is defined by the accumulation of excessive amounts of ECM proteins, such as collagen and fibronectin.[45] Fibrotic remodeling is driven by the phenotypic shift of cardiac fibroblasts (**CFs**) in the ventricular wall into activated myofibroblasts. Myofibroblasts are marked by their expression of alpha smooth muscle actin (***α-SMA***), and periostin (***Postn***).[218] Myofibroblasts secrete and compact ECM components

such as collagen types I and III as they become contractile, allowing for short-term adaptation to tissue injury.[48–51,219,220] These changes result in increasing ECM stiffness during pathological remodeling, which is transmitted to CFs by their focal adhesions. During prolonged pressure overload, increased ECM stiffness results in a positive feedback loop whereby CFs continue to differentiate into myofibroblasts, creating a stiff, non-compliant myocardium. These changes lead to impaired cardiomyocyte contraction, cardiac dysfunction, and heart failure.[11,45,221]

Focal adhesions are protein complexes which link the cytoskeleton of CFs with the ECM via integrin receptors on the cellular membrane and mechanosensitive proteins. Integrins, through activation of their cytoplasmic tails, bind to actin via mechanosensitive proteins, including talin, vinculin, and α-actinin.[86,87,222] As ECM rigidity increases, outside-in signaling through focal adhesions causes stress fibers within CFs to form (expression of actin fibers and α-SMA instead of depolymerized G-actin) as more mechanosensitive proteins are recruited to focal adhesions and these stress fibers allow CFs to contract.[223] This contractility is transmitted to the ECM through inside-out signaling through focal adhesions and allows CFs to compact the ECM leading to more defined and rigid ECM in the heart.[80–82]

Talins are a family of large, dimeric, cytoskeletal proteins that link the actin cytoskeleton via connections to the cytoplasmic domain of the integrin β subunit.[224,225] The two talin genes of vertebrates, *Tln1* and *Tln2*, encode very similar proteins with 74% amino acid sequence identity.[226] In the adult heart, Tln1 and Tln2 are both highly expressed in CFs, while cardiomyocytes express Tln2 predominantly.[128] Tln2 has a stronger affinity for F-actin, allowing it to make stronger bonds than Tln1 and, therefore, is expressed highly in cells under constant forces, such as cardiomyocytes.[121] Under pressure overload of the heart, Tln1 protein levels were increased 4-weeks post-TAC in CMs and whole heart tissue, with no change in Tln2 expression.[126] This is consistent with protein levels of Tln1 and Tln2 taken from patients with end-stage, non-ischemic dilated cardiomyopathy (DCM), and suggests that Tln1 upregulation plays a

key response in CM response to injury.[126] While deletion of talins in cardiomyocytes has been evaluated, the effect of talin deletion in CFs in unknown.

Here, we describe the effects of TAC-induced pressure overload on the hypertrophic and fibrotic response when Tln1 is deleted from myofibroblasts. Additionally, we use siRNA to knockdown Tln1 *in vitro* in myofibroblasts to characterize the morphological changes in myofibroblasts when Tln1 is removed.

4.2 Methods

Mice

All animal protocols were approved by the Institutional Animal Care and Use Committee at Vanderbilt University. Tln1 myofibroblast-specific knockout mice were created by crossing the $Tln1^{flox/flox}$ mice, provided by Dr. Roy Zent (Vanderbilt University Medical Center), with the *Postn*-Cre mice, provided by Dr. Jeffery Molkentin (Cincinnati Children's Hospital).[40] All mice were crossed with the *Rosa26*-stop-tdTomato reporter mice (Jackson Laboratory, Stock No. 007914) to visually verify Cre activation (**Figure 6**).[227] For brevity, these mice will be referred to as $Tln1^{MF-/-}$ mice. The sequences for the genotyping primers are listed in **Table 3**.

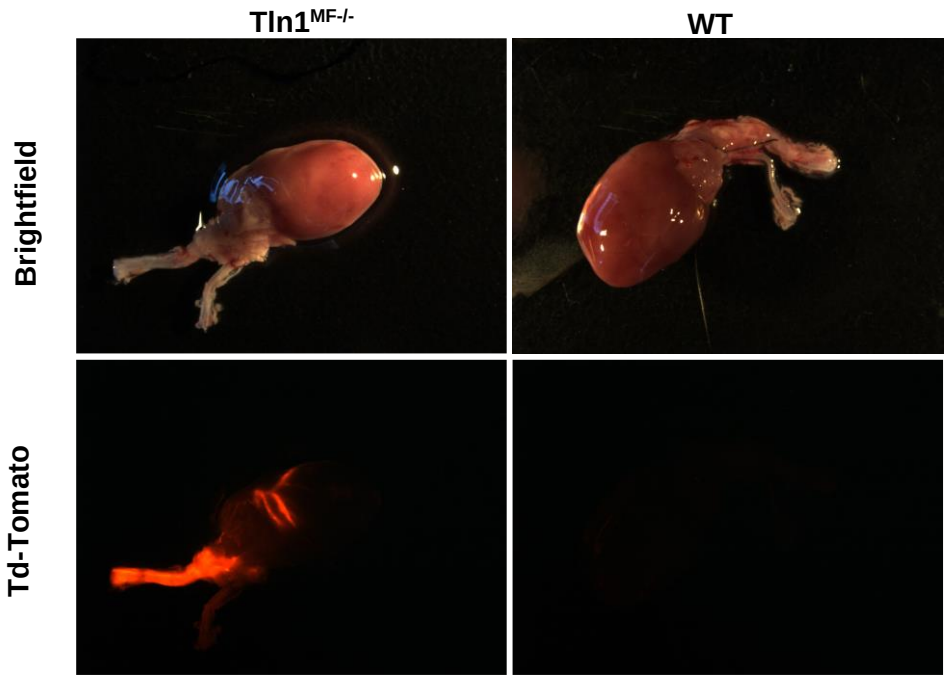

Figure 6: *Postn*-Cre activation after TAC. Pictures of WT and Tln1$^{MF-/-}$ hearts and carotid arteries under brightfield and Td-Tomato filters 6 weeks post-TAC.

Gene	Primer Name	Primer Sequence
Talin1	Primer A	AAGCAGGAACAAAAGTAGGTCTCC
	Primer B	GCATCGTCTTCACCACATTCC
Postn Cre	Postn Primer A	TCTGTAAGGCCATCGCAAGCT
	Mutant Primater A	GGTGGGACATTTGAGTTGCT
	Primer B	AATAAGTAAAACAGCTCCCCT
TdTomato	WT Primer A	AAGGGAGCTGCAGTGGAGTA
	WT Primer B	CCGAAAATCTGTGGGAAG TC
	Homozygous Primer A	GGCATTAAAGCAGCGTATCC
	Homozygous Primer B	CTGTTCCTGTACGGCATGG

Table 3: Primers used for genotyping.

Animal Studies – Transverse aortic constriction

All mice were started on tamoxifen chow at 8-weeks of age and were given tamoxifen chow throughout the duration of the experiment. Transverse aortic constriction (**TAC**) was induced in 10-week-old mice (**Figure 7**).[228] Briefly, mice were anesthetized with a single intraperitoneal injection of a mixture of ketamine and xylazine. Following a 3-4 mm upper partial sternotomy, a 6/0 silk suture is threaded through the eye of a ligation aid was passed under the aortic arch and tied over a blunted 27-guage needle. Sham-operated animals underwent the same surgical preparation but without aortic arch constriction. The success of TAC surgery can be seen by a decrease in peak left ventricular outflow tract velocity time integral (**LVOT VTI**) and hypertrophy of the tied carotid artery.

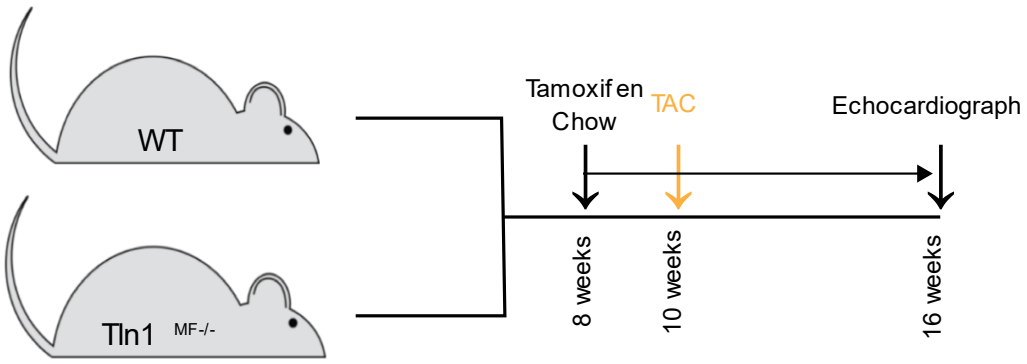

Figure 7: Experimental approach of TAC injury. 8-week-old WT and Tln1$^{MF-/-}$ mice were given tamoxifen chow 2 weeks prior to injury and kept on tamoxifen chow throughout the experiment. At 10-weeks of age transverse aortic constriction (TAC) or sham surgery was performed. 6-weeks later echocardiography was performed, and mice were euthanized.

Euthanasia

Mice were either euthanized with CO_2 exposure in accordance with Vanderbilt University Medical Center's Division of Animal Care Guidelines. Littermates were used and treatment groups were distributed throughout cages and litters.

Echocardiography

Blinded echocardiographic measurements were taken from short-axis cardiac M-mode images captured at mid-papillary level of non-anesthetized mice on a Vevo2100 small-animal ultrasound system (VisualSonics). Three independent measurements were analyzed per mouse for each timepoint.

Quantitative Polymerase Chain Reaction

Quantitative PCR (**qPCR**) was performed on flash frozen LV tissue dissected from experimental mice. The sequences for the primers used are listed in **Figure 4**. Gene expression was compared to the housekeeping gene *Gapdh*.

Gene	Forward	Reverse
Gapdh	ATGTTCCAGTATGACTCCACTCACG	GAAGACACCAGTAGACTCCACGACA
α-SMA	CACCCAGGGCCAGAGTCA	TCTCGTCTTCGTCGCACATG
Nppa	CCATATTGGAGCAAATCCTGTGT	CAGGTTCTTGAAATCCATCAGATCT
Tln1	GGCCCTCCCAACGACTTT	AGCCTCTAGCCAGATGCCTTT
Fn1	CTTTGGCAGTGGTCATTTCAG	ATTCTCCCTTTCCATTCCCG

Table 4: Primers used for qPCR.

Histology

Upon euthanasia, hearts were perfused with PBS-/-, excised, and submerged in 3M potassium chloride to arrest hearts in diastole. Hearts were bisected along the transverse plane of the heart. Tissue was frozen and cryosectioned at 7 µm thickness. Picrosirius red staining (**PSR**) (Fisher Scientific #50-300-77) was used to identify ECM (red) and cytoplasm (yellow). Images were analyzed using a semiautomated image-processing pipeline that was developed based on color segmentation.[227] Left and right carotid arteries were taken and fixed in formaldehyde. Carotids were then frozen and cryosectioned at 7 µm thickness. Carotids were elastin stained (Sigma-Aldrich, HT25A-1), and imaged to determine the elastin/media ratio.

Western Blot

Cells were lysed in RIPA buffer and frozen at -80°C. Protein lysates were denatured via β-mercaptoethanol and heat (five minutes at 95°C). 10% polyacrylamide gels were used for gel electrophoresis to separate proteins. Proteins were transferred to nitrocellulose membranes (LI-COR 926) and blocked with Odyssey Blocking Buffer (LI-COR 927) to prevent non-specific antibody binding. Membranes were incubated serially in primary antibody followed by fluorescently tagged secondary antibodies. LI-COR odyssey fluorescent scanner was used to image membranes and Image Studio Lite was used to analyze the images and perform the densitometry. Antibodies used were αTubulin for normalizing total protein Tln1 (ab71333).

Cell isolation and Culture

WT animals were mated with mice harboring the *Immorto* gene to allow for serial cell-culture of littermate WT cell lines. CFs were isolated from eight-week-old mice. Hearts were excised, minced, and digested in > 175 units/mL collagenase type 2 (Worthington Biochemical, LS004202) at 37° with mixing for 45 minutes. Digested tissue was centrifuged, filtered through a

40 µm filter, and cells were plated on gelatin-coated dishes. Cells were cultured at 33°C in DMEM supplemented with 10% FBS, 1% penicillin/streptomycin, and 10 µg/mL recombinant murine interferon γ to induce activation of the simian virus 40 T antigen. Prior to experiments (overnight), cells were incubated at 37°C in the same media lacking interferon γ (complete media) to deactivate the T antigen that confers immortalization.

siRNA knockdown

siRNA knockdown of Tln1 was performed in isolated cardiac fibroblasts with X-treme GENE siRNA (Roche, 04476093001) in 6-well plates when cells were 60% confluent (**Tln1 KD**). Scramble siRNA was added to control cells (**Scr**). 24 hours after siRNA was added, media was changed, and cells were lifted and plated for experiments. Western blot was used to verify knockdown over 120h post-siRNA addition. Western blot was used to verify knockdown over 120h post-siRNA addition (**Figure 8**).

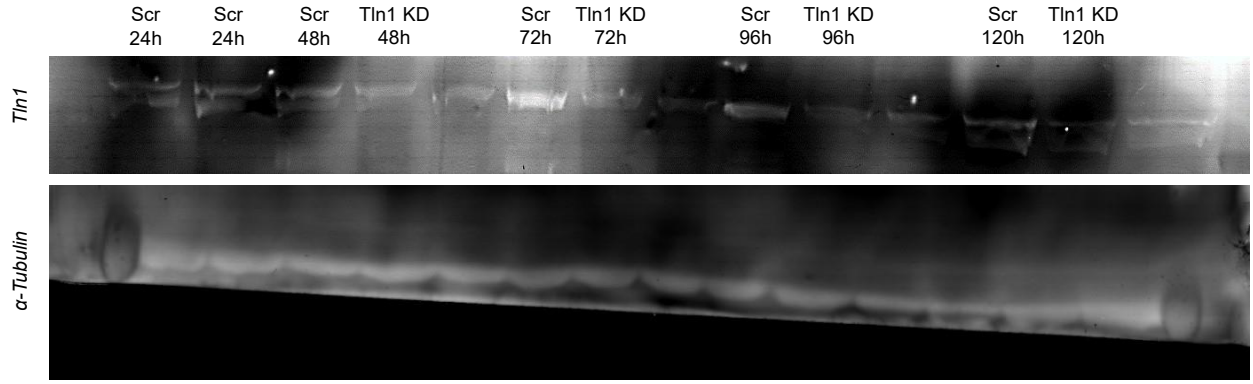

Figure 8: Western blot of Tln1 siRNA knockdown. siRNA Tln1 KD in cardiac fibroblasts with α-Tubulin used as the loading control. All marked sections on the blot are the concentration of siRNA used for all experiments.

Equalbiaxial Strain

Equalbiaxial strain was implemented on isolated cells for 24 hours using the FlexCell 3000 machine (FlexCell International Corporation) (**Figure 9**). Briefly, cells were plated 24h after siRNA was added onto fibronectin flexcell plates. Plates were then exposed to 10% strain for 24 hours. Control plates were not exposed to any strain.

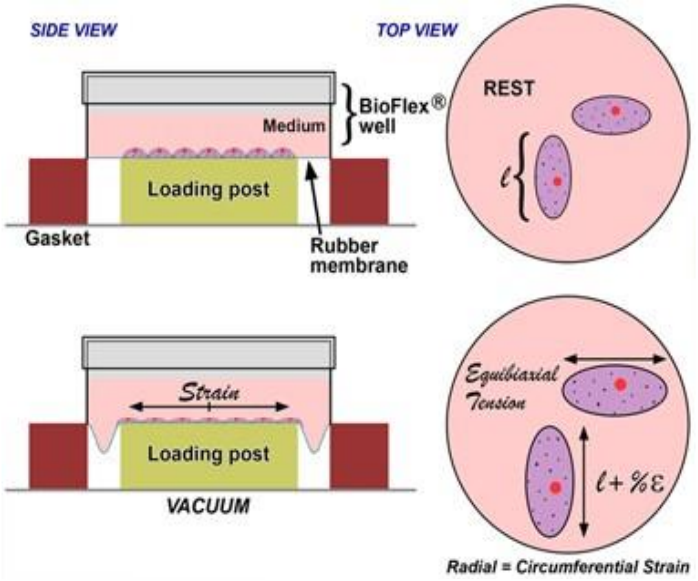

Figure 9: Flexcell diagram. Diagram of how the FlexCell 3000 applies equalbiaxial strain to cells.

MTT Assay

Cells were pated into 96-well plates 24 hours after siRNA was added. MTT (Roche, 11465007001) was added to the cells at 24 and 48 hours later and imaged using a colorimetric reader.

Gel Contraction Assay

Cells were suspended in complete media were used to create a 50:50 mixture with a bovine collagen solution (Advanced Biomatrix, 5005) for a final collagen concentration of 1.5 mg/mL collagen and 200,000 cells/mL. 250 µL of solution was pipetted unto a Teflon ring within a suspension cell culture plate. Following 1.5 hours of polymerization, complete media was added, and the collagen gel was released from both the Teflon mold and bottom of the plate. Gels were imaged immediately after release as well as six, 48, 72, 96 hours following siRNA addition. Gel area was measured at each time point using ImageJ (NIH) and normalized to original gel area.

Scratch Wound Assay

Cells were plated into 24-well plates 24 hours after siRNA was added. 24 hours after this, when all cells were 100% confluent, a 1mL pipet tip end was used to create a uniform scratch wound 'X' shape in each well. Pictures were taken after the scratch wound was inflicted, and all timepoints were normalized to these original images. Cells were then imaged every 6 hours.

Immunostaining

Cells were plated on glass coverslips coated in fibronectin 24 hours after siRNA was added to cells. 48 hours later, cells were fixed and permeabilized at 37oC. They were then washed and blocked in 1% BSA for 1 hours at room temperature. Primary antibodies were added overnight at 4oC. Talin (ab71333). Cells were washed, and then secondary antibodies were added overnight at 4oC. D-a-Ms IgG 647, α-SMA-Cy3 (Sigma-Aldrich, C6198), Phalloidin Alexa-Flour 488 (A12379). Cells were washed and then mounted with ProLongGold with DAPI (Invitrogen, P36941) and imaged.

Statistical Analysis

Data was compiled and shown as the means ± SEM. Data was evaluated using unpaired, two-tailed t-tests with Welch's correction (95% confidence interval) using GraphPad Prism software (GraphPad Inc., San Diego, CA). A p value < 0.05 was considered significant.

4.3 Results

4.3.1 TAC injury results in pressure overload of the heart that leads to both HFpEF and HFrEF in WT and mice with myofibroblast deletion of Tln1

A Tln1 floxed mouse ($Tln1^{flox/flox}$) was crossed with the myofibroblast specific *Postn*-Cre, referred to as **$Tln1^{MF-/-}$**. We then performed TAC on male WT and $Tln1^{MF-/-}$ mice for 6 weeks (**Figure 7**). All TAC mice had an increase in peak left ventricular outflow tract velocity time integral (**LVOT VTI**) as compared to sham controls (both $p \leq 0.0001$), indicating successful TAC (**Figure 10**), and tdTomato was verified in TAC mice (**Figure 6**).

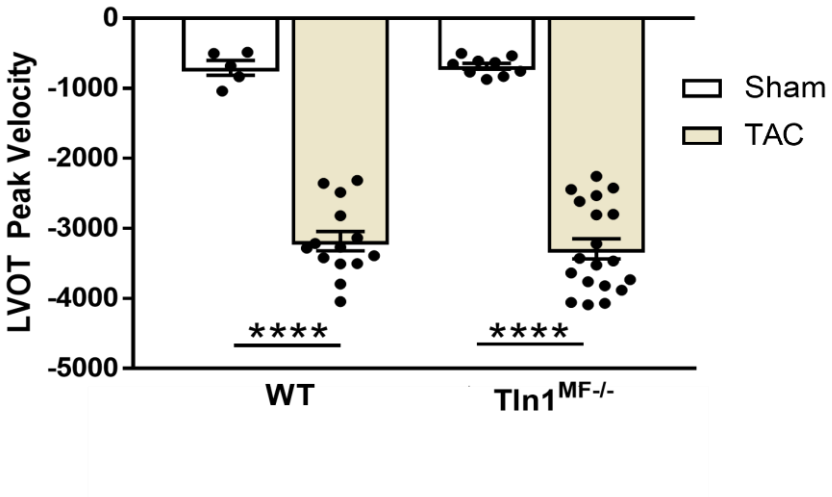

Figure 10: LVOT Peak Velocity after TAC. Peak left ventricular outflow tract velocity time integral (LVOT Peak V) 6 weeks after TAC to confirm successful TAC procedure. Mean±SEM, ****P<0.0001 between groups noted with bar. All statistics were done with a two-tailed t-tests with Welch's correction.

Additionally, the left and right carotid arteries were collected, and elastin staining showed increased injury in the carotid that was banded, indicating successful TAC (**Figure 11**).

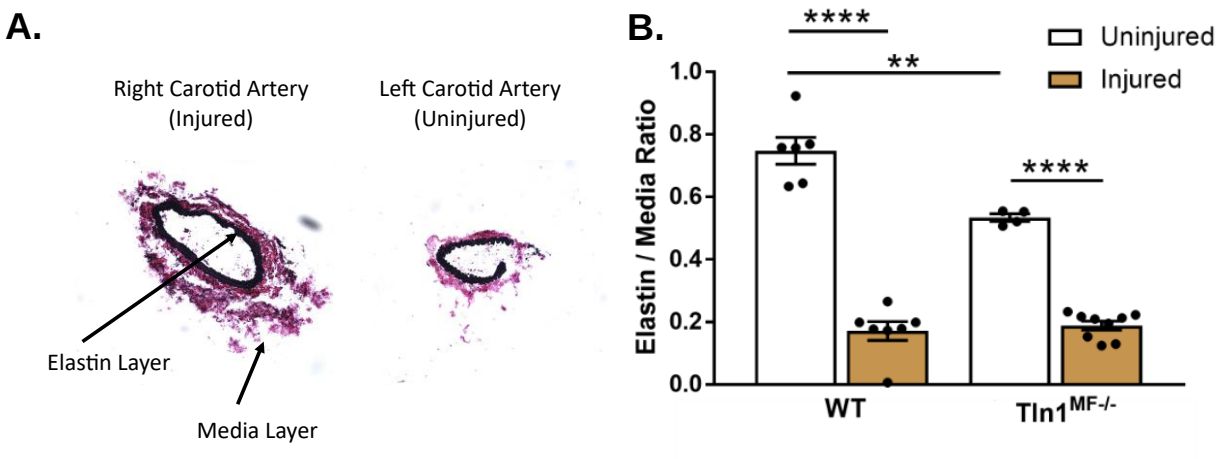

Figure 11: Elastin staining of carotid arteries after TAC. A. Representative pictures of elastin stain of both carotid arteries 6-weeks post TAC of a $Tln1^{MF-/-}$ mouse. The left carotid is uninjured, and the right carotid is injured as this carotid was next to the ligation site of the TAC. **B.** Elastin / Media ratio of the injured and uninjured carotid arteries for each mouse 6-weeks after TAC. Mean±SEM, **P<0.01, ****P<0.0001 between groups noted with bar. All statistics were done with a two-tailed t-tests with Welch's correction.

At 6-week post-TAC, 17.64% of WT mice and 31.58% of $Tln1^{MF-/-}$ mice had EF < 40%, indicating development of HFrEF (**Figure 12**). Due to the incidence of HFrEF not being prevalent in either the WT or $Tln1^{MF-/-}$ mice, we decided to focus on TAC-induced HFpEF (EF ≥ 40%) for the remainder of this study (**Figure 12**).

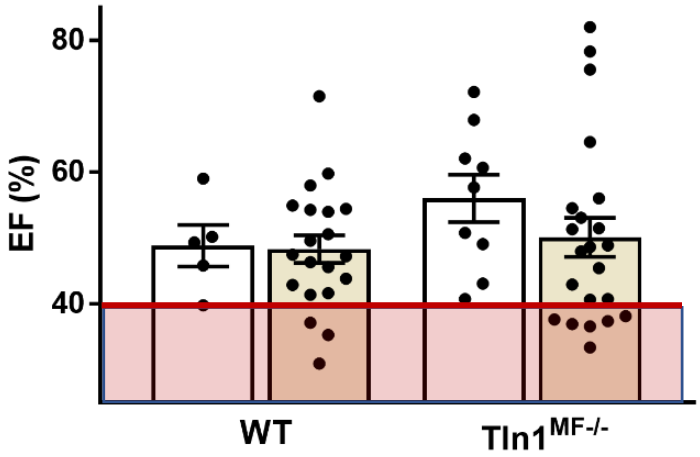

Figure 12: EF of mice after TAC injury. Ejection Fraction (EF) of mice taken 6-weeks post-TAC. Mice that had an EF < 40% and were classified as having HFrEF (seen shaded in red), and mice that had an EF ≥ 40% were classified as having HFpEF. Mean±SEM, **P<0.01, ***P<0.001 between groups noted with bar. All statistics were done with a two-tailed t-tests with Welch's correction.

4.3.2 Myofibroblast deletion of Tln1 results in myocardial injury and cardiomyocyte hypertrophy in response to TAC injury with HFpEF

Expression of *Nppa* was quantified in the left ventricle to assess myocardial injury. $Tln1^{MF-/-}$ mice had an increase in *Nppa* ($p \leq 0.05$) compared to their saline controls at 6 weeks post-TAC. This increase in *Nppa* was not seen in the WT TAC mice (**Figure 13a**). Ventricle weights were taken 6-weeks post-TAC to assess myocardial remodeling. Ventricle to body weight ratio at 6-week post TAC was increased in the $Tln1^{MF-/-}$ mice ($p \leq 0.001$) (**Figure 13b**).

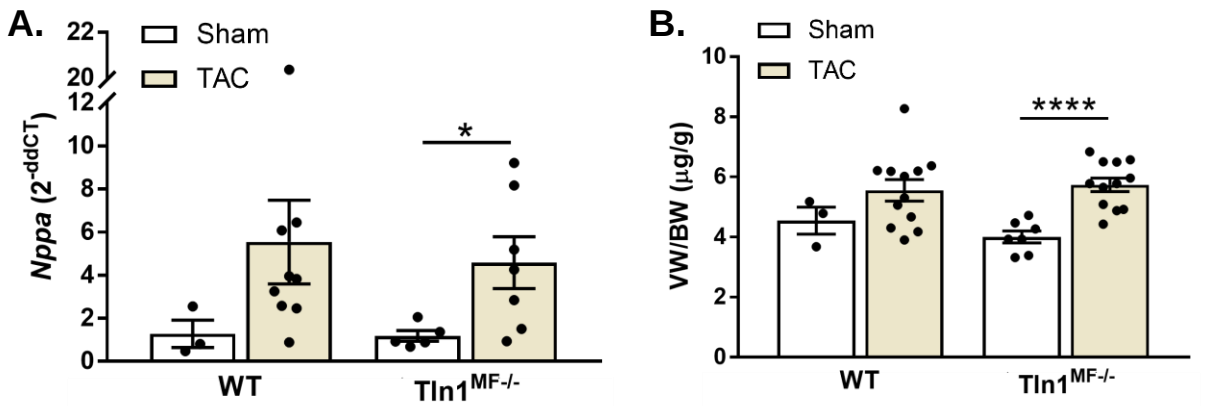

Figure 13: qPCR of *Nppa* and ventricle weight after TAC injury. A. Quantitative polymerase chain reaction analysis of *Nppa*, the gene encoding the heart failure marker natriuretic peptide A, at 6-weeks post-TAC, **B.** Ventricles to body weight ratio (VW/BW) at 6-weeks post-TAC. Mean±SEM, *P<0.05, ****P<0.0001 between groups noted with bar. All statistics were done with a two-tailed t-tests with Welch's correction.

This was supported by measurements of ventricle thickness through echocardiography. Echocardiographic measurement of LV mass showed an increase in the $Tln1^{MF-/-}$ mice ($p \leq 0.01$) (**Figure 14**). This increase in LV mass was additionally measured in increased thickness of the septum and posterior wall as the $Tln1^{MF-/-}$ mice had a greater increase in LVPW;d, IVS;d, and IVS;d (all $p \leq 0.01$) compared to sham as the WT mice (all $p \leq 0.05$) (**Figure 14**).

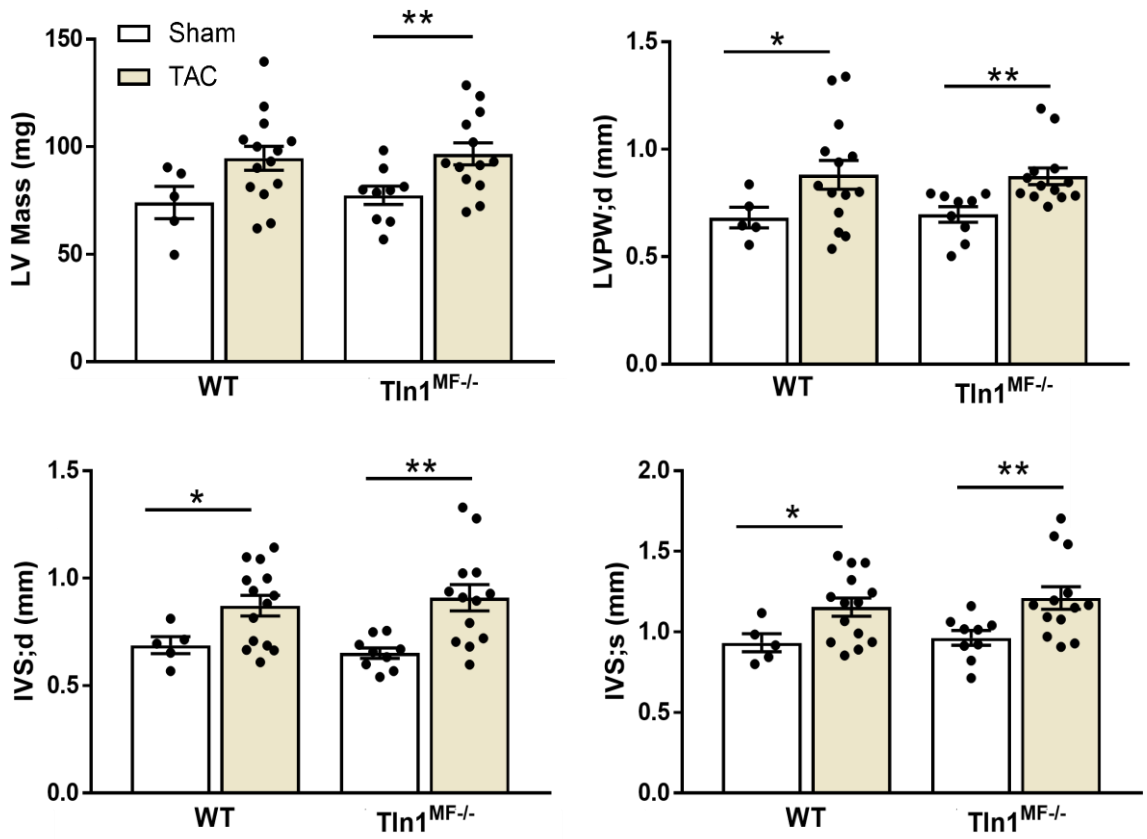

Figure 14: Echocardiographic assessment of LV thickness after TAC injury. Echocardiographic analysis of left ventricular (LV) mass, diastolic LV posterior wall thickness (LVPW;d), diastolic and systolic internal ventricular septum thickness (IVS;d), (IVS;s) 6-weeks post-TAC. Mean±SEM, *P<0.05, **P<0.01 between groups noted with bar. All statistics were done with a two-tailed t-tests with Welch's correction.

Dry lung to body weight ratio was not changed in the TAC mice groups, showing that no congestion occurred (**Figure 15**). This indicates morphological evidence of enhanced hypertrophic response of cardiomyocytes to TAC injury during HFpEF.

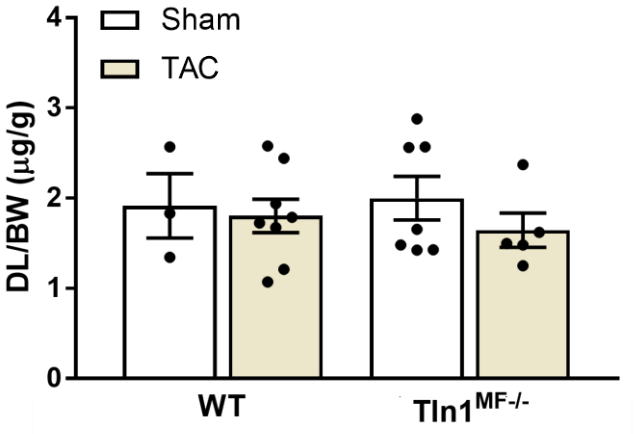

Figure 15: DL/BW ratio in TAC injured mice. Dry lung to body weight (DL/BW) ratio of mice 6-weeks post-TAC. Mean±SEM, *P<0.05 between groups noted with bar. All statistics were done with a two-tailed t-tests with Welch's correction.

4.3.3 Myofibroblast deletion of Tln1 results in no change in cardiac fibrosis burden following TAC with HFpEF

Interstitial fibrosis and fibroblast activation was measured using picrosirius red staining and mRNA expression of α-SMA respectively to determine the effects of myofibroblast Tln1. Image quantification of PSR staining showed that WT and $Tln1^{MF-/-}$ mice did not have an increase in interstitial fibrosis as compared to sham animals 6 weeks post-TAC (**Figure 16a**). Additionally, α-SMA was not increased in the WT or $Tln1^{MF-/-}$ TAC mice (**Figure 16b**).

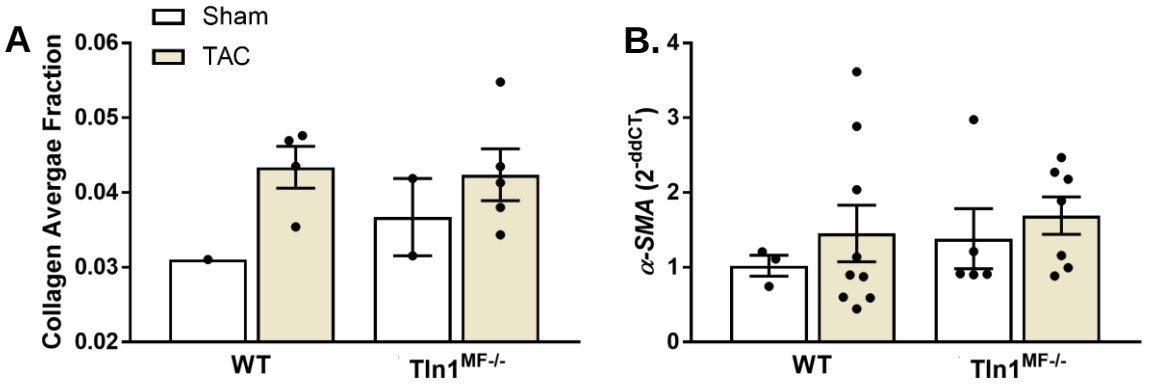

Figure 16: Measurement of interstitial fibrosis in TAC injured mice. A. Quantification of picrosirius red (PSR) staining of hearts. Collagen (red pixels) and heart tissue (yellow) was used to calculate the average collagen fraction in each heart 6-weeks post-TAC **B.** Quantitative polymerase chain reaction analysis of α-SMA, the gene encoding the myofibroblast marker alpha-smooth muscle actin. Mean±SEM, *P<0.05 between groups noted with bar. All statistics were done with a two-tailed t-tests with Welch's correction.

4.3.4 siRNA knockdown of Tln1 in myofibroblasts alters cellular proliferation, migration, and contraction

To try and determine the characteristical changes that are occurring in myofibroblasts with loss of Tln1, we used siRNA to knockdown Tln1 expression *in vitro* in myofibroblasts. siRNA knockdown of Tln1 (**Tln1 KD**) resulted in an average reduction of 75% in Tln1 at 24h, an 88% reduction at 48h, an 80% reduction at 72h, and a 79% reduction at 96h compared to siRNA scramble (**Scr**) controls at the same timepoint (**Figure 17**).

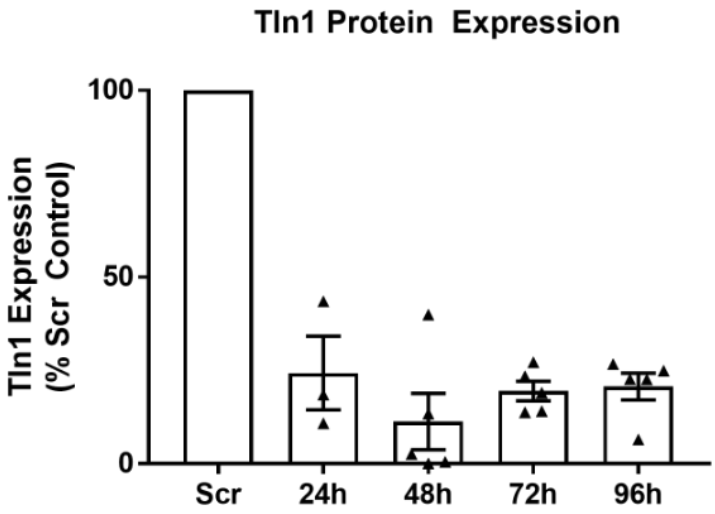

Figure 17: siRNA knockdown of *Tln1* in CFs. Percent knockdown of Tln1 in cardiac fibroblasts using siRNA at 24–96-hour timepoints. Data shown as a percent reduction of Tln1 as compared to Scramble (Scr) control at each timepoint.

WT and Tln1 KD cell were exposed to 10% strain for 24 hours. Tln1 KD cell had increased mRNA expression of fibronectin (***Fn1***) ($p \leq 0.05$) and *α-SMA* ($p \leq 0.001$) (**Figure 18**).

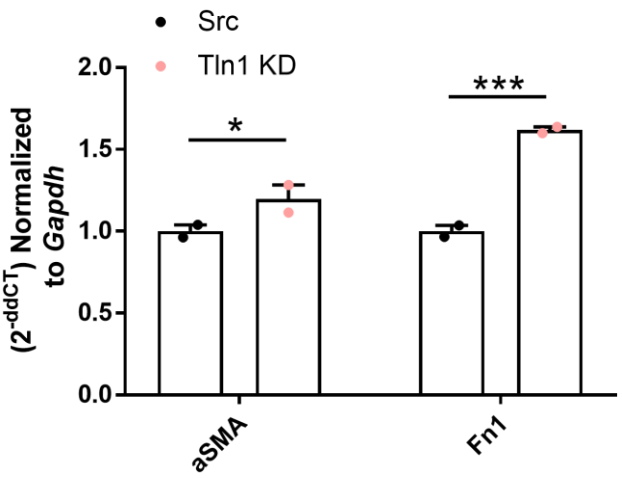

Figure 18: qPCR of *α-SMA* and *Fn1* in Tln1 KD and Scr cells aft 10% strain. Quantitative polymerase chain reaction analysis of *αSMA*, the gene encoding alpha-smooth muscle actin, at 6-weeks post-TAC. Mean±SEM, *P<0.05, ***P<0.001 between groups noted with bar. All statistics were done with a two-tailed t-tests with Welch's correction.

We next characterized proliferation, migration, and contraction in the Tln1 KD myofibroblasts. Proliferation, as measured by MTT assay, was decreased in the Tln1 KD cells at 48h ($p \leq 0.001$) and 72h post-KD ($p \leq 0.001$) as compared to Scr controls (**Figure 19a**). This was confirmed via immunofluorescence where Tln1 KD cells plated at the same concentration failed to proliferate to the same extent as Scr myofibroblasts after 56 hours (**Figure 19b**). Interestingly, the Tln1 KD cells also appeared to have less expression of α-SMA as compared to Scr myofibroblasts.

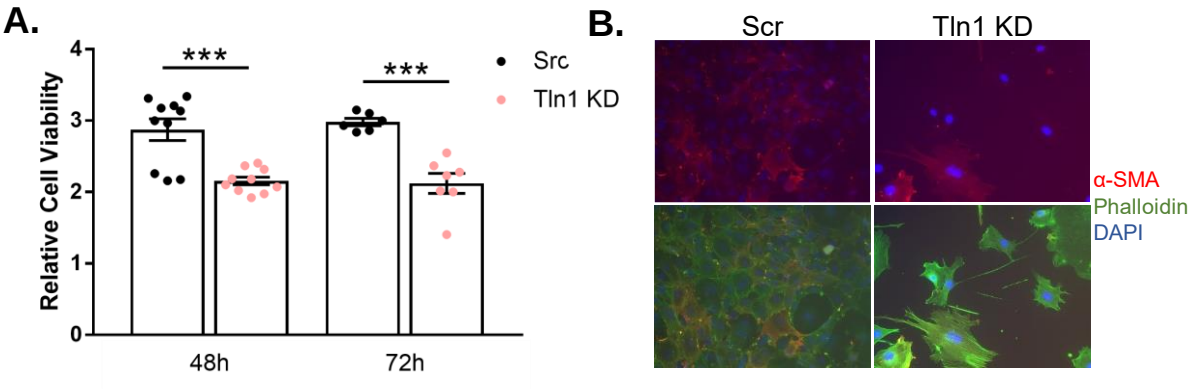

Figure 19: Cell proliferation measurement in Tln1 KD and Scr CFs. A. MTT Assay measuring proliferation of siRNA knockdown of Tln1 in CFs (Tln1 KD) and siRNA scramble (Scr) controls at 48h and 72h after siRNA was introduced. **B.** Immunofluorescence of Tln1 KD and Scr CFs 48h aft siRNA was introduced, and 56 hours after being plated on fibronectin-coated coverslips. Mean±SEM, ***P<0.001 between groups noted with bar. All statistics were done with a two-tailed t-tests with Welch's correction.

Migration, measured by the scratch wound assay, decreased in the Tln1 KD myofibroblasts ($p \leq 0.01$) by 66h after KD **(Figure 20a**). Finally, we measured cell contraction using a collagen gel assay. Contractility was reduced in Tln1 KD cells compared to Scr cells ($p \leq 0.0001$) at 96h (**Figure 20b**).

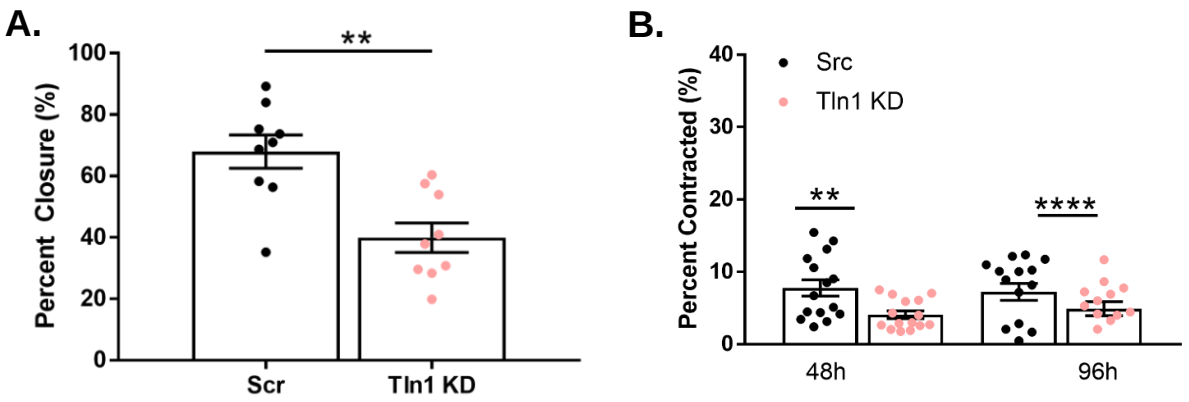

Figure 20: Scratch wound and gel contraction assays of Tln1 KD and Scr CFs. Scratch Wound and Contraction Assays of cardiac fibroblasts (CFs) cells with siRNA knockdown of Tln1 (Tln1 KD) or siRNA scramble (Scr). siRNA was added to CFs at 0h. **A.** CFs were plated at 24h after siRNA was added, and scratch wound was created at 48h. Percent closure was measured at 66h post-siRNA. **B.** CFs were plated inside collagen gels at 24h post-siRNA, and percent contraction was measured at 48-96h after siRNA was added to CFs. Mean±SEM, **P<0.01, ****P<0.001 between groups noted with bar. All statistics were done with a two-tailed t-tests with Welch's correction.

4.4 Discussion

The purpose of the present study was to evaluate the functional significance of Tln1 in myofibroblasts during pressure overload injury of the heart. This was accomplished by developing a novel transgenic mouse where Tln1 was deleted from myofibroblasts using the *Postn* Cre system. $Tln1^{-/-}$ myofibroblasts were further characterized through siRNA knockdown *in vitro*. The results suggest that mechanotransdution in myofibroblasts through Tln1 may be an important mediator of cardiomyocyte hypertrophy during pressure overload injury of the heart that results in HFpEF.

WT and $Tln1^{MF-/-}$ mice underwent TAC for 6 weeks to evaluate the hemodynamic and fibrotic response to prolonged pressure overload of the heart. We observed 17.64% of WT and 31.58% of $Tln1^{MF-/-}$ mice developed EF < 40%, indicating the development of HFrEF. This is surprising as TAC was developed as a method to study pressure overload-induced HF leading to HFrEF.[174] There are a couple potential reasons there was not a larger development of mice with HFrEF in this study. We may not have waited long enough post-TAC to allow more mice to progress from HFpEF to HFrEF. A second explanation is that the TAC procedure is technically demanding, highly operator dependent, and is variable depending on mouse weight, age, and genetic background. While we tried to control many variables including weight, gender, and age of the mice, there may have been too much inter-animal variability. However, the amount of variability that is inherent in the TAC procedure, even with the same operator performing all the TAC surgeries, could have resulted in a less-intensive pressure overload of the heart, resulting in the majority of WT and $Tln1^{MF-/-}$ mice having HFpEF at 6 weeks post-TAC. Using our TAC as a model of HFrEF could be done with larger a sample size, but there are many logistical and ethical barriers to such large-scale studies when there are other models of HFrEF that are currently used in mice to study HFrEF disease.

WT and Tln1$^{MF-/-}$ mice that developed HFpEF did not develop more interstitial fibrosis as compared to sham animals (**Figure 16**). Due to the *Rosa26*-TdTomato reporter activating in the Tln1$^{MF-/-}$ mice after TAC (**Figure 6**), we know there are myofibroblasts present during injury. Therefore, the TAC injury at this timepoint most likely did not produce enough pressure overload in the heart to cause a large interstitial fibrotic response. To better understand the contribution of Tln1 in myofibroblasts during HFpEF to interstitial fibrosis, Tln1$^{MF-/-}$ mice should be subjected to either a more severe TAC injury, or another injury model, such as AngII infusion, that more reliably results in the development of interstitial fibrosis.[135]

Due to the WT and Tln1$^{MF-/-}$ TAC HFpEF mice not having a difference in interstitial fibrosis, our findings suggest that an increase in ventricular wall stiffness in not the primary factor driving a larger cardiomyocyte hypertrophy in the Tln1$^{MF-/-}$ mice post-TAC. However, increased mRNA expression of *Nppa* in the Tln1$^{MF-/-}$ mice post-TAC indicates that there is a greater myocardial injury in mice with myofibroblast loss of Tln1. Therefore, this change in cardiomyocyte hypertrophy could be attributed to compensation for a change in myofibroblast function due to loss of Tln1.

Past studies have shown that talins can partially compensate for each other when one is removed. This was demonstrated in skeletal muscle tissue, where knockdown of Tln2 in muscle *in vivo* resulted in successful assembly of integrin complexes at costameres and MTJs.[123] However, with aging, defects in the MTJs occurred. Likewise, when Tln1 was knocked down in muscle *in vivo* the same results were seen, with MTJ defects occurring over time.[124] This shows that while talins can partially offset each other, they cannot completely compensate. Additionally, talins ability to compensate for each other may be tissue specific and dependent on if one talin form is dominantly expressed. In the heart, myofibroblasts, which equally express Tln1 and Tln2, are tasked with responding to the initial response to injury.[128] To do this, they must migrate to the cite of injury, proliferate, and then lay down ECM.[45,46] Our studies show that loss of Tln1 in myofibroblasts, through siRNA knockdown, results in myofibroblasts with decreased migration,

proliferation, and contraction, indicating that Tln2 cannot completely compensate for loss of Tln1 (**Figure 19** and **Figure 20**). This would lead us to hypothesize that myofibroblasts without Tln1 would not be able to respond to injury as quickly in the heart and create and compact interstitial fibrosis at the site of injury.

When TAC was imposed on the WT and $Tln1^{MF-/-}$ mice we did not observe an increase in interstitial fibrosis in the WT mice in our HFpEF cohort. This could be due to TAC inducing pressure overload of the entire heart, and not an acute injury. Therefore, even if loss of Tln1 in myofibroblasts reduces their ability to migrate and contract, it is not translated into a response post-TAC, suggesting that migration and proliferation to the site of injury are not vital requirements for myofibroblasts when responding to TAC injury. Because *Nppa* is increased in the $Tln1^{MF-/-}$ mice post-TAC, we know that there is increased myocardial injury. Therefore, there could be some signaling changes between the myofibroblasts and the cardiomyocytes, resulting in cardiomyocyte hypertrophy as a response to the increased pressure in the heart. To better test the loss of Tln1 in myofibroblasts, a more acute injury should be used, like myocardial infarction, or a model that results in a large increase in interstitial fibrosis post-injury.

In conclusion, this study demonstrates that deletion of Tln1 in myofibroblasts results in cells that have reduced ability to migrate, proliferate, and contract. In a mouse model of TAC with HFpEF, the loss of myofibroblast Tln1 enhances cardiac hypertrophy following TAC. Moving forward, we aim to find a model of hypertension that is more reproducible so that we can better draw conclusions across genetic mouse models and mouse genders. Additionally, due the potential effect of tamoxifen on the heart, we aim to perform a specific knockdown of Tln1 in CFs so that tamoxifen can be given prior to injury to induce the Cre and not throughout the injury.[229] In addition, we want to look at the development of pressure overload induced hypertension in a Tln2-null mouse and the Tln2-null mouse with a Tln1 knockout in cardiac fibroblasts to better understand the contribution of both talins in cardiac fibroblasts during cardiac injury.

Chapter 5

Creating and Validating Models of Heart Failure Injury and Creation of the Tln2-Null; Cardiac Fibroblast-Specific Tln1 Knockout Mouse

5.1 Introduction

Hypertension is one of the main underlying conditions that leads to HFpEF in humans, and deterioration into HFrEF.[4,23,24] Hypertension injury is exacerbated when pressure in the LV increases, resulting in the proliferation of fibroblasts, hypertrophy of vascular smooth muscle cells, and pathological deposition of interstitial collagen. This leads to increased myocardial wall stress which causes LV hypertrophy to compensate for the increased pressure.[28] Pharmacological models of hypertension focus on chronic adrenergic stimulation and chronic vasoconstriction. This is accomplished though administration of isoproterenol (**ISO**), phenylephrine (**PE**), and/or angiotensin II (**AngII**).[217] ISO is a nonselective β-adrenergic agonist that can lead to cardiac hypertrophy, reduced EF, ventricular dysfunction, and cardiomyocyte apoptosis.[194] PE is a α-adrenergic agonist that causes vasoconstriction, resulting in decreased EF, myocardial hypertrophy, systolic dysfunction, and increased *Nppa* expression.[199] AngII, another potent vasoconstrictive hormone, induces hypertension, TGF-β and aldosterone secretion resulting in the development of cardiac hypertrophy.[200] Additionally, it has been shown that mice on different generic backgrounds have an interstitial fibrotic response when injured with AngII.[230]

Cardiomyocyte hypertrophy and interstitial fibrosis are the two principle components of myocardial remodeling in response to pressure overload of the heart.[48,214] During pressure

overload of the heart, CFs in the ventricular walls undergo a phenotypic shift to activated myofibroblasts. Myofibroblasts secrete and compact ECM components leading to interstitial fibrosis.

In vitro studies that removed Tln1 and Tln2 in fibroblasts resulted in cells that balled up and did not form new focal adhesion protrusions.[231] Furthermore, in a study of myocardial infarction (MI), myofibroblasts were removed from the heart using the *Postn*-Cre that expressed diphtheria toxin. This resulted in the death of 80% of mice by 4 days post-MI.[40] This study illustrates that myofibroblasts mediate the cardiac fibrotic response to an acute injury, and are necessary for preserving heart function.

Many different markers have been used to identify myofibroblasts in the heart including *α-SMA*, *Postn*, and *Col1a1*.[40] However, none of these markers universally mark all myofibroblast-like cells in the heart. Postn is the most common driver used for Cre genetic models when trying to knockdown myofibroblast protein expression. However, *Postn* is only expressed in myofibroblasts and not in inactivated CFs. Recent genetic lineage tracing has identified Tcf21 as the best universal marker of all CFs. *Tcf21* is found in almost all CFs and this expression persists during myofibroblasts activation.[40] For this reason, we used *Tcf21* as the driver for our Cre to remove Tln1 from CFs and myofibroblasts in the context of cardiac injury. To better understand the specific contribution of talins in the heart, we created a novel mouse model that has a germline deletion of the *Tln2* gene and has a tamoxifen-inducible, *Tcf21* Cre-driven deletion of *Tln1* gene specifically in CFs. $Tln2^{-/-}$ mice have normal cardiac structure and function up to 12 months of age.[127] Therefore, $Tln2^{-/-}$ mice were used as our control.

Here, we describe the creation and validation of mouse models of ISO, PE & AngII, and AngII alone to develop a working reproducible model of hypertension that allows for the quantification of cardiac hypertrophy and interstitial fibrosis. We then describe the creation of a

novel *Tln2* null mouse with a CF-specific deletion of *Tln1* and the cardiac phenotypes that occur during MI and AngII injuries. We hypothesis that with removal of Tln1 and Tln2 from cardiac fibroblasts, we will render a myofibroblast cell that cannot respond MI injury.

5.2 Methods

Mice

All animal protocols were approved by the Institutional Animal Care and Use Committee at Vanderbilt University. Tln1 myofibroblast-specific knockout mice were created by crossing the $Tln1^{flox/flox}$ mice, provided by Dr. Roy Zent (Vanderbilt University Medical Center), with the *Postn*-Cre mice, provided by Dr. Jeffery Molkentin (Cincinnati Children's Hospital) [40]. All mice were crossed with the *Rosa26*-stop-tdTomato reporter mice (Jackson Laboratory, Stock No. 007914) to visually verify Cre activation (**Figure 6**).[227]

Tln2 null, Tln1 CF-specific knockout mice were created by crossing the $Tln2^{-/-}$;$Tln1^{flox/flox}$ mice, provided by Dr. Roy Zent (Vanderbilt University Medical Center)[111,123,232], with the *Tcf21*-Cre mice, provided by Dr. Michelle Tallquist (University of Hawaii) [233]. All mice were crossed with the *Rosa26*-stop-tdTomato reporter mice (Jackson Laboratory, Stock No. 007914) to visually verify Cre activation (**Figure 29**).[227] The sequences for the primers used are listed in **Table 5**.

Gene	Primer Name	Primer Sequence
Talin1	Primer A	AAGCAGGAACAAAAGTAGGTCTCC
	Primer B	GCATCGTCTTCACCACATTCC
Talin2	Primer A	CAAACTGAATGAAGGCCCAACAG
	Primer B	TCTCCACTTACTCCTTGCCC
	Primer C	GCCGAGGCTACATGGAGTCAGTAT
Tcf21 Cre	Primer A	CAAACCCTAGCACAAATCACTCGC
	Primer B	GCTTCCGATATCCAGATCCAGAC
	Primer C	TTCTCCAGGCTCAAGACCAC
TdTomato	WT Primer A	AAGGGAGCTGCAGTGGAGTA
	WT Primer B	CCGAAAATCTGTGGGAAG TC
	Homozygous Primer A	GGCATTAAAGCAGCGTATCC
	Homozygous Primer B	CTGTTCCTGTACGGCATGG
Postn Cre	Postn Primer A	TCTGTAAGGCCATCGCAAGCT
	Mutant Primater A	GGTGGGACATTTGAGTTGCT
	Primer B	AATAAGTAAAACAGCTCCCCT

Table 5: Primers used for genotyping mice.

Animal Studies - Isoproterenol

All mice were started on tamoxifen chow at 10 weeks of age to activate the *Postn*-Cre. Chronic hypertension was imposed via isoproterenol (**ISO**) injection through intraperitoneal injection on 12-week-old mice at a concentration of 180mg/kg/day for 1 week (**Figure 21**). Control mice were given saline injections.

Animal Studies - Angiotensin II and Phenylephrine

All mice were started on tamoxifen chow at 11 weeks of age to activate the *Postn*-Cre. Chronic hypertension was imposed via angiotensin II (**AngII**) at 1.5mg/kg/day and phenylephrine (PE) at 50mg/kg/day infusion through mini osmotic pumps (Alzet Corp, 1004) on 12-week-old mice at a concentration of 180mg/kg/day for 4 weeks (**Figure 23**). Control mice were given saline pumps.

Animal Studies - Myocardial Infarction

MI was induced in 12-week-old mice by permanent coronary artery ligation, as previously described [234–236]. Briefly, mice were anesthetized with 2% isoflurane inhalation. A small incision was made over the left chest and dissection and retraction of the pectoral major and minor muscles was performed. A small hole was punctured in the fourth intercostal space and gently held open with a mosquito clamp. Using gentle pressure superior and inferior to the heart, the heart was popped out of the chest. A 6-0 silk suture was used to ligate the left main descending coronary artery approximately 3 mm from its origin. The heart was immediately placed back into the chest cavity, air was manually evacuated, the muscle was replaced, and the skin sutured. Mice were then taken out to 3-weeeks before dissections (**Figure 28**).

Animal Studies - Angiotensin II

All mice were given tamoxifen injections (2 mg in PBS-/-)/day for 5 days at 9 weeks of age to activate the Tcf21-Cre. Chronic hypertension was imposed via AngII infusion (1.5mg/kg/day) through mini osmotic pumps (Alzet Corp, 1004) on 12-week-old male and female mice at a concentration of 1.5mg/kg/day (**Figure 31**). Control mice were given saline pumps.

Euthanasia

Mice were either euthanized with CO_2 exposure or via exsanguination followed by removal of the heart under isoflurane INH continuous at 1-5% in accordance with Vanderbilt University Medical Center's Division of Animal Care Guidelines. Littermates were used and treatment groups were distributed throughout cages and litters.

Echocardiography

Blinded echocardiographic measurements were taken from short-axis cardiac M-mode images captured at mid-papillary level of non-anesthetized mice on a Vevo2100 small-animal ultrasound system (VisualSonics). Three independent measurements were analyzed per mouse for each timepoint.

Systolic blood pressure

Systolic blood pressure was measured using a noninvasive tail-cuff platform (Hatteras Instruments). Two rounds of 10 measurements were taken for each mouse and averaged for each mouse at each timepoint. Four mice were excluded from this study as their systolic blood pressure 8 weeks post AngII infusion did not indicate hypertension injury, and one control mouse was excluded for having a systolic blood pressure higher than all AngII mice, indicating vascular defect.

Quantitative Polymerase Chain Reaction

Quantitative PCR (qPCR) was performed on flash frozen LV tissue dissected from experimental mice. The sequences for the primers used are listed in **Table 4**. Gene expression was compared to the housekeeping gene *Gapdh*.

Histology

Upon euthanasia, hearts were perfused with PBS-/-, excised, and submerged in 3M potassium chloride to arrest hearts in diastole. Hearts were bisected along the transverse plane of the heart. Tissue was frozen and cryosectioned at 7 µm thickness. Picrosirius red staining (**PSR**) (Fisher Scientific #50-300-77) was used to identify ECM (red) and cytoplasm (yellow).

Images were analyzed using a semiautomated image-processing pipeline that was developed based on color segmentation.[227]

Statistical Analysis

Data was compiled and shown as the means ± SEM. Data was evaluated using unpaired, two-tailed t-tests with Welch's correction (95% confidence interval) using GraphPad Prism software (GraphPad Inc., San Diego, CA). A p value < 0.05 was considered significant.

5.3 Validation of heart failure mouse models

5.3.1 Isoproterenol injections

First, we validated a model of ISO injury to find a reliable reproducible model that produced cardiac hypertrophy and interstitial fibrosis. ISO or saline was administered to WT mice through intraperitoneal injection, and cardiac function and ventricular weight were measured at 4-weeks post-injury to determine injury and induction of hypertension (**Figure 21**).

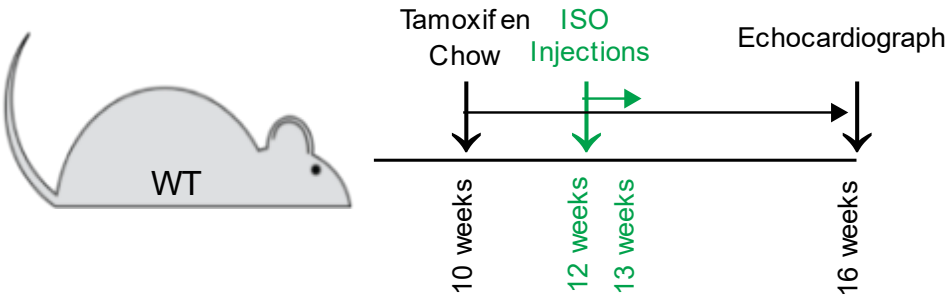

Figure 21: Experimental approach for ISO injection injury. Ten-week-old WT mice were given tamoxifen chow 2 weeks prior to injury and kept on tamoxifen chow throughout the experiment. At twelve weeks, isoproterenol (ISO) or control (saline) was injected into mice one daily for a week. Treatment was ceased four weeks after initial injury, and echocardiography was performed.

Echocardiography analysis at 4-weeks post-injury showed that there was no change in EF (**Figure 22a**). Measurements of ventricular weight / body weight illustrated that there was no change in ventricular mass in the ISO mice compared to saline controls (**Figure 22b**). These measurements indicate that our treatment of mice with ISO was not successful in inducing HFrEF and cardiac hypertrophy.

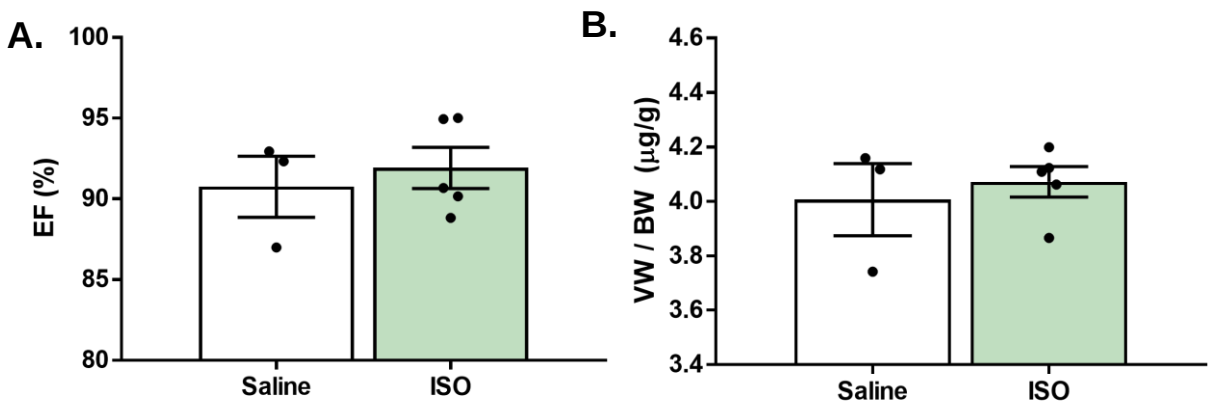

Figure 22: EF and ventricular weight of ISO injured mice. A. Echocardiographic analysis of ejection fraction (EF) 4 weeks post-isoproterenol (ISO) or saline pumps, **B.** Ventricles to body weight ratio (VW/BW) at 4 weeks post-ISO or saline pumps. Mean±SEM, *P<0.05 between groups noted with bar. All statistics were done with a two-tailed t-tests with Welch's correction.

5.3.2 Angiotensin II & Phenylephrine osmotic pumps

Next, we tried a more aggressive pharmacological treatment of mice with PE, a nonselective β-adrenergic agonist, and AngII, a vasoconstirive hormone, to try and induce HFrEF. WT mice were subjected to either AngII & PE or saline through osmotic pumps for 4-weeks, and echocardiography, ventricular weights, and interstitial fibrosis were measured to determine the degree of injury (**Figure 23**).

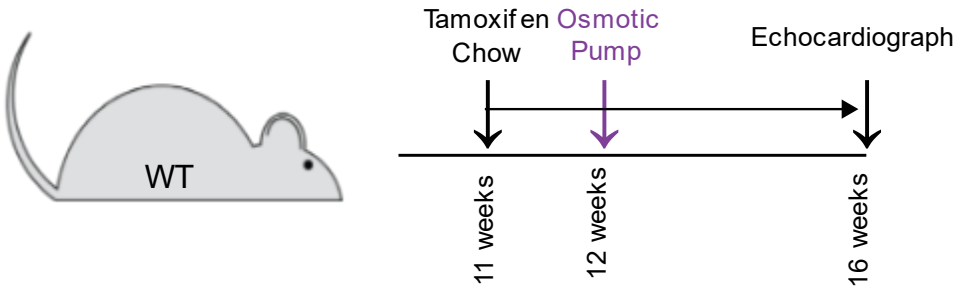

Figure 23: Experimental approach of AngII & PE injury. Eleven-week-old male WT mice were given tamoxifen chow 1 week prior to injury and kept on tamoxifen chow throughout the experiment. At twelve weeks, pumps were surgically implanted in mice with angiotensin II (AngII) and phenylephrine (PE), or control (saline). Treatment was ceased four weeks after initial injury, and echocardiography was performed.

After 4-weeks, echocardiography was performed to assess cardiac function. EF was not changed between the saline and the AngII & PE groups (**Figure 24**).

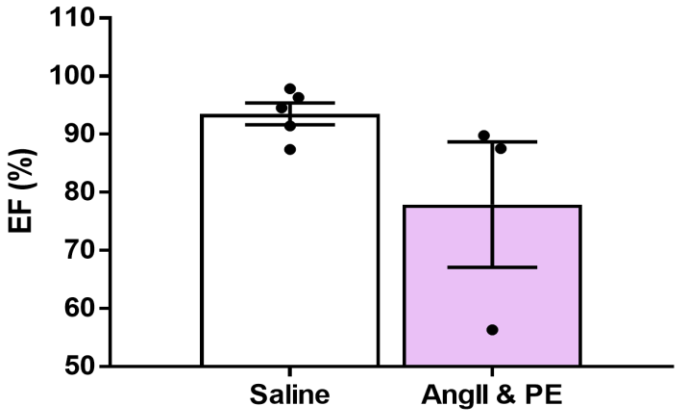

Figure 24: EF of AngII & PE injured mice. Echocardiographic analysis of ejection fraction (EF) four weeks after pumps implant of angiotensin II (AngII) and phenylephrine (PE) or saline pumps. Mean±SEM, *P<0.05 between groups noted with bar. All statistics were done with a two-tailed t-tests with Welch's correction.

Mouse ventricle / body weight was measured and revealed no difference between the sham and the AngII & PE groups (**Figure 25a**). This was additionally seen though echocardiography at 4-weeks post-injury (**Figure 25b**).

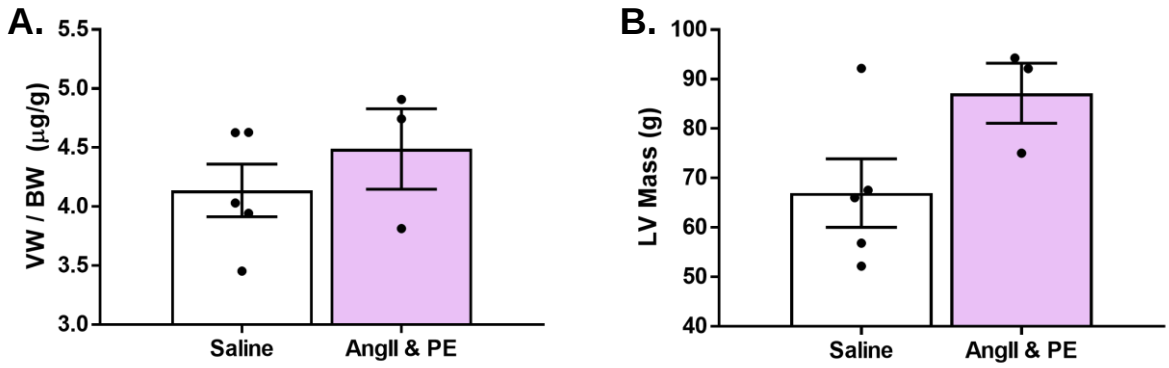

Figure 25: Measurements of ventricle weights in AngII & PE injured mice. A. Ventricle to body weight ratio (VW/BW) 4 weeks post-pump implantation of angiotensin II (AngII) and phenylephrine (PE) or saline, **B.** Echocardiographic analysis of left ventricle (LV) mass 4 weeks post-pump implants. Mean±SEM, *P<0.05 between groups noted with bar. All statistics were done with a two-tailed t-tests with Welch's correction.

Interstitial fibrosis was measured for saline and AngII & PE treated hearts. Quantification of fibrosis showed that there was a significant increase in interstitial fibrosis in the AnII & PE mice ($p \leq 0.001$) as compared to saline mice (**Figure 26**). This indicates that while our treatment of mice with AngII & PE was successful in inducing interstitial fibrosis, it did not cause cardiomyocyte hypertrophy or a reduction in EF at 4-weeks post injury.

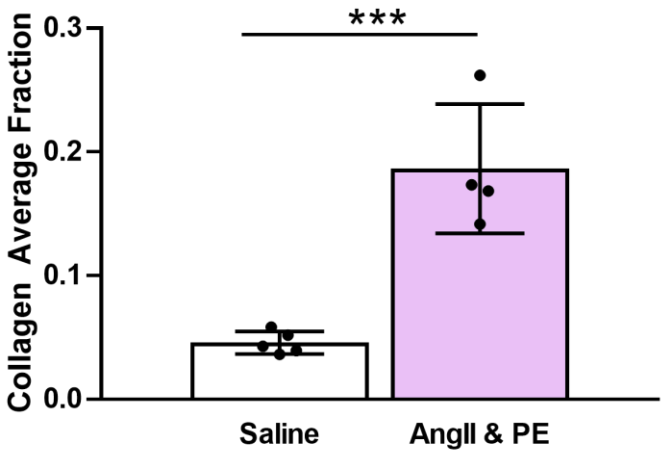

Figure 26: Measurement of interstitial fibrosis in AngII & PE injured mice. Quantification of picrosirius red (PSR) staining of hearts four weeks after pump implantation. Collagen (red pixels) and heart tissue (yellow) was used to calculate the average collagen fraction in each heart. Mean±SEM, ***P<0.005 between groups noted with bar. All statistics were done with a two-tailed t-tests with Welch's correction.

5.4 Creation and validation of a Tln2 null, CF-specific deletion of Tln1

The COVID19 pandemic severely reduced the amount of animal work that could be performed which limited the amount of injury validation performed in WT mice. However, during

the time of reduced lab activity we successfully developed the Tln2-null, CF specific knockout out of Tln1 (**Tln2$^{-/-}$;Tln1$^{CF-/-}$**) mice. When the pandemic was better controlled, we resumed testing models of HF in the Tln2$^{-/-}$;Tln1$^{CF-/-}$ mice, with **Tln2$^{-/-}$** as our controls.

Echocardiography, body weight, and systolic blood pressure at 12 weeks of age, after 5 days of tamoxifen injections, showed no difference between the Tln2$^{-/-}$ and Tln2$^{-/-}$;Tln1$^{CF-/-}$ mice (**Figure 27**), indicating that under basal conditions, Tln1 deletion from CFs doesn't result in overall morphometric or functional changes in the heart.

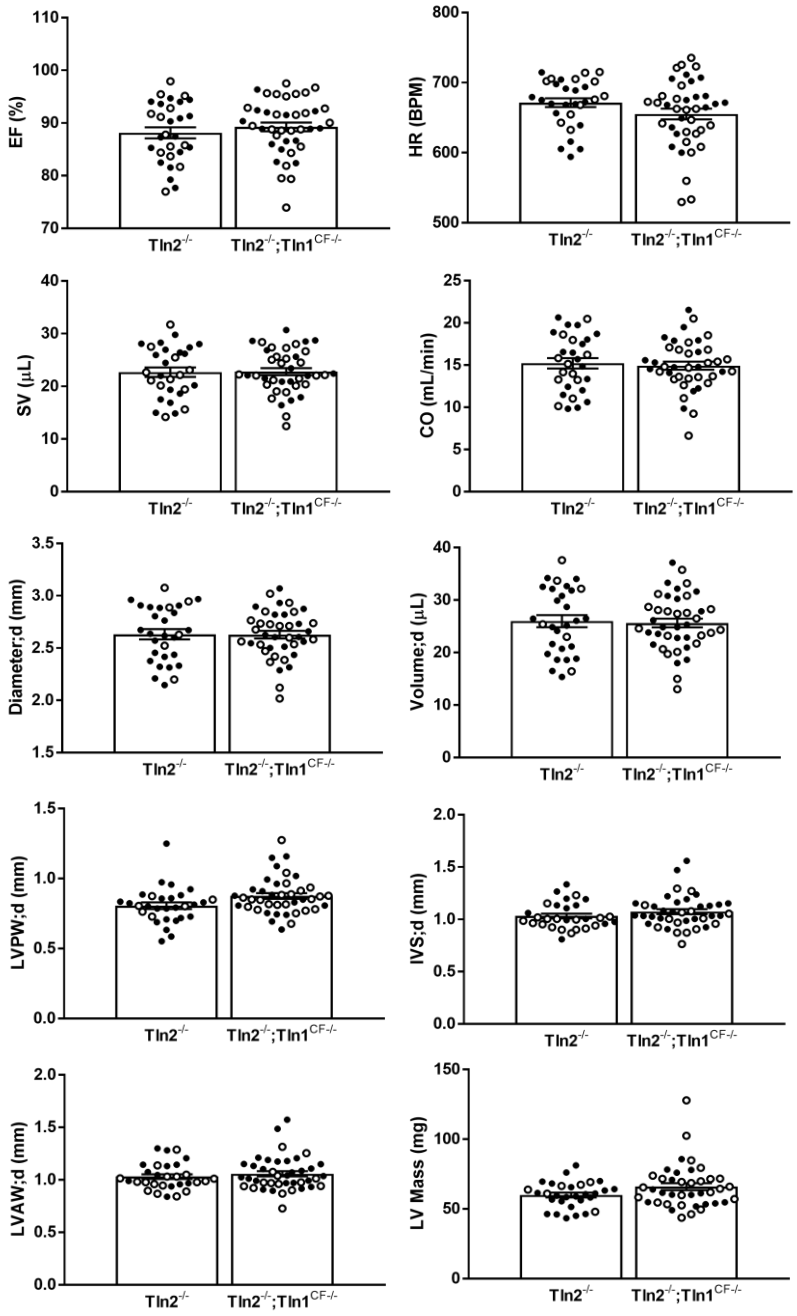

Figure 27: Echocardiographic analysis of Tln2$^{-/-}$; Tln1$^{CF-/-}$ and Tln2$^{-/-}$ mice at 12 weeks of age. Echocardiographic analysis of ejection fraction (EF), heart rate (HR), stroke volume (SV), cardiac output (CO) to assess cardiac function in mice at 12 weeks of age. Echocardiographic analysis of LV internal volume diameter during diastole (Diamere;d), LV chamber volume during diastole (Volume;d), LV posterior wall thickness during diastole (LVPW;d), interventricular septal thickness during diastole (IVS;d), and LV anterior wall thickness during diastole (LVAW; d) to assess cardiac hypertrophy in mice at 12 weeks of age. Filled black circles denote female mince, and white filled circles denote male mice. Mean±SEM, *P<0.05 between groups noted with bar. All statistics were done with a two-tailed t-tests with Welch's correction.

5.4.1 Mice with a global deletion of Tln2 and CF-specific deletion of Tln1 does not affect the ability of mice to survive myocardial infarction injury.

Next, we wanted to assess if CFs and myofibroblasts were still functional in the heart when Tln2 and Tln1 were removed from CFs. We performed MI on male and female $Tln2^{-/-}$ and $Tln2^{-/-}$;$Tln1^{CF-/-}$ mice for 3-weeks to assess the ability of Tln1 and Tln2 null CFs to respond to acute injury (**Figure 28**).

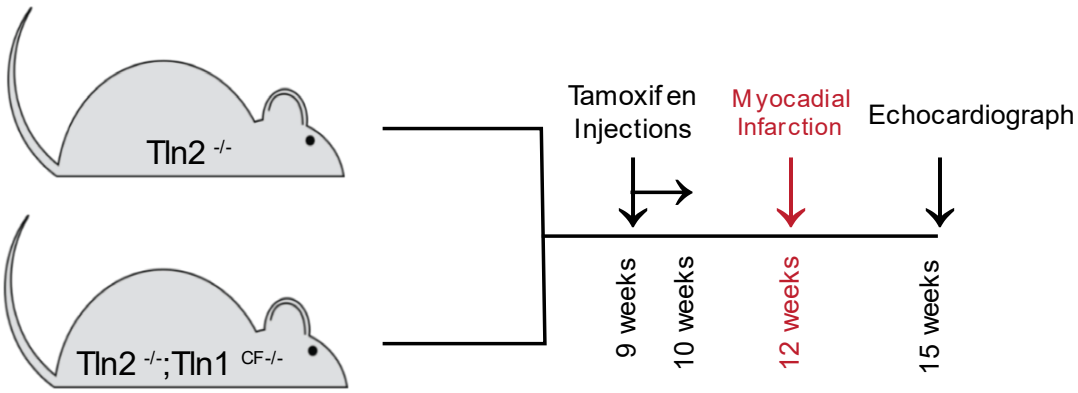

Figure 28: Experimental approach for MI injury. Nine-week-old mice were subjected to 5 consecutive days of tamoxifen injections. At twelve weeks, myocardial infarction (MI) or sham surgery was performed. Treatment was ceased three weeks after initial injury, and echocardiography was performed.

Rosa26-TdTomato expression was checked to ensure activation of the Tcf21-Cre (**Figure 29**).

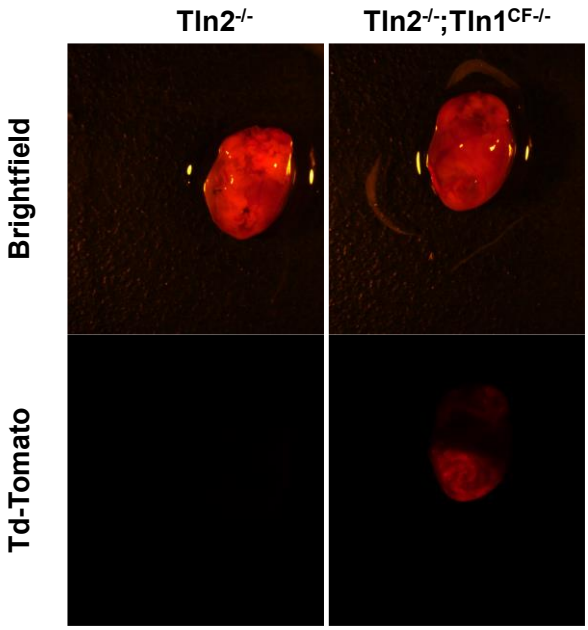

Figure 29: *Tcf21*-Cre expression in mice after MI injury. Representative pictures of hearts 3 weeks post-MI taken under brightfield and a Td-Tomato filter. *Tcf21*-Cre activation was seen only in the $Tln2^{-/-}$;$Tln1^{CF-/-}$ mice as depicted by florescence under the Td-Tomato filter.

There was an initial increase in death in the $Tln2^{-/-}$;$Tln1^{CF-/-}$ mice as they died more rapidly in response to MI injury (50% death at 1 day post-MI compared to 25% in $Tln2^{-/-}$ mice). However, 6-days post-MI, survival curves level out with 40% or more survival in both genotypes out to 21-days post-MI injury (**Figure 30**). This indicates that loss of Tln1 and Tln2 in CFs does not affect the overall survival of mice during MI as compared to mice that just have CF Tln1.

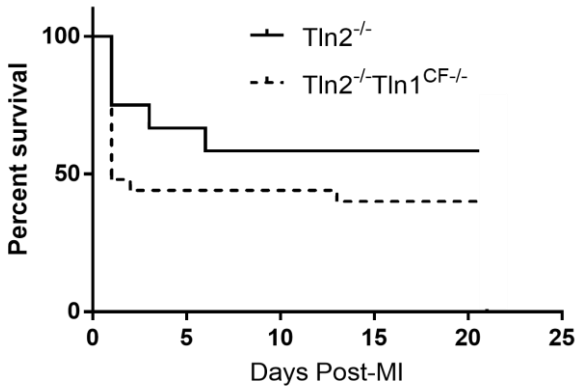

Figure 30: Survival curves pos-MI injury. Survival curves for Tln2$^{-/-}$ and Tln2$^{-/-}$;Tln1$^{CF-/-}$ mice after myocardial infarction (MI) up to 21 days.

5.4.2 AngII-injury in Tln2-null mice results in cardiac hypertrophy

To induce a pressure-overload of the heart in a hypertension model, AngII was given through osmotic pumps for 4-weeks to Tln2$^{-/-}$ and Tln2$^{-/-}$;Tln1$^{CF-/-}$ mice (**Figure 31**).

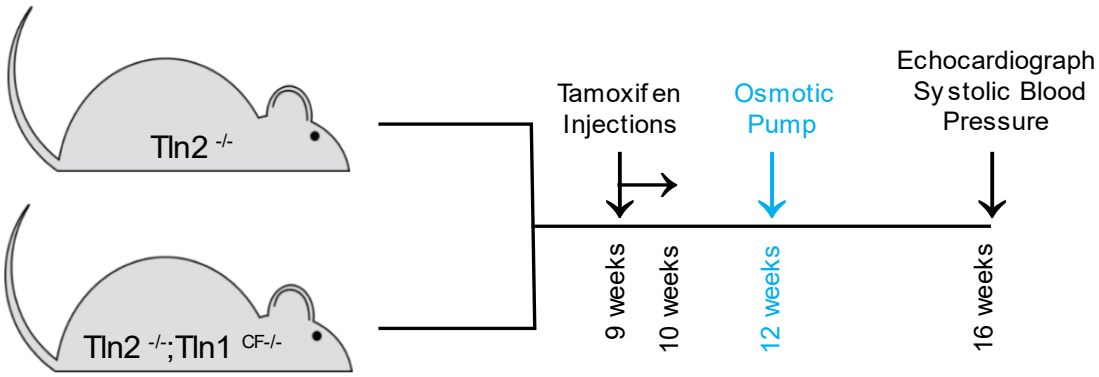

Figure 31: Experimental approach for AngII injury. Nine-week-old mice were subjected to 5 consecutive days of tamoxifen injections. At twelve weeks, pumps were surgically implanted in mice with angiotensin II (AngII), or control (saline). Treatment was ceased four weeks after initial injury, and echocardiography was performed, and systolic blood pressure was performed.

SBP was measured at 4-weeks post-AngII infusion as a marker of increased pressure overload in the heart. At 4-weeks, both $Tln2^{-/-}$ ($p \leq 0.001$) and $Tln2^{-/-}$;$Tln1^{CF-/-}$ ($p \leq 0.01$) mice had an increase in SBP as compared to saline mice (**Figure 32**), with no differences seen between the AngII injured animals.

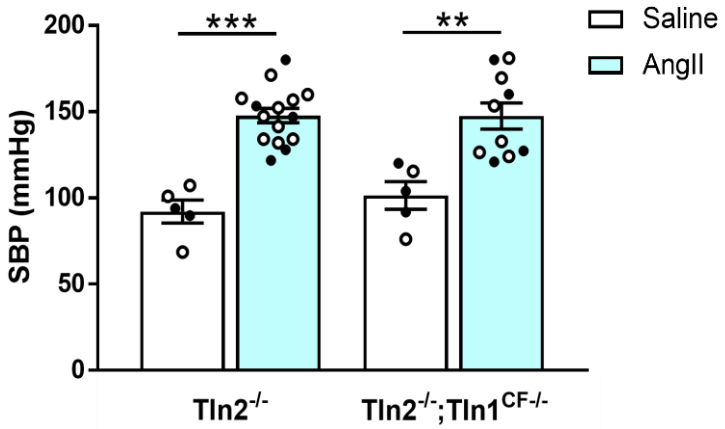

Figure 32: SBP of mice after AngII injury. Systolic blood pressure (SBP) 4-weeks post pump implantation. Mean±SEM, **P<0.01, ***P<0.001 between groups noted with bar. All statistics were done with a two-tailed t-tests with Welch's correction.

Echocardiographic measurements showed no change in EF between $Tln2^{-/-}$ and $Tln2^{-/-}$;$Tln1^{CF-/-}$ and their saline controls (**Figure 33**).

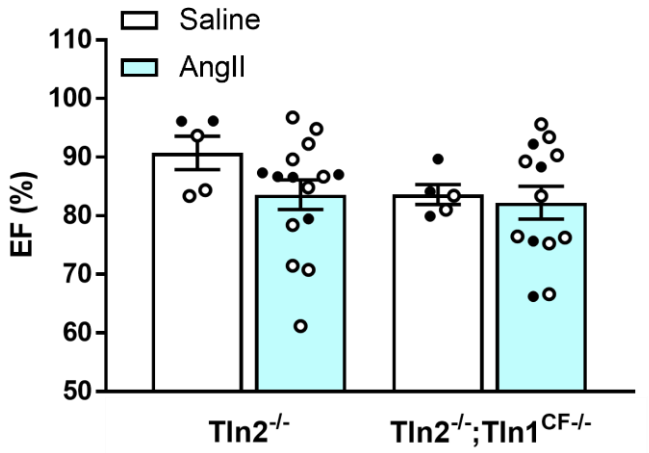

Figure 33: EF in mice after AngII injury. Echocardiographic analysis of ejection fraction (EF) 4-weeks after pump implantation. Mean±SEM, *P<0.05 between groups noted with bar. All statistics were done with a two-tailed t-tests with Welch's correction.

Echocardiographic measurements additionally show a trend towards increasing LV mass in AngII inured mice in both $Tln2^{-/-}$ and $Tln2^{-/-}$;$Tln1^{CF-/-}$ mice. This is also seen in LV/body weight (**LV/BW**) ratios taken during dissections, with the $Tln2^{-/-}$ AngII mice already having an increase LV/BW ratio as compared to their same controls ($p < 0.05$) (**Figure 34**).

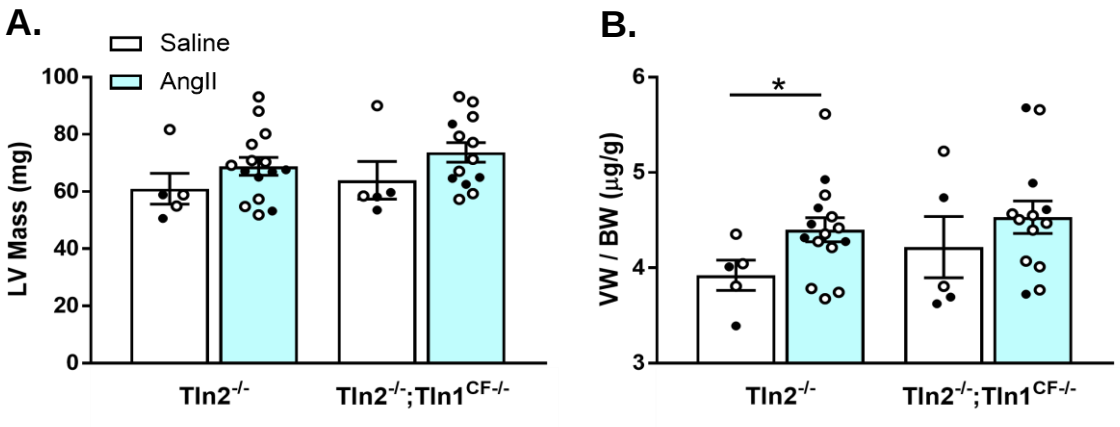

Figure 34: Measurements of ventricle weight after AngII injury. A. Echocardiographic analysis of ejection fraction (EF) at 4-weeks post pump implantation, **B.** Ventricle to body weight (VW/BW) ratio 4 weeks post-pump implantation. Mean±SEM, *P<0.05 between groups noted with bar. All statistics were done with a two-tailed t-tests with Welch's correction.

Interstitial fibrosis was quantified through PSR staining. There were no changes seen between $Tln2^{-/-}$ and $Tln2^{-/-}$;$Tln1^{CF-/-}$ mice at 4-weeks after AngII infusion (**Figure 35**).

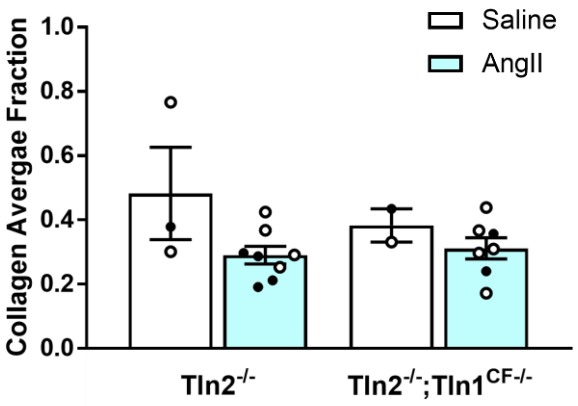

Figure 35: Measurement of interstitial fibrosis after AngII injury. Quantification of picrosirius red (PSR) staining of hearts. Collagen (red pixels) and heart tissue (yellow) was used to calculate the average collagen fraction in each heart 4 weeks after pump implantation. Mean±SEM, *P<0.05between groups noted with bar. All statistics were done with a two-tailed t-tests with Welch's correction.

5.5 Discussion

We successfully created a novel Tln2-null, CF-specific knockdown of Tln1 mouse and tested this mouse in a model of MI to see if fibroblasts lacking both talin isoforms had an altered response to acute injury. We expected there to be significant death in the $Tln2^{-/-}$;$Tln1^{CF-/-}$ mice in the first 2 days post-MI, as we anticipated that removal of both talins would not allow myofibroblasts to migrate to the site of acute injury and lay down the ECM to create the scar needed to survive MI. While there was an increase in death in the $Tln2^{-/-}$;$Tln1^{CF-/-}$ mice initially post-MI compared to the $Tln2^{-/-}$ mice, this death leveled off to approximately the same survival percentage at 3 weeks post-MI. This indicates that the loss of Tln1 in CFs influences the ability of mice to survive acute cardiac injury. However, although there was approximately 50% death in the $Tln2^{-/-}$;$Tln1^{CF-/-}$ mice initially post-MI, this was not close to the death seen when myofibroblasts were removed from the heart with diphtheria toxin during MI,[40] indicating that even with loss of talins in CF prior to MI, myofibroblasts are still able to respond to acute injury. Additionally, because survival rates do not continue to decrease after 2 days in the $Tln2^{-/-}$;$Tln1^{CF-/-}$ mice, this may indicate that talins in CFs do not play a large role after the initial injury response during acute injury to the heart. Due to MI being an acute injury, we next decided to subject $Tln2^{-/-}$ and $Tln2^{-/-}$;$Tln1^{CF-/-}$ mice to a prolonged pressure overload injury to try and tease out the contribution of Tln1 and Tln2 in CFs during the remodeling process (**Chapter 6**).

We also set out to create and validate a model of HF that was reproducible and resulted in cardiac hypertrophy and interstitial fibrosis. We turned to pharmacological agonists of hypertension due to greater reliability and reproducibility when compared to surgical interventions. However, we did not see the expected results when using models of ISO, and PE & AngII injury. An explanation for this could be the overall weight of our mice. The WT mice used to test these models were the same background as our talin mutant mice and were on average smaller than the typical C57BL/6J mouse. Due to this, dosages taken from the literature for C57BL/6J mice

may not have been optimal to induce HF in experimental mice. All experiments were performed in multiple groups using fresh ISO or PE & AngII which should rule out a reagent issue causing a problem.

While a 4-week model of AngII injury did not produce the anticipated effect, we decided to extend this injury model out to 8 weeks since we were seeing an increase in SBP that indicated the development of systemic hypertension. Extending to 8-weeks induced measurable increases in blood pressure, cardiac hypertrophy, and fibrosis (**Chapter 6**). This model was chosen going forward as it also allows for standardized dosing and consistency across different genetic backgrounds.

Chapter 6

Loss of Talin in Cardiac Fibroblasts Results in Augmented Ventricular Cardiomyocyte Hypertrophy in Response to Pressure Overload

Text for Chapter 6 was adapted from **Noll NA**, et al. *Loss of talin in fibroblasts results in augmented ventricular cardiomyocyte hypertrophy in response to pressure overload*. The American Journal of Physiology-Heart and Circulatory Physiology. In review December 2021.

6.1 Abstract

Pressure overload of the heart is characterized by concentric hypertrophy and interstitial fibrosis. Cardiac fibroblasts (**CFs**) in the ventricular wall become activated during injury and synthesize and compact extracellular matrix, which causes interstitial fibrosis and stiffening of the ventricular heart walls. Talin1 (**Tln1**) and Talin2 (**Tln2**) are mechanosensitive proteins that participate in focal adhesion transmission of signals from the extracellular environment to the actin cytoskeleton of CFs. The aim of the present study was to determine whether removal of Tln1 and Tln2 from CFs would reduce interstitial fibrosis and cardiac hypertrophy. Twelve-week-old male and female Tln2 null (**Tln2$^{-/-}$**) and Tln2 null; CF-specific Tln1 knockout (**Tln2$^{-/-}$;Tln1$^{CF-/-}$**) mice were given angiotensin-II (**AngII**) (1.5mg/kg/day) or saline through osmotic pumps for 8 weeks. Cardiomyocyte area and ventricle weight to body weight ratio were increased in the AngII infused Tln2$^{-/-}$;Tln1$^{CF-/-}$ mice. Additionally, the systolic blood pressure was increased to a greater extent in the Tln2$^{-/-}$;Tln1$^{CF-/-}$ mice after AngII infusion compared to the Tln2$^{-/-}$ mice. There was no difference in interstitial fibrosis or markers of fibroblast to myofibroblast transition in the AngII infused mice of either genotype. Collectively, these data indicate that the absence of Tln1 and Tln2 in CFs

results in cardiomyocyte hypertrophy in response to Ang II, without a change in interstitial fibrosis. These findings have important implications for the role of mechanosensitive proteins in CFs, and their impact on cardiomyocyte function in the pathogenesis of hypertension and cardiac hypertrophy.

6.2 Introduction

Adverse myocardial remodeling in response to pressure overload is a leading cause of heart failure.[4,23,24] The two principal components of myocardial remodeling in the context of pressure overload are cardiac hypertrophy and interstitial fibrosis.[48,214] These adaptations cause the heart to initially normalize left ventricle (**LV**) wall stress and maintain cardiac output.[215,216] However, as remodeling continues, interstitial fibrosis causes a stiffening of the heart walls leading to impaired cardiomyocyte contraction and heart failure.

Cardiac fibrosis is a key feature of the remodeling response and is defined by the accumulation of excessive amounts of extracellular matrix (**ECM**) proteins, such as collagen and fibronectin.[45] Fibrotic remodeling is driven by the phenotypic shift of cardiac fibroblasts (**CFs**) in the ventricular wall into activated myofibroblasts. Myofibroblasts secrete and compact ECM components such as collagen types I and III as they become contractile, indicated by their expression of alpha smooth muscle actin (***α-SMA***), allowing for short-term adaptation to tissue injury.[48–51,219,220] These changes result in increasing ECM stiffness during pathological remodeling, which is transmitted to CFs by their focal adhesions. During prolonged pressure overload, increased ECM stiffness results in a positive feedback loop whereby CFs continue to differentiate into myofibroblasts, creating a stiff, non-compliant myocardium. These changes lead to impaired cardiomyocyte contraction, cardiac dysfunction, and heart failure.[11,45,221]

Focal adhesions are protein complexes which link the cytoskeleton of CFs with the ECM via integrin receptors on the cellular membrane and mechanosensitive proteins. Integrins, through activation of their cytoplasmic tails, bind to actin via mechanosensitive proteins, including talin, vinculin, and α-actinin.[86,87,222] As ECM rigidity increases, outside-in signaling through focal adhesions causes stress fibers within CFs to form (expression of actin fibers and α-SMA instead of depolymerized G-actin) as more mechanosensitive proteins are recruited to focal adhesions and these stress fibers allow CFs to contract.[223] This contractility is transmitted to the ECM through inside-out signaling through focal adhesions and allows CFs to compact the ECM leading to more defined and rigid ECM in the heart.[80–82]

.Talins are a family of large, dimeric, cytoskeletal proteins that link the actin cytoskeleton via connections to the cytoplasmic domain of the integrin β subunit.[224,225] The two talin genes of vertebrates, *Tln1* and *Tln2*, encode very similar proteins with 74% amino acid sequence identity.[226] In the adult heart, Tln1 and Tln2 are both highly expressed in CFs, while cardiomyocytes express Tln2 predominantly.[128] Tln2 has a stronger affinity for F-actin, allowing it to make stronger bonds than Tln1 and, therefore, is expressed highly in cells under constant forces, such as cardiomyocytes.[121] When Tln2 was deleted from cardiomyocytes in a Tln2 knockout mouse, cardiac structure and function are not affected up to one year of age, as Tln1 is upregulated and functionally replaces Tln2.[127] This expression pattern may be protectively redundant in adult mice, however during development, Tln2 cannot replace Tln1 function in the entire embryo, as Tln1 knockout mice leads to an embryonically lethal phenotype by E8.5-9.0.[122] Likewise, when Tln1 and Tln2 are both deleted from cardiomyocytes in adult mice, dilated cardiomyopathy develops spontaneously and results in death by 24 weeks of age, highlighting the need for a form of talin in cardiomyocytes to maintain function.[127] While deletion of talins in cardiomyocytes has been evaluated, the effect of talin deletion in CFs in unknown.

Here, we describe the effects on AngII-induced cardiac injury on the hypertrophic and fibrotic response when Tln1 is deleted from CFs in the global Tln2 knockout mouse. We hypothesized that the absence of Tln1 and Tln2 from CFs would result in the attenuation of adverse myocardial remodeling in response to pressure overload.

6.3 Methods

Animal Studies

All animal protocols were approved by the Institutional Animal Care and Use Committee at Vanderbilt University. Tln2 null, CF-specific knockout mice were created by crossing the $Tln2^{-/-}$;$Tln1^{flox/flox}$ mice, provided by Dr. Roy Zent (Vanderbilt University Medical Center)[111,123,232], with the Tcf21-Cre mice, provided by Dr. Michelle Tallquist (University of Hawaii) [233]. All mice were crossed with the *Rosa26*-stop-tdTomato reporter mice (Jackson Laboratory, Stock No. 007914) to visually verify Cre activation (**Figure 29**).[227] The sequences for the primers used are listed in **Table 5**.

All mice were given tamoxifen injections (2 mg in PBS-/-)/day for 5 days at 9 weeks of age to activate the *Tcf21*-Cre. Echocardiography and body weight at 12 weeks of age showed no difference between $Tln2^{-/-}$ and $Tln2^{-/-}$;$Tln1^{CF-/-}$ mice (**Figure 36**).

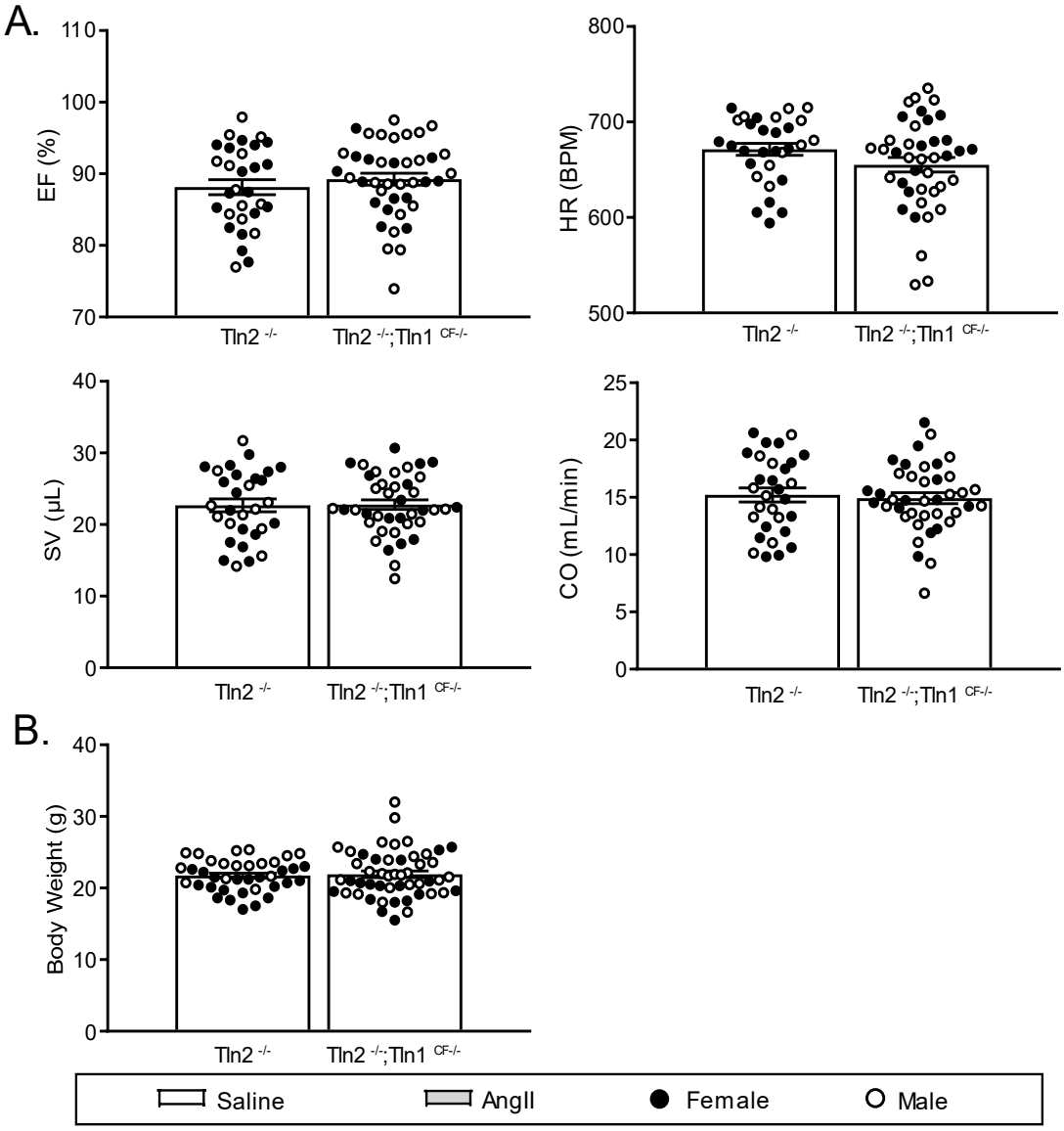

Figure 36: Echocardiographic measurements at 12 weeks of age under basal conditions. A. Echocardiographic analysis of ejection fraction (EF), heart rate (HR), stroke volume (SV) and cardiac output (CO) at 12 weeks of age, **B.** Mouse body weight at 12 weeks of age. A-B. Mean±SEM, *P<0.05 between groups noted with bar. All statistics were done with a two-tailed t-tests with Welch's correction.

These mice were then randomly assigned to receive AngII or saline through osmotic pumps. Chronic hypertension was imposed via AngII infusion through mini osmotic pumps (Alzet Corp, 1004) on 12-week-old male and female mice at a concentration of 1.5mg/kg/day. Control

mice were given saline pumps. This surgery was repeated in all mice at 16 weeks of age (**Figure 37**). Mice were either euthanized with CO_2 exposure or via exsanguination followed by removal of the heart under isoflurane INH continuous at 1-5% in accordance with Vanderbilt University Medical Center's Division of Animal Care Guidelines. Littermates were used and treatment groups were distributed throughout cages and litters.

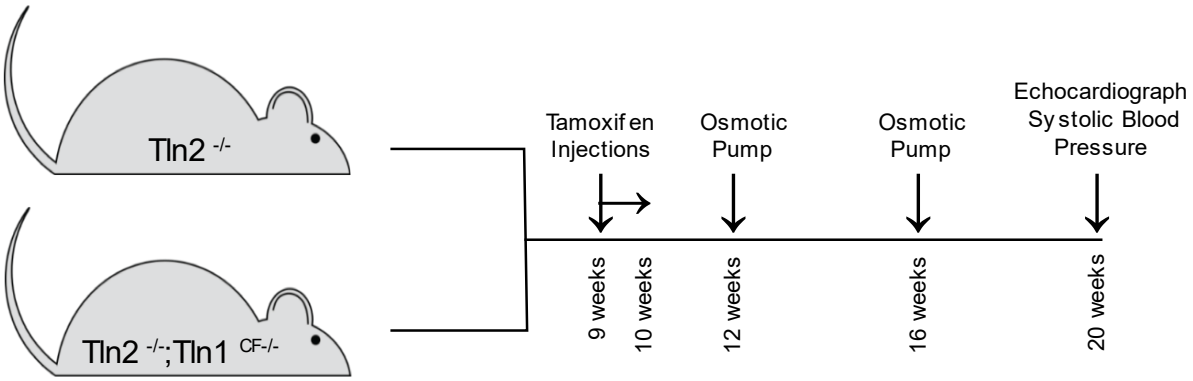

Figure 37: Experimental approach of 8-week AngII injury. Nine-week-old mice were subjected to 5 consecutive days of tamoxifen injections. At twelve and sixteen-weeks, pumps were surgically implanted in mice with angiotensin II-treatment (AngII), or control (saline). Treatment was ceased eight weeks after initial injury, and echocardiography and systolic blood pressure was performed.

Systolic blood pressure

Systolic blood pressure was measured using a noninvasive tail-cuff platform (Hatteras Instruments). Two rounds of 10 measurements were taken for each mouse and averaged for each mouse at each timepoint. Four mice were excluded from this study as their systolic blood pressure 8 weeks post AngII infusion did not indicate hypertension injury, and one control mouse was

excluded for having a systolic blood pressure higher than all AngII mice, indicating vascular defect.

Echocardiography

Blinded echocardiographic measurements were taken from short-axis cardiac M-mode images captured at mid-papillary level of non-anesthetized mice on a Vevo2100 small-animal ultrasound system (VisualSonics). Three independent measurements were analyzed per mouse for each timepoint.

Quantitative PCR

Quantitative PCR (**qPCR**) was performed on flash frozen LV tissue dissected from experimental mice. The sequences for the primers used are listed in **Table 4**. Gene expression was compared to the housekeeping gene *Gapdh*.

Histology

Upon euthanasia, hearts were perfused with PBS-/-, excised, and submerged in 3M potassium chloride to arrest hearts in diastole. Hearts were bisected along the transverse plane of the heart. Tissue was frozen and cryosectioned at 7 µm thickness. Picrosirius red staining (Fisher Scientific #50-300-77) was used to identify ECM (red) and cytoplasm (yellow). Images were analyzed using a semiautomated image-processing pipeline that was developed based on color segmentation.[227] Wheat germ agglutinin (**WGA**) staining (Invitrogen, #W11261) was performed for 30 min at room temp to quantify cardiomyocyte area, which was calculated using ImageJ.[237] A minimum of two LV images per animal were quantified.

RNA Sequencing

Left Ventricles (**LVs**) from dissected hearts were homogenized in TRIzol reagent, and RNA was isolated with the Zymo Direct-zol RNA Microprep Kit (Zymo, R2060). RNA integrity was measured with an Agilent Bioanalyzer before library preparations (**Table 6**). Sequencing and read alignment was performed by the Vanderbilt Technologies for Advanced Genomics (**VANTAGE**) center as described in Snider et al. to an average depth of 57.9 M reads per sample.[227] Differential expression analysis was performed with DEseq2 with Cook's outliers to filter low gene counts (mean count < 6) and $P_{adj} = 0.01$.[227,238] Protein-coding genes with an absolute log_2 fold change > 1 were analyzed. Visualizations were generated with ggplot2 in R. RNA sequencing (RNAseq) data has been deposited in the Gene Expression Omnibus (**GEO**) of NCBI under accession code GSE189323.

Sample #	Sample	Mouse Gender	RIN	Total Yield (Reads)
1	$Tln2^{-/-}$	Female	7.9	58,527,039
2	$Tln2^{-/-}$	Female	7.6	53,114,305
3	$Tln2^{-/-}$	Female	7.9	51,995,179
4	$Tln2^{-/-}$	Female	8.1	53,155,641
5	$Tln2^{-/-}$	Male	7.4	63,308,193
6	$Tln2^{-/-}$	Male	8.1	55,557,228
7	$Tln2^{-/-}$	Male	8.0	61,759,284
8	$Tln2^{-/-}$	Male	7.9	56,708,543
9	$Tln2^{-/-};Tln1^{-/-}$	Female	7.8	58,828,204
10	$Tln2^{-/-};Tln1^{-/-}$	Female	5.4	55,351,935
11	$Tln2^{-/-};Tln1^{-/-}$	Female	7.6	63,439,261
12	$Tln2^{-/-};Tln1^{-/-}$	Female	7.8	61,297,446
13	$Tln2^{-/-};Tln1^{-/-}$	Male	7.9	42,751,671
14	$Tln2^{-/-};Tln1^{-/-}$	Male	7.5	52,768,925
15	$Tln2^{-/-};Tln1^{-/-}$	Male	6.9	88,967,671
16	$Tln2^{-/-};Tln1^{-/-}$	Male	7.1	49,048,848

Table 6: RIN numbers for RNAseq. Descriptions of RNA integrity (RIN) and number of sequencing reads for each sample used in RNA sequencing (RNAseq).

Statistical Analysis

Data was compiled and shown as the means ± SEM. Data was evaluated using unpaired, two-tailed t-tests with Welch's correction (95% confidence interval) using GraphPad Prism software (GraphPad Inc., San Diego, CA). A p value < 0.05 was considered significant.

6.4 Results

6.4.1 Global deletion of Tln2 and CF-specific deletion of Tln1 causes a mild stress response in adult mice

Due to the ability of Tln2 to compensate for the loss of Tln1, we developed a strategy to delete both talin genes from CFs to determine the role of Tln1 in CFs during cardiac injury. We crossed the talin knockout mouse ($Tln2^{-/-}$;$Tln1^{flox/flox}$) with the fibroblast specific *Tcf21*-Cre, referred to as **$Tln2^{-/-}$;$Tln1^{CF-/-}$** mouse. **$Tln2^{-/-}$** mice have no cardiac phenotype up to one year of age, and therefore served as our control.[127] At 20 weeks of age, there was no increase in systolic blood pressure in either of the two saline groups indicating there was no pressure overload injury to the hearts (**Figure 38a**). At 20 weeks of age, $Tln2^{-/-}$;$Tln1^{CF-/-}$ mice had a significant increase in expression of the myocardial injury marker, atrial natriuretic peptide (*Nppa*) compared to the $Tln2^{-/-}$ mice ($p \leq 0.05$) **(Figure 38b**). Measurements of cardiac hypertrophy, and interstitial fibrosis were not changed at 20 weeks of age. Overall, this data suggests that under basal conditions, a mild stress response occurs in the ventricular myocardium when Tln1 is deleted from CFs, but this deletion does not result in overall morphologic or functional changes in the heart.

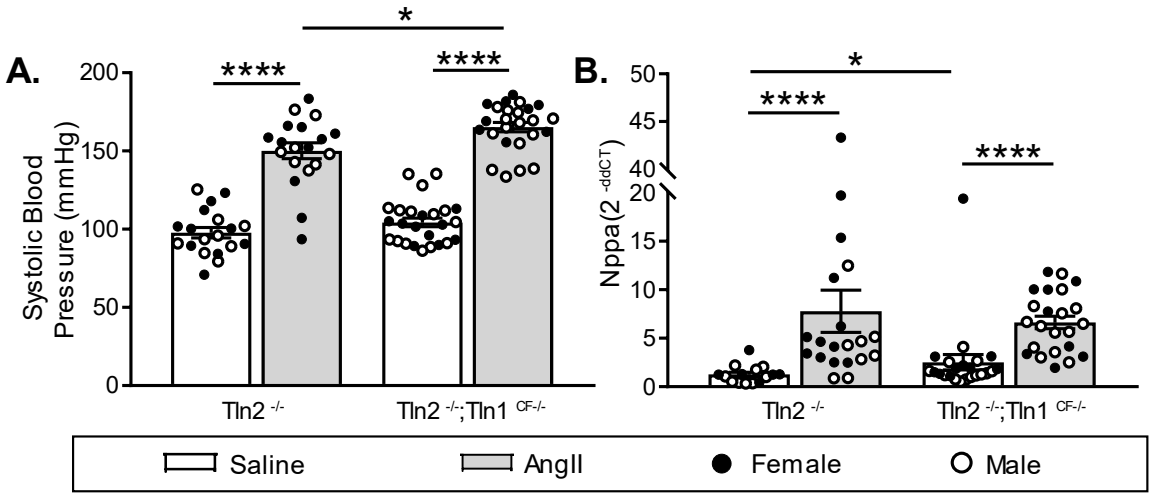

Figure 38: Measurements of SBP and mRNA *Nppa* expression in 8 week AngII injured mice. A. Systolic blood pressure at 20 weeks of age, **B.** Quantitative polymerase chain reaction analysis of Nppa, the gene encoding the heart failure marker natriuretic peptide A, at 20 weeks of age. A-B. Mean±SEM, *P<0.05, ****P<0.001 between groups noted with bar. All statistics were done with a two-tailed t-tests with Welch's correction.

6.4.2 Mice with a global deletion of Tln2 and CF-specific deletion of Tln1 develop exaggerated systolic hypertension in response to AngII infusion

Given the absence of significant changes at baseline, we then subjected $Tln2^{-/-}$ and $Tln2^{-/-}$;$Tln1^{CF-/-}$ mice to AngII or saline for 8 weeks (**Figure 37**). Both AngII groups had an increase in systolic blood pressure compared to respective saline controls at 8 weeks post-AngII infusion ($p \leq 0.001$) (**Figure 38a**). Additionally, the $Tln2^{-/-}$;$Tln1^{CF-/-}$ mice had a significant increase in systolic blood pressure compared to the $Tln2^{-/-}$ mice after AngII infusion ($p \leq 0.05$) (**Figure 38a**).

6.4.3 CF deletion of Tln1 and Tln2 does not affect heart hemodynamics during AngII infusion

Expression of *Nppa* was quantified in the left ventricle to assess myocardial injury. $Tln2^{-/-}$ and $Tln2^{-/-}$;$Tln1^{CF-/-}$ mice had an increase in *Nppa* (both $p \leq 0.001$) compared to their saline controls at 8 weeks post-AngII infusion (**Figure 38b**). Heart hemodynamics was assessed through

echocardiographic analysis. An unchanging ejection fraction (**EF**) and heart rate (**HR**) (**Figure 39a**) with a decrease in stroke volume (**SV**) and cardiac output (**CO**) in all AngII groups (both $p \leq 0.001$) indicate a decrease in end diastolic volume in all mice with AngII infusion (**Figure 39b**).

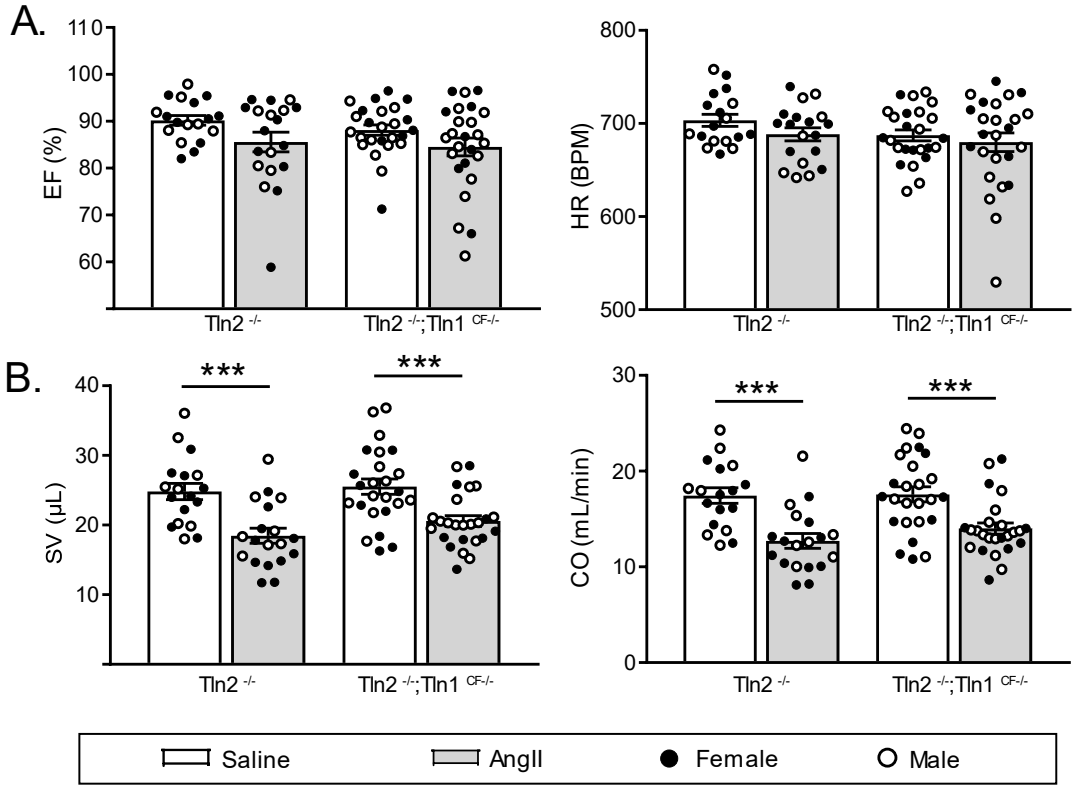

Figure 39: Echocardiographic measurements of heart function in 8-week AngII injured mice. A. Echocardiographic analysis of ejection fraction (EF) and heart rate (HR) at 20 weeks of age, **B.** Echocardiographic analysis of stroke volume (SV) and cardiac output (CO) at 20 weeks of age. A-B. Mean±SEM, ***P<0.005 between groups noted with bar. All statistics were done with a two-tailed t-tests with Welch's correction.

Dry lung/ body weight ratio was not changed in the AngII groups, showing that no congestion occurred (**Figure 40**).

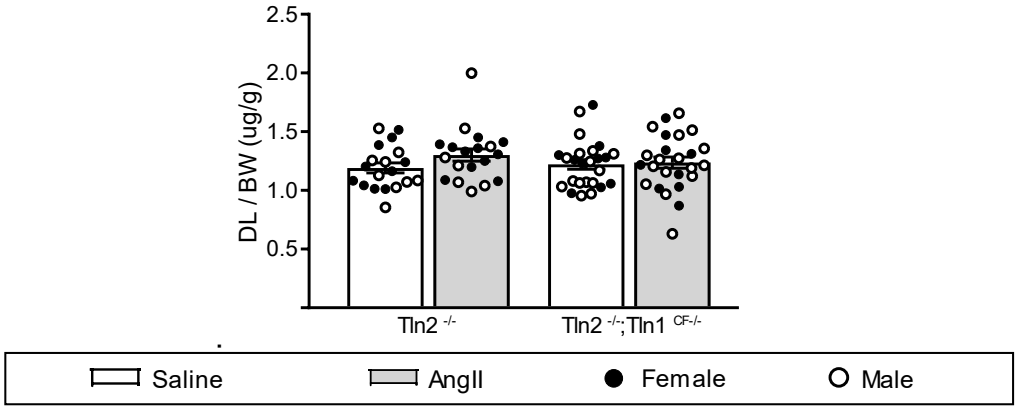

Figure 40: DL/BW ratio in 8-week AngII injured mice. A. Echocardiographic analysis of ejection fraction (EF) and heart rate (HR) at 20 weeks of age, **B.** Echocardiographic analysis of stroke volume (SV) and cardiac output (CO) at 20 weeks of age. A-B. Mean±SEM, ***P<0.005 between groups noted with bar. All statistics were done with a two-tailed t-tests with Welch's correction.

6.4.4 CF deletion of Tln1 and Tln2 results in cardiomyocyte hypertrophy in response to AngII infusion

Cardiac hypertrophy in the setting of pressure overload is a result of cardiomyocyte hypertrophy and interstitial fibrosis. $Tln2^{-/-};Tln1^{CF-/-}$ mice had a significant increase in ventricle/end body weight compared to their saline controls ($p \leq 0.05$) at 8 weeks post AngII infusion (**Figure 41**).

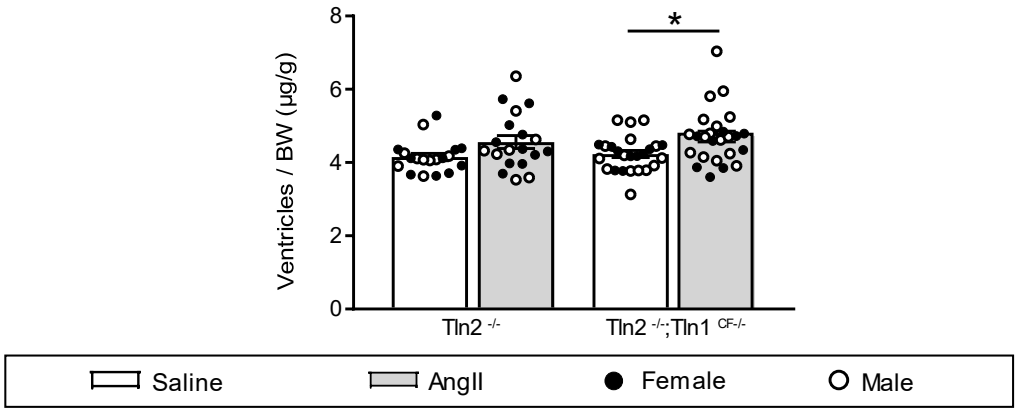

Figure 41: Ventricle / BW ratio in 8-week AngII injured mice. Ventricles to body weight ratio at 20 weeks of age. Mean±SEM, *P<0.05 between groups noted with bar. All statistics were done with a two-tailed t-tests with Welch's correction.

This was supported by measurements of cardiomyocyte hypertrophy. Histologic analysis showed that the $Tln2^{-/-}$;$Tln1^{CF-/-}$ mice had an increase in cardiomyocyte area ($p \leq 0.01$) at 8 weeks post AngII treatment, whereas the $Tln2^{-/-}$ mice had no change (**Figure 42**). This indicates that there is morphometric and histological evidence of enhanced hypertrophic response of cardiomyocytes to AngII infusion in mice with loss of Tln1 in CFs.

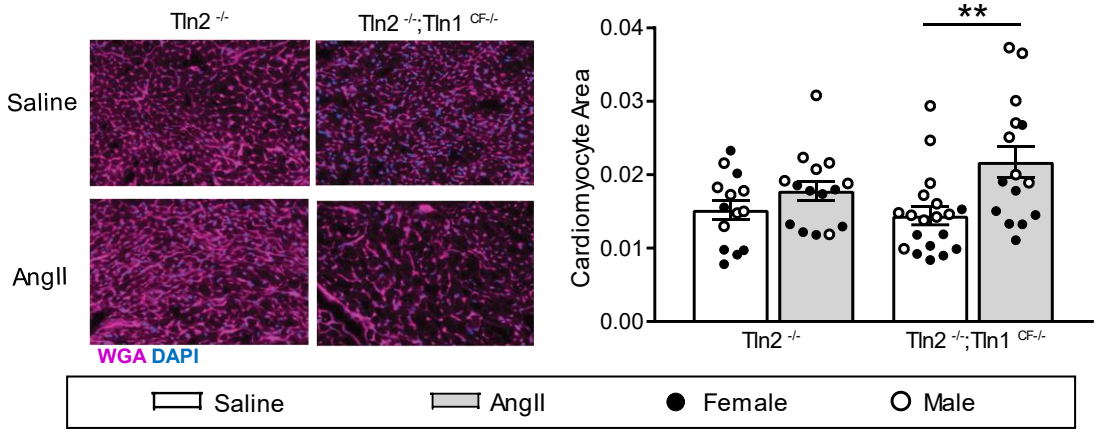

Figure 42: WGA staining of cardiomyocyte area in 8-week AngII injured mice. Representative images of wheat germ agglutinin (WGA) stain on the left ventricle of mice at 20 weeks of age. Quantification of WGA staining to determine cardiomyocyte area. Mean±SEM, **P<0.01 between groups noted with bar. All statistics were done with a two-tailed t-tests with Welch's correction.

6.4.5 CF deletion of Tln1 and Tln2 results in no change in cardiac fibrosis burden following AngII infusion

To measure the effects of CF Tln1 and Tln2 on fibrotic remodeling we measured interstitial fibrosis and fibroblast activation following AngII infusion. Picrosirius red staining was performed on transverse sections of the heart and quantified to determine fibrosis. Image quantification of the ratio of the fibrotic to non-fibrotic tissue showed that the $Tln2^{-/-}$ and $Tln2^{-/-};Tln1^{CF-/-}$ mice both had a significant increase ($p \leq 0.005$) in fibrosis at 8 weeks of AngII infusion compared to saline controls, but were not significantly different from each other (**Figure 43**).

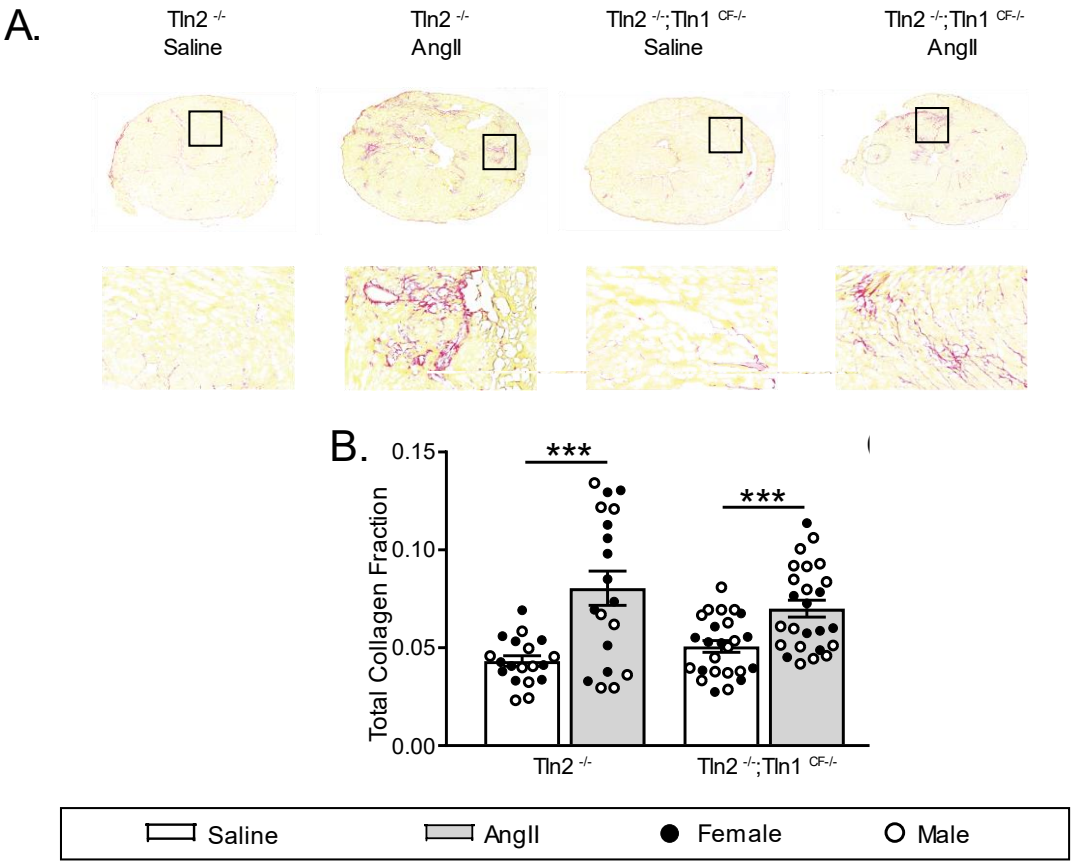

Figure 43: Measurements of interstitial fibrosis in 8-week AngII injured mice. A. Representative images of picrosirius red (PSR) stained hearts at 20 weeks of age at 20x and their corresponding 40x images indicated with black boxes, **B.** Quantification of PSR staining of hearts. Collagen (red pixels) and heart tissue (yellow) was used to calculate the average collagen fraction in each heart. Mean±SEM, ***P<0.005 between groups noted with bar. All statistics were done with a two-tailed t-tests with Welch's correction

α-SMA, a marker of CF to myofibroblast transition, was increased in both the AngII-treated $Tln2^{-/-}$ and $Tln2^{-/-}$;$Tln1^{CF-/-}$ (both $p \leq 0.001$) mice (**Figure 44**). This indicates that the loss of both talins in CFs does not result in a change in the fibrotic response to AngII infusion.

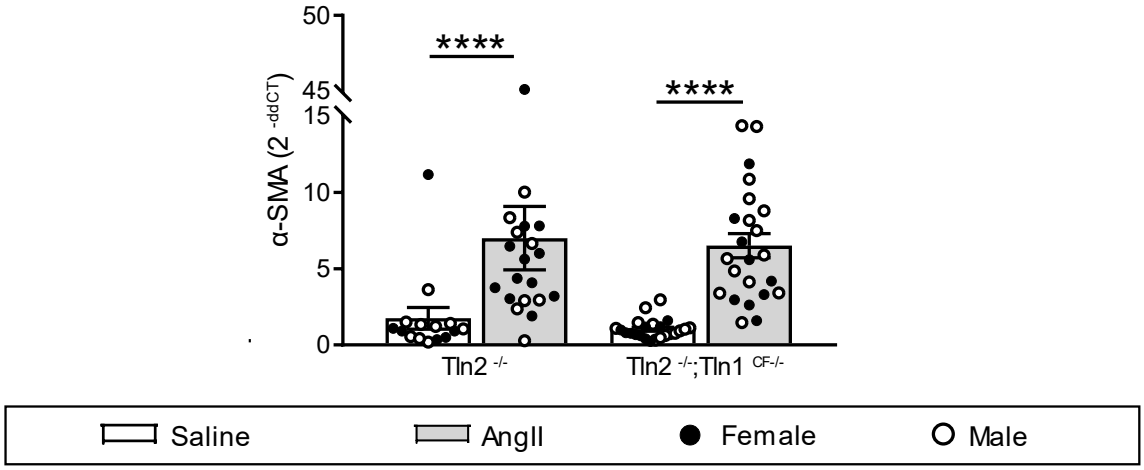

Figure 44: qPCR expression of *α-SMA* in 8-week AngII injured mice. Quantitative polymerase chain reaction analysis of α-SMA, the gene encoding the myofibroblast marker alpha-smooth muscle actin. Mean±SEM, ****P<0.001 between groups noted with bar. All statistics were done with a two-tailed t-tests with Welch's correction.

6.4.6 Global deletion of Tln2 and CF-specific deletion of Tln1 causes a change in genes associated with fibrosis and cardiac hypertrophy

To further understand the increase in cardiomyocyte hypertrophy in the AnII-injured Tln2$^{-/-}$;Tln1$^{CF-/-}$ mice, we used RNAseq to investigate genetic changes associated with loss of talin in CFs. RNAseq analysis of LV tissue from Tln2$^{-/-}$ and the Tln2$^{-/-}$;Tln1$^{CF-/-}$ hearts 8 weeks post-AngII infusion yielded 10 differentially expressed genes between the Tln2$^{-/-}$ and the Tln2$^{-/-}$;Tln1$^{CF-/-}$ genotypes. (P_{adj} < 0.01 and absolute $\log_2$ fold change > 1). These top 10 enriched genes are annotated on the volcano plot in **Figure 45**.

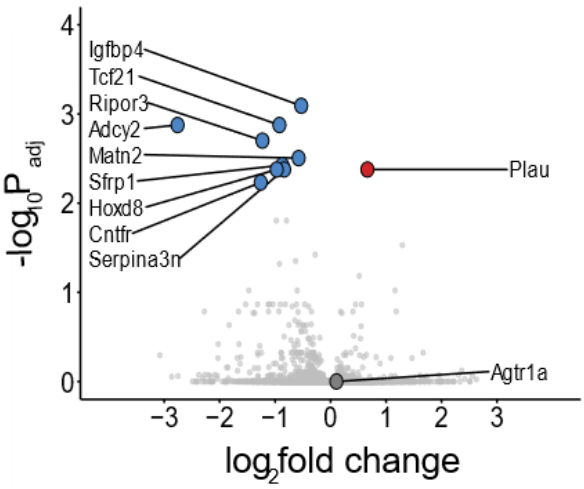

Figure 45: Volcano plot showing enriched genes from RNAseq. RNAseq comparing Tln2$^{-/-}$ and Tln2$^{-/-}$;Tln1$^{CF-/-}$ left ventricles shows changes to genes involved in fibrosis and cardiac hypertrophy. Volcano plot showing the significantly (Padj < 0.01) altered genes in Tln2$^{-/-}$;Tln1$^{CF-/-}$ left ventricle tissue following AngII-induced injury.

Manually categorizing these genes based on literature searches, these genes fell mostly into two categories: genes associated with fibrosis (*Igfbp4, Sfrp1, Tcf21, Plau, Serpina3n, Cntfr*) and genes associated with cardiac hypertrophy (*Igfbp4, Sfrp1, Serpina3n, Cntfr*) (**Table 7**).

	PubMed Results	
Gene	**Fibrosis**	**Cardiac Hypertrophy**
Igfbp4	13	2
Tcf21	19	0
Adcy2	1	0
Ripor3	0	0
Matn2	2	0
Sfrp1	27	2
Serpina3n	4	1
Plau	14	0
Hoxd8	0	0
Cntfr	3	1

Table 7: PubMed results for top 10 enriched genes in studies of fibrosis and cardiac hypertrophy

6.5 Discussion

The purpose of the present study was to evaluate the functional significance of talins in CFs during AngII-induced injury. This was accomplished by developing a novel transgenic mouse: a Tln2 null mouse with Tln1 specifically deleted in CFs. The results suggest that mechanotransdution in CFs through Tln1 and Tln2 may be important mediators of cardiomyocyte hypertrophy and interstitial fibrosis.

Under basal conditions, the $Tln2^{-/-}$;$Tln1^{CF-/-}$ mice had an increase in *Nppa*, indicating that there was an increase in myocardial stress in these mice. This did not manifest into changes in cardiac function through 20 weeks of age, suggesting that talins in CFs are not needed to maintain cardiac function under basal conditions. The increase in *Nppa* does suggest that the myocardium of the $Tln2^{-/-}$;$Tln1^{CF-/-}$ mice is under more stress, indicating that cardiomyocytes compensate for the additional stress placed on the heart due to dysfunctional fibroblasts. To further understand this phenomenon, we subjected the $Tln2^{-/-}$ and $Tln2^{-/-}$;$Tln1^{CF-/-}$ mice to AngII infusion for 8 weeks to evaluate cardiomyocyte response under prolonged pressure overload of the heart. We found that absence of Tln1 and Tln2 in CFs results in an increase in cardiomyocyte hypertrophy with AngII infusion but did not affect interstitial fibrosis.

Because $Tln2^{-/-}$ and $Tln2^{-/-}$;$Tln1^{CF-/-}$ mice under AngII infusion have no difference in interstitial fibrosis, our findings suggest that an increase in ventricular wall stiffness is not the primary factor driving cardiomyocyte hypertrophy in the $Tln2^{-/-}$;$Tln1^{CF-/-}$ mice. Therefore, this change in cardiomyocyte hypertrophy could be attributed to the increase in afterload, apparent in the increased systolic blood pressure in the $Tln2^{-/-}$;$Tln1^{CF-/-}$ mice under AngII infusion. The increase in systolic blood pressure seen in the $Tln2^{-/-}$;$Tln1^{CF-/-}$ mice could be the result of using *Tcf21* as the driver for the Cre. Tcf21 is highly expressed in resident CFs and myofibroblasts, and is considered the best marker of all fibroblast populations in the heart [40]. However, Tcf21 is also

expressed in podocytes in the kidney.[239] Integrin adhesions are necessary for podocytes to withstand the hydrostatic pressure in the kidney, and injured podocytes results in an increase in systolic blood pressure.[240,241] Therefore, systolic blood pressure could be increased in the $Tln2^{-/-}$;$Tln1^{CF-/-}$ mice due to Tln1 and Tln2 being removed from podocytes, resulting in podocyte injury. This increase in systolic blood pressure would result in more ventricular wall stress in the heart, resulting in cardiomyocyte hypertrophy in response to increased wall stress and intraventricular pressure.

Contrary to the development of enhanced cardiomyocyte hypertrophy in the $Tln2^{-/-}$;$Tln1^{CF-/-}$ mice under AngII infusion, there was no change in interstitial fibrosis between the $Tln2^{-/-}$ and $Tln2^{-/-}$;$Tln1^{CF-/-}$ mice under AngII infusion. With the absence of Tln1 and Tln2 in CFs we expected to see a decrease in interstitial fibrosis in the $Tln2^{-/-}$;$Tln1^{CF-/-}$ mice as the ability of CFs to sense ECM stiffness through focal adhesions would be impaired. However, this does not mean that the absence of Tln1 and Tln2 in CFs did not alter ECM deposition in these mice. $Tln2^{-/-}$;$Tln1^{CF-/-}$ mice had higher systolic blood pressure than the $Tln2^{-/-}$ mice after 8 weeks of AngII infusion, indicating that the $Tln2^{-/-}$;$Tln1^{CF-/-}$ hearts were under more pressure. The higher systolic blood pressure would result in an increase in LV wall stress, and we would therefore expect to see more interstitial fibrosis in the ventricles of a heart that had a higher systolic blood pressure. Because we do not see this in the $Tln2^{-/-}$;$Tln1^{CF-/-}$ mice, our data suggests that absence of Tln1 and Tln2 in CFs is hampering the ability of CFs to produce ECM in response to increased LV pressure. Due to the limitations of our current study, we cannot say if this is a protective mechanism that prevents the increase in interstitial fibrosis, or merely delays the onset of interstitial fibrosis during constant AngII infusion. To answer these questions, this study should be repeated over a longer time course and with a higher concentration of AngII in order to distinguish if this phenotype only occurs during a lesser injury, or also occurs during a more progressive intense injury.

Our data indicate that CF-specific Tln1 deletion is involved in the development of hypertension and hypertrophy in response to hemodynamic stress. RNAseq analysis of the LV after 8 weeks of AngII infusion showed a decrease in *Cntfr* and *Sfrp1* in $Tln2^{-/-}$;$Tln1^{CF-/-}$ mice, with no change in the angiotensin type 1 receptor (*Agtr1a*) as compared to $Tln2^{-/-}$ mice. Overexpression of *Cntfr* in mouse cardiomyocytes has been shown to be cardioprotective against AngII-induced injury, suggesting that cardiomyocytes in the $Tln2^{-/-}$;$Tln1^{CF-/-}$ mice are under more stress and have additional injury due to their decreased expression of *Cntf.*[242] Additionally, $Sfrp1^{-/-}$ mice develop dilated cardiomyopathy at 1 year of age with cardiomyocyte hypertrophy.[243] Therefore, reduction in *Sfrp1* may mediate the development of AngII-induced cardiac hypertrophy during the presence of disrupted mechanical signaling in CFs. The relationship between talins and *Cntfr* and *Sfrp1* has not been studied and should be examined in the future to elucidate the mechanisms of signaling leading to cardiomyocyte hypertrophy with loss of Tln1 in CFs.

In conclusion, this study demonstrates that global deletion of Tln2 and CF-specific deletion of Tln1 results in enhanced hypertension and cardiac hypertrophy following Ang II infusion. Furthermore, the absence of Tln1 and Tln2 in CFs may prevent the development of fibrosis in the setting of enhanced AngII induced pressure overload.

Chapter 7

Discussion and Future Directions

7.1 Summary and broader impact

This work investigated the role of the two talin proteins, Tln1 and Tln2, in the context of multiple models of hypertension-induced injury through pressure overload of the heart. HF is one of the leading causes of death worldwide, and there is no indication that its prevalence is decreasing. While there have been advances in lowering death rates in patients with acute cardiac events leading to HFrEF, prolonged slow development of HFpEF rates continue to rise. Hypertension is one of the main underlying conditions that leads to HFpEF, and clinically presents as an increase in blood pressure.[5,12] Therefore, the most common therapeutics (Thiazide-type diuretics, CCBs, and ACE inhibitors/ARBs) used in treating hypertension function through wide-spread mechanisms of action to lower SBP.[71] During pressure overload, interstitial fibrosis, and cardiomyocyte hypertrophy lead to concentric remodeling of the heart.[16] While treatments to lower blood pressure have proven useful in slowing down the progression of hypertension induced HF, the results obtained can be improved as these pharmacologic therapeutics do not address the underlying cardiac injury; namely cardiac hypertrophy and interstitial fibrosis.

To address these challenges, we utilized multiple novel genetic mice to selectively delete the focal adhesion proteins Tln1 and Tln2 from CFs and myofibroblasts so that we could target interstitial remodeling during hypertension. Additionally, we utilized several injury models of hypertension and pressure overload in mice, as well as an acute heart failure model, to determine the contribution of CF talins to cardiac disease.

We initially started by characterizing CFs *in vitro* with loss of Tln1 using an siRNA knockdown in WT CFs (Tln1 KD). Myofibroblasts were characterized as they are the cells primarily responsible for depositing and contracting the ECM in heart injury.[45,46] First, we exposed these cells to strain to activate CF to myofibroblasts transition. α-SMA, a gene that is associated with CF to myofibroblast transition, was upregulated in Tln1 KD cells. Additionally, α-SMA is associated with increased cellular ability to contract. Gel contraction assays, however, showed that there was a significant decrease in Tln1 KD cells' ability to contract as compared to Scr controls. This suggests that while the Tln1 KD cells have an increased expression of mRNA genes associated with contraction, this is not translated to cellular contraction. This indicates that Tln1 has a function in fibroblasts in regulating the contractile units inside the cell. We know that Tln1 connects the actin cytoskeleton to the ECM, so loss of Tln1 could be disrupting these connections, and resulting in the decreased contractility phenotype. However, because these fibroblasts still have Tln2, they still have some functional connections to the ECM, and therefore the fibroblasts are still receiving signals to produce more α-SMA to cause contraction, hence the increased mRNA expression. This indicates that intact Tln2 in these fibroblasts are still able to confer some contractile properties in Tln1 KD cells. We additionally identified changes in cell viability and migration in myofibroblasts lacking Tln1. Overall, these characteristic changes we observed in the Tln1 KD myofibroblasts led us to move to a mouse model of pressure overload of the heart to further study the specific effects of myofibroblast loss of Tln1.

To further investigate the changes in myofibroblasts with loss of Tln1 in the heart, we created a novel myofibroblast Tln1-specific knockout mouse ($Tln1^{MF-/-}$ mice) and subjected these and WT mice to 6-weeks of TAC. 6-weeks post TAC, we observed a decrease in LVOT Peak Velocity in the TAC mice as compared to sham, indicating that the surgery was successful in causing pressure overload in the heart. Through echocardiography, we observed that most of the TAC animals, WT and $Tln1^{MF-/-}$ mice, did not have a decrease in EF as expected. Because cardiac

remodeling is different in HFpEF and HFrEF, we decided to focus just on the mice that had EF > 40% 6-weeks post-TAC to ensure that we were analyzing only mice undergoing the concentric remodeling seen in HFpEF. Once we removed mice from our experiment that had an EF < 40%, we looked at measures of interstitial fibrosis. We observed that there was no change in interstitial fibrosis between the WT and Tln1$^{MF-/-}$ mice after TAC. Furthermore, there was no difference in interstitial fibrosis between either of these TAC mice and their sham controls. This suggests that either our TAC model did not produce enough pressure overload of the heart to cause a fibrotic response, or our time point in this mouse model was not far enough out for us to start seeing the fibrotic response. To establish why this model is not producing the interstitial fibrotic response we expected, this TAC model should be continued for twice as long. Additionally, a smaller gauge needle can be used for the aortic constriction to cause a greater severity of ligation and greater pressure overload of the heart.

While this was not what we expected to see, we proceeded to investigate measurements of cardiac hypertrophy, as hypertrophy in addition to interstitial fibrosis are the hallmarks of HF. Vertical/body weight ratio 6-weeks post-TAC was increased in just the Tln1$^{MF-/-}$ mice compared to sham animals, indicating the presence of cardiac hypertrophy. This was validated though echocardiography where LV mass in just the Tln1$^{MF-/-}$ TAC mice was increased. Additionally, the WT and Tln1$^{MF-/-}$ TAC mice all had an increase in LVPW;d, IVS;d, and IVS;s. However, the Tln1$^{MF-/-}$ TAC mice had a larger increase in these echocardiographic measurements compared to sham animals indicating that concentric remodeling in the Tln1$^{MF-/-}$ TAC mice was occurring to a greater extent than the WT mice. This indicates that loss of Tln1 in myofibroblasts results in an increase in cardiomyocyte hypertrophy during pressure overload of the heart. Since we are only removing Tln1 from the CFs, this points to loss of Tln1 in CFs causing a change that results indirectly in cardiomyocyte hypertrophy. We know from prior measurements that the interstitial fibrosis is not

changing, therefore, loss of Tln1 in CFs is most likely causing a chemical or electrical signaling change between CFs and cardiomyocytes, resulting hypertrophy.

Since it has been shown in literature that Tln1 and Tln2 often have similar roles in cells that highly express both talin proteins, we wanted to then assess interstitial fibrosis when there is loss of both Tln1 and Tln2 in CFs. We created a novel genetic mouse that was null for Tln2 with a CF Tln1-specific knockout ($Tln2^{-/-}$;$Tln1^{CF-/-}$) using the *Tcf21*-Cre. It has been shown *in vitro* that removal of Tln1 and Tln2 from fibroblasts results in fibroblasts that do not migrate, proliferate, or form cellular protrusions.[231] Additionally, *in vivo* studies of mice exposed to MI result in death four days post-MI with removal of mouse myofibroblasts.[218] We hypothesized that removal of Tln1 and Tln2 from CFs would theoretically be like removing CFs from the heart, and therefore would also result in mouse death during acute injury. To test this, we exposed the $Tln2^{-/-}$;$Tln1^{CF-/-}$ mice to MI. While these mice had a 60% mortality 4 days post-MI, this was less death than when all myofibroblasts were ablated. To survive MI, a collagenous scar must be formed through the deposition of collagen in place of apoptotic cardiomyocytes. Formation of this scar in the $Tln2^{-/-}$;$Tln1^{CF-/-}$ mice suggests that CFs with loss of Tln1 and Tln2 are still able to function, proliferate, and lay down ECM to some extent.

We then decided to look at CF Tln1 and Tln2 in an AngII model of prolonged pressure overload of the heart to try to identify the contribution of CF Tln1 and Tln2 in a non-acute injury model. When the $Tln2^{-/-}$;$Tln1^{CF-/-}$ mice were exposed to 8 weeks of AngII infusion, we measured an increase in SBP, indicating that pressure overload of the heart was occurring. Interestingly, the SBP of the $Tln2^{-/-}$;$Tln1^{CF-/-}$ mice was greater than the $Tln2^{-/-}$, which were serving as our control. While this could mean that loss of Tln1 and Tln2 in CFs results in an alteration in blood pressure, *Tcf21*, the driver of our Cre system, could also be resulting in this change. *Tcf21* is expressed in podocytes in the kidney, as well as CFs and myofibroblasts in the heart.[239] Injury of podocytes cell, such as loss of Tln1, can result in increased systolic blood pressure.[240,241] This could be

causing the increased SBP that we seen between the $Tln2^{-/-}$ and $Tln2^{-/-}$;$Tln1^{CF-/-}$ AngII injured mice.

We proceeded to investigate the hypertrophic response of cardiomyocytes to pressure overload injury of the heart. We observed that *Nppa*, a marker of myocardial injury, was increased in both the $Tln2^{-/-}$;$Tln1^{CF-/-}$ and $Tln2^{-/-}$ mice after AngII-injury. Echocardiography showed that both the $Tln2^{-/-}$;$Tln1^{CF-/-}$ and $Tln2^{-/-}$ mice both had a decrease in SV and CO after AngII injury, indicating that cardiomyocyte remodeling was occurring. We further investigated these histological changes associated with our echocardiographic observations. Ventricle / body weight was increased in just the $Tln2^{-/-}$;$Tln1^{CF-/-}$ mice after AngII-injury. WGA staining additionally showed that there was increased cardiomyocyte hypertrophy in the $Tln2^{-/-}$;$Tln1^{CF-/-}$ mice that was not seen in the $Tln2^{-/-}$ mice. These observations together suggest that loss of Tln1 and Tln2 in CFs results in cardiomyocyte hypertrophy during pressure overload injury of the heart. The increase in cardiomyocyte hypertrophy mirrors the same results that we saw in the $Tln1^{MF-/-}$ TAC mice signifying that loss of Tln2 in CFs is not changing the response to pressure overload injury in the heart, and that loss of Tln1 in CFs is driving the morphologic remodeling that we are seeing.

Finally, we investigated the interstitial fibrosis changes associated with pressure overload injury in the heart. Through histology, we observed an increase in fibrosis in both the $Tln2^{-/-}$ and $Tln2^{-/-}$;$Tln1^{CF-/-}$ mice after AngII-injury, with no difference between the AngII-injured mice. This was surprising as we expected to see an increase in interstitial fibrosis in the $Tln2^{-/-}$;$Tln1^{CF-/-}$ mice after AngII-injury since there was an increase in SBP in these mice, suggesting that they were experiencing a higher degree of injury. This indicates that loss of Tln1 and Tln2 in CFs can augment interstitial fibrosis during pressure overload of the heart.

In conclusion, we set out to target the focal adhesion proteins, Tln1 and Tln2, in the effector cells of fibrosis (i.e. CFs and myofibroblasts) to control the fibrotic response and limit the

adverse fibrotic remodeling in the heart during pressure overload injury. These studies have identified a novel role of Tln1 and Tln2 in CF and myofibroblasts in regulating the hypertrophic response of cardiomyocytes to pressure overload injury in the heart. Removal of Tln1 and Tln2 from CFs resulted in cells that have a decreased ability to migrate, proliferate, and contract. This was seen in a decrease in interstitial fibrosis after pressure overload injury of the heart, even in the face of greater SBP. Taken together, this work has identified CF Tln1 and Tln2 as novel mediators of cardiomyocyte behavior in the heart. Further work needs to be done to determine the contribution of increased SBP during loss of Tln1 and Tln2 in CFs before this work should be looked at in other contexts of heart disease.

7.2 Future directions

The present work advances our understanding of CF Tln1 and Tln2 in the context of pressure overload remodeling of the heart. However, it has also raised important questions that can be used to direct future research into this topic. In particular, this research should be expanded by investigating the signaling between cardiac fibroblasts and cardiomyocytes. While we began the investigation of CF and myofibroblasts change *in vitro* we only looked at the overall characteristic changes in these cells with loss of Tln1 through siRNA knockdown. With the creation of the $Tln1^{MF-/-}$ mouse, CFs from these mice can be isolated and then exposed to a Cre-recombinase *in vitro* to ensure a more complete knockdown of Tln1. Additionally, myofibroblasts produce multiple cytokines (TNF-a, IL-1B, IL-6, TNF-b), vasoactive peptides, and growth factors (AngII, TN-1, ANP, BNP, VEGEF), which can increase collagen synthesis in CFs, while also inducing cardiomyocyte hypertrophy.[58] Therefore, the production of these cytokines, peptides, and growth factors should be measured in $Tln1^{-/-}$ myofibroblasts. Media can be collected from Tln1-null CFs and immunoprecipitation assay can be performed to measure the above factors. Additionally, TGF-β, AngII, or ISO can be added to CF's 24 hours prior to media collection to look specifically at activated CFs. Additionally, CFs should be co-cultured with cardiomyocytes to see how changes in CF signaling alter cardiomyocyte physiology *in vitro*.

Limitations of the work described in this dissertation could be addressed with a variety of studies to directly and incrementally expand the data presented. First, podocyte injury should be assessed when Tln1 is removed with the *Tcf21* Cre through collection of kidneys and measuring the podocyte injury markers of podoplanin and synaptopodin.[244] Since podocyte injury can result in an increase in blood pressure, assessment of podocyte injury should be measured to rule out their contribution to injury as an increase in SBP results in further cardiomyocyte hypertrophy and interstitial fibrosis in the heart. If podocyte injury is found to contribute to regulating SBP, then this experiment should be repeated using a different driver of the Cre system for Tln1 removal. Other

common markers for CFs include fibroblast specific protein 1 (*FSP1*) and platelet-derived growth factor receptor-α (*PDGFRα*), and they maybe more viable drivers for the Cre system.[218]

Secondly, SBP was used to confirm a systemic increase in blood pressure, but pressure overload was not confirmed in ventricular pressure. This could be done through measuring the outflow of blood through the aorta, as was done during the initial TAC study. Furthermore, noninvasive measurements could be used to assess the changes in cardiomyocyte function. Echocardiography could be used to measure the contractility and relaxation of the heart through global longitudinal strain measurements, and electrocardiogram could be used to measure the electrical conduction of the heart. This would allow us to see if altered interstitial fibrosis in the heart is leading to cardiomyocyte defects and allow for a more targeted approach to study cardiomyocyte and CF crosstalk in an electrical, stiffness, or chemical signaling context. Additionally, mice should be kept on AngII-infusion for more than 8 weeks to allow for greater cardiac decompensation to occur to further confirm that a decrease in interstitial fibrosis in the $Tln2^{-/-}$;$Tln1^{CF-/-}$ mice is still seen during longer injury with increased SBP, and is not just delaying the onset of increased interstitial fibrosis.

Further experiments should also include determining if there is an alteration in collagen deposition and processing. While we did begin investigation into alteration in the transcription of MMPs and TIMPs, further research should be done to determine the thickness of collagen, types of collagen present, and location of interstitial fibrosis in the AngII injured hearts. Polarized light images of PSR staining reflect different colors based on the thickness of collagen fibers. Using a MatLab program previously developed in our lab to quantify the coloration,[227] we can quantify the proportion of thinner, less mature collagen fibers compared to thicker more mature collagen fibers in the interstitial fibrosis. Additionally, the type of collagen present should be investigated. In the healthy heart, ~85% of the ECM is composed of thicker collagen I fibers to conifer tensile strength, and ~11% of collagen type III fibers that maintain the elasticity of the ECM.[43] These proportions

change during injury, and the amount of Collagen type III increases. The ratios of collagens should be measured to give an idea of elasticity of the ventricular heart wall. This should be done both through qPCR and immunostaining. Atomic force microscopy (AFM) should also be used to measure the stiffness of the interstitial fibrosis to additionally gain insight on alteration in collagen deposition.

Lastly, the location of interstitial fibrosis in the heart should be characterized. Histological sections of the heart can be subdivided into LV posterior wall, LV anterior wall, septum, and right ventricle. PSR staining can then be quantified in each of these sections and correlated to WGA quantification in these same histological sections and correlated to echocardiographic measurements of LV Mass, LVPW, LVAW, and IVS. This would allow for a better determination of the contribution of interstitial fibrosis and cardiomyocyte hypertrophy to the overall hypertrophy in each section of the heart.

In terms of RNA sequencing, we would like to have improved selection criteria for the mice that we use to see if we can detect more subtle changes. While we did control for an increase in SBP and used an equal number of male and female mice, we had no other variables to determine the severity of pressure overload injury in each of these mice. Additional measurements that could be used would be ventricle/body weight ratio during dissections, and measurement of mRNA *Nppa* to try and only use mice with more severe injury. We would also like to include control animals in the RNA sequencing. From our data, we know that the $Tln2^{-/-}$;$Tln1^{CF-/-}$ mice have a slight increase in *Nppa* under basal conditions at 12-weeks indicating a slight stress response. Therefore, comparing the AngII mice with a control for both genotypes may elucidate more genetic changes that were masked by only comparing mice that were exposed to AngII-injury in our current study.

In the present RNA sequencing set up, we use LV tissue, resulting in the changes seen in the RNA sequencing mostly reflecting changes in cardiomyocytes since they are producing most of the RNA used in this study. This could be masking CF changes. In order to highlight only CF changes in the $Tln2^{-/-}$;$Tln1^{CF-/-}$ and $Tln2^{-/-}$ cells, we could alter our breeding strategy such that our control animals express $Tcf21^{MCM}$ and the *Rosa26* td-Tomato reporter but do not have the $Tln1^{fl/fl}$ allele. This would ensure that all *Tcf21*+ CFs are fluorescent in both the control and the experimental groups, but only the experimental group would lack *Tln1* expression. Then, injured and sham hearts could collected and flow sorted for only Td-Tomato+ cells. These cells could then be used for RNA sequencing to determine the genetic changes specifically between CFs in both the $Tln2^{-/-}$ and $Tln2^{-/-}$;$Tln1^{CF-/-}$ mice.

Collectively, the work presented in this dissertation contributes to the understanding of Tln1 and Tln2 function in CFs and myofibroblasts in cardiovascular pathologies, specifically pressure overload induced hypertension. This work applies a variety of tools to garner a better understanding of interstitial fibrosis which could be applied to other fibrotic processes. This includes the creation and validation of two novel genetic mice in multiple models of cardiovascular disease. Lastly, this work highlights the interconnectedness of cardiomyocytes, CFs, and the ECM in the heart, and that changing the response of one to cardiac injury results in indirect changes in the others.

REFERENCES

1. Masoudi FA, Havranek EP, Smith G, et al. Gender, age, and heart failure with preserved left ventricular systolic function. *J Am Coll Cardiol*. 2003;41(2):217-223. doi:10.1016/S0735-1097(02)02696-7

2. Roger VL, Weston SA, Redfield MM, et al. Trends in Heart Failure Incidence and Survival in a Community-Based Population. *JAMA*. 2004;292(3):344. doi:10.1001/jama.292.3.344

3. Mozaffarian D, Benjamin EJ, Go AS, et al. Executive Summary: Heart Disease and Stroke Statistics—2016 Update A Report From the American Heart Association. *Circulation*. 2016;133:447-454. doi:10.1161/CIR.0000000000000366

4. Hawkins NM, Petrie MC, Jhund PS, Chalmers GW, Dunn FG, McMurray JJV. Heart failure and chronic obstructive pulmonary disease: Diagnostic pitfalls and epidemiology. *Eur J Heart Fail*. 2009;11(2):130-139. doi:10.1093/eurjhf/hfn013

5. Song JJ, Ma Z, Wang J, Chen LX, Zhong JC. Gender Differences in Hypertension. *J Cardiovasc Transl Res*. 2020;13(1):47-54. doi:10.1007/S12265-019-09888-Z/TABLES/1

6. What is Heart Failure? | American Heart Association. https://www.heart.org/en/health-topics/heart-failure/what-is-heart-failure. Accessed November 21, 2021.

7. Pfeffer MA. Heart Failure and Hypertension: Importance of Prevention. *Med Clin North Am*. 2017;101(1):19-28. doi:10.1016/J.MCNA.2016.08.012

8. Jessup M, Brozena S. Heart Failure. *http://dx.doi.org/101056/NEJMra021498*. 2009;348(20):2007-2018. doi:10.1056/NEJMRA021498

9. Di Palo KE, Barone NJ. Hypertension and Heart Failure: Prevention, Targets, and Treatment. *Heart Fail Clin*. 2020;16(1):99-106. doi:10.1016/J.HFC.2019.09.001

10. Chugh SS, Reinier K, Teodorescu C, et al. Epidemiology of Sudden Cardiac Death: Clinical and Research Implications. *Prog Cardiovasc Dis*. 2008;51(3):213-228. doi:10.1016/j.pcad.2008.06.003

11. Simmonds SJ, Cuijpers I, Heymans S, Jones EA V. Cellular and Molecular Differences between HFpEF and HFrEF: A Step Ahead in an Improved Pathological Understanding. *Cells*. 2020;9(1):242. doi:10.3390/cells9010242

12. Kass DA, Bronzwaer JGF, Paulus WJ. What mechanisms underlie diastolic dysfunction in heart failure? *Circ Res*. 2004;94(12):1533-1542. doi:10.1161/01.RES.0000129254.25507.d6

13. Tsao CW, Lyass A, Enserro D, et al. Temporal Trends in the Incidence of and Mortality Associated with Heart Failure with Preserved and Reduced Ejection Fraction. *JACC Heart Fail*. 2018;6(8):678. doi:10.1016/J.JCHF.2018.03.006

14. Hogg K, Swedberg K, McMurray J. Heart Failure with Preserved Left Ventricular Systolic Function: Epidemiology, Clinical Characteristics, and Prognosis. *J Am Coll Cardiol*. 2004;43(3):317-327. doi:10.1016/j.jacc.2003.07.046

15. Borlaung BA, Redfield MM. Diastolic and Systolic Heart Failure are Distinct Phenotypes of the Heart Failure Syndrome. *Circulation*. 2011;123(18):2014.

doi:10.1161/CIRCULATIONAHA.110.954388

16. Levy D. The Progression From Hypertension to Congestive Heart Failure. *JAMA J Am Med Assoc*. 1996;275(20):1557. doi:10.1001/JAMA.1996.03530440037034

17. Janicki JS, Brower GL, Gardner JD, Chancey AL, Stewart JA. The dynamic interaction between matrix metalloproteinase activity and adverse myocardial remodeling. *Heart Fail Rev*. 2004;9(1):33-42. doi:10.1023/B:HREV.0000011392.03037.7E

18. González A, Ravassa S, Beaumont J, López B, Díez J. New Targets to Treat the Structural Remodeling of the Myocardium. *J Am Coll Cardiol*. 2011;58(18):1833-1843. doi:10.1016/J.JACC.2011.06.058

19. Gurusamy N, Das DK. Autophagy, Redox Signaling, and Ventricular Remodeling. *Antioxid Redox Signal*. 2009;11(8):1975. doi:10.1089/ARS.2009.2524

20. Tsutsui H, Kinugawa S, Matsushima S. Oxidative stress and heart failure. *Am J Physiol - Hear Circ Physiol*. 2011;301(6):2181-2190. doi:10.1152/AJPHEART.00554.2011/ASSET/IMAGES/LARGE/ZH40121101550006.JPEG

21. Penn MS. The Role of Leukocyte-Generated Oxidants in Left Ventricular Remodeling. *Am J Cardiol*. 2008;101(10):S30-S33. doi:10.1016/J.AMJCARD.2008.02.005

22. Palazzuoli A, Ruocco G, Beltrami M, Nuti R, Cleland JG. Combined use of lung ultrasound, B-type natriuretic peptide, and echocardiography for outcome prediction in patients with acute HFrEF and HFpEF. *Clin Res Cardiol*. 2018;107(7):586-596. doi:10.1007/s00392-018-1221-7

23. Kannan A, Janardhanan R. Hypertension as a risk factor for heart failure. *Curr Hypertens Rep*. 2014;16(7). doi:10.1007/s11906-014-0447-7

24. Gradman AH, Alfayoumi F. From Left Ventricular Hypertrophy to Congestive Heart Failure: Management of Hypertensive Heart Disease. *Prog Cardiovasc Dis*. 2006;48(5):326-341. doi:10.1016/j.pcad.2006.02.001

25. Reboussin DM, Allen NB, Griswold ME, et al. Systematic review for the 2017 ACC/AHA/AAPA/ABC/ ACPM/AGS/APhA/ASH/ASPC/NMA/PCNA guideline for the prevention, detection, evaluation, and management of high blood pressure in adults a report of the American College of Cardiology/American Heart Association Task Force on Clinical practice guidelines. *Hypertension*. 2018;71(6):E116-E135. doi:10.1161/HYP.0000000000000067

26. Whelton PK, Carey RM, Aronow WS, et al. 2017 ACC/AHA/AAPA/ABC/ACPM/AGS/APhA/ ASH/ASPC/NMA/PCNA guideline for the prevention, detection, evaluation, and management of high blood pressure in adults a report of the American College of Cardiology/American Heart Association Task Force on Clinical practice guidelines. *Hypertension*. 2021;71(6):E13-E115. doi:10.1161/HYP.0000000000000065

27. Ettehad D, Emdin CA, Kiran A, et al. Blood pressure lowering for prevention of cardiovascular disease and death: A systematic review and meta-analysis. *Lancet*. 2016;387(10022):957-967. doi:10.1016/S0140-6736(15)01225-8/ATTACHMENT/603C0742-74C8-441A-9C4C-C02740B35023/MMC1.PDF

28. Taylor DA. Hypertensive Crisis A Review of Pathophysiology and Treatment.

doi:10.1016/j.cnc.2015.08.003

29. CV Physiology | Welcome to Cardiovascular Physiology Concepts. https://www.cvphysiology.com/. Accessed November 21, 2021.

30. Rodriguez MA, Kumar SK, De Caro M. Hypertensive crisis. *Cardiol Rev*. 2010;18(2):102-107. doi:10.1097/CRD.0B013E3181C307B7

31. Fischer D, Rossa S, Landmesser U, et al. Endothelial dysfunction in patients with chronic heart failure is independently associated with increased incidence of hospitalization, cardiac transplantation, or death. *Eur Heart J*. 2005;26(1):65-69. doi:10.1093/EURHEARTJ/EHI001

32. Katz SD, Biasucci L, Sabba C, et al. Impaired endothelium-mediated vasodilation in the peripheral vasculature of patients with congestive heart failure. *J Am Coll Cardiol*. 1992;19(5):918-925. doi:10.1016/0735-1097(92)90271-N

33. Kubo SH, Rector TS, Bank AJ, Williams RE, Heifetz SM. Endothelium-dependent vasodilation is attenuated in patients with heart failure. *Circulation*. 1991;84(4):1589-1596. doi:10.1161/01.CIR.84.4.1589

34. Witman MAH, Fjeldstad AS, Mcdaniel J, et al. Vascular Function and the Role of Oxidative Stress in Heart Failure, Heart Transplant, and Beyond. *Hypertension*. 2012;60(3):659-668. doi:10.1161/HYPERTENSIONAHA.112.193318

35. Treasure CB, Vita JA, Cox DA, et al. Endothelium-dependent dilation of the coronary microvasculature is impaired in dilated cardiomyopathy. *Circulation*. 1990;81(3):772-779. doi:10.1161/01.CIR.81.3.772

36. Torre-Amione G, Kapadia S, Benedict C, Oral H, Young JB, Mann DL. Proinflammatory cytokine levels in patients with depressed left ventricular ejection fraction: A report from the studies of left ventricular dysfunction (SOLVD). *J Am Coll Cardiol*. 1996;27(5):1201-1206. doi:10.1016/0735-1097(95)00589-7

37. Marti CN, Gheorghiade M, Kalogeropoulos AP, Georgiopoulou V V., Quyyumi AA, Butler J. Endothelial Dysfunction, Arterial Stiffness, and Heart Failure. *J Am Coll Cardiol*. 2012;60(16):1455-1469. doi:10.1016/J.JACC.2011.11.082

38. Jugdutt BI. Ventricular remodeling after infarction and the extracellular collagen matrix: When is enough enough? *Circulation*. 2003;108(11):1395-1403. doi:10.1161/01.CIR.0000085658.98621.49

39. Kohl P, Camelliti P, Burton FL, Smith GL. Electrical coupling of fibroblasts and myocytes: relevance for cardiac propagation. *J Electrocardiol*. 2005;38(4):45-50. doi:10.1016/J.JELECTROCARD.2005.06.096

40. Kanisicak O, Khalil H, Ivey MJ, et al. Genetic lineage tracing defines myofibroblast origin and function in the injured heart. *Nat Commun*. 2016;7. doi:10.1038/ncomms12260

41. Snider P, Standley KN, Wang J, Azhar M, Doetschman T, Conway SJ. Origin of cardiac fibroblasts and the role of periostin. *Circ Res*. 2009;105(10):934-947. doi:10.1161/CIRCRESAHA.109.201400

42. Porter KE, Turner NA. Cardiac fibroblasts: At the heart of myocardial remodeling. *Pharmacol Ther*. 2009;123(2):255-278. doi:10.1016/J.PHARMTHERA.2009.05.002

43. Weber KT. Cardiac interstitium in health and disease: The fibrillar collagen network. *J Am Coll Cardiol*. 1989;13(7):1637-1652. doi:10.1016/0735-1097(89)90360-4

44. Goshima K, Tonomura Y. Synchronized beating of embryonic mouse myocardial cells mediated by FL cells in monolayer culture. *Exp Cell Res*. 1969;56(2):387-392. doi:10.1016/0014-4827(69)90029-9

45. Suthahar N, Meijers WC, Silljé HHW, de Boer RA. From Inflammation to Fibrosis—Molecular and Cellular Mechanisms of Myocardial Tissue Remodelling and Perspectives on Differential Treatment Opportunities. *Curr Heart Fail Rep*. 2017;14(4):235-250. doi:10.1007/s11897-017-0343-y

46. Chen W, Frangogiannis NG. Fibroblasts in post-infarction inflammation and cardiac repair. 2012. doi:10.1016/j.bbamcr.2012.08.023

47. Dale Brown R, Jones GM, Laird RE, Hudson P, Long CS. Cytokines regulate matrix metalloproteinases and migration in cardiac fibroblasts.

48. Creemers EE, Pinto YM. Molecular mechanisms that control interstitial fibrosis in the pressure-overloaded heart. *Cardiovasc Res*. 2011;89(2):265-272. doi:10.1093/cvr/cvq308

49. Heymans S, González A, Pizard A, et al. Searching for new mechanisms of myocardial fibrosis with diagnostic and/or therapeutic potential. *Eur J Heart Fail*. 2015;17:764-771. doi:10.1002/ejhf.312

50. Hinz B. Formation and function of the myofibroblast during tissue repair. *J Invest Dermatol*. 2007;127(3):526-537. doi:10.1038/sj.jid.5700613

51. Kong P, Christia P, Frangogiannis NG. The pathogenesis of cardiac fibrosis. *Cell Mol Life Sci*. 2014;71(4):549-574. doi:10.1007/s00018-013-1349-6

52. Monkley SJ, Pritchard CA, Critchley DR. Analysis of the Mammalian Talin2 Gene TLN2. *Biochem Biophys Res Commun*. 2001;286(5):880-885. doi:10.1006/BBRC.2001.5497

53. Desmoulire A, Redard M, Darby I, Gabbiani G. Apoptosis Mediates the Decrease in Cellularity during the Transition between Granulation Tissue and Scar. *Ame?ican jouirnal Pathol*. 1995;146(1).

54. Tyagi SC, Campbell SE, Reddy HK, Tjahja E, Voelker DJ. Matrix metailoproteinase activity expression in infarcted, noninfarcted and dilated cardiomyopathic human hearts. *Mol Cell Biochem*. 1996;155:13-21.

55. Li Y-Q, Ballinger JR, Nordal RA, Su Z-F, Wong CS. Hypoxia in Radiation-induced Blood-Spinal Cord Barrier Breakdown. *CANCER Res*. 2001;61:3348-3354. http://cancerres.aacrjournals.org/content/canres/61/8/3348.full.pdf. Accessed July 14, 2017.

56. Thomas C V., Coker ML, Zellner JL, Handy JR, Crumbley AJ, Spinale FG. Increased Matrix Metalloproteinase Activity and Selective Upregulation in LV Myocardium From Patients With End-Stage Dilated Cardiomyopathy. *Circulation*. 1998;97(17):1708-1715. doi:10.1161/01.CIR.97.17.1708

57. Pan CH, Wen CH, Lin CS. Interplay of angiotensin II and angiotensin(1–7) in the regulation of matrix metalloproteinases of human cardiocytes. *Exp Physiol*. 2008;93(5):599-612. doi:10.1113/EXPPHYSIOL.2007.041830

58. Crabos M, Roth M, Hahn AWA, Erne P. Characterization of angiotensin II receptors in cultured adult rat cardiac fibroblasts. Coupling to signaling systems and gene expression. *J Clin Invest*. 1994;93(6):2372. doi:10.1172/JCI117243

59. Baicu CF, Stroud JD, Livesay VA, et al. Changes in extracellular collagen matrix alter myocardial systolic performance. *Am J Physiol - Hear Circ Physiol*. 2003;284(1 53-1):122-132. doi:10.1152/AJPHEART.00233.2002/ASSET/IMAGES/LARGE/H40132011008.JPEG

60. Wang J, Hoshijima M, Lam J, et al. Cardiomyopathy associated with microcirculation dysfunction in laminin α4 chain-deficient mice. *J Biol Chem*. 2006;281(1):213-220. doi:10.1074/JBC.M505061200/ATTACHMENT/19E00D6A-1BA9-4458-A568-E64998061A07/MMC1.PDF

61. Role of Myocardial Collagen in Severe Aortic Stenosis With Preserved Ejection Fraction and Symptoms of Heart Failure. https://www.revespcardiol.org/en-linkresolver-role-myocardial-collagen-in-severe-S1885585716304625. Accessed November 19, 2021.

62. Kasner M, Westermann D, Lopez B, et al. Diastolic Tissue Doppler Indexes Correlate With the Degree of Collagen Expression and Cross-Linking in Heart Failure and Normal Ejection Fraction. *J Am Coll Cardiol*. 2011;57(8):977-985. doi:10.1016/J.JACC.2010.10.024

63. Yajima T. Viral myocarditis: potential defense mechanisms within the cardiomyocyte against virus infection. *Future Microbiol*. 2011;6(5):551. doi:10.2217/FMB.11.40

64. Seferovic´1 PM, Seferovic´1 S, Paulus WJ. Clinical diabetic cardiomyopathy: a two-faced disease with restrictive and dilated phenotypes. doi:10.1093/eurheartj/ehv134

65. Post-ischemic apoptotic death of rat neonatal cardiomyocytes - PubMed. https://pubmed.ncbi.nlm.nih.gov/17180028/. Accessed November 19, 2021.

66. Cheng W, Li B, Kajstura J, et al. Stretch-induced programmed myocyte cell death. *J Clin Invest*. 1995;96(5):2247. doi:10.1172/JCI118280

67. Zile MR, Gaasch WH, Carroll JD, et al. Heart Failure With a Normal Ejection Fraction. *Circulation*. 2001;10(2):72-75. doi:10.1161/HC3201.094226

68. Zile MR, Gottdiener JS, Hetzel SJ, et al. Prevalence and significance of alterations in cardiac structure and function in patients with heart failure and a preserved ejection fraction. *Circulation*. 2011;124(23):2491-2501. doi:10.1161/CIRCULATIONAHA.110.011031

69. A Randomized Trial of Intensive versus Standard Blood-Pressure Control. *N Engl J Med*. 2015;373(22):2103-2116. doi:10.1056/NEJMOA1511939/SUPPL_FILE/NEJMOA1511939_DISCLOSURES.PDF

70. Mozaffarian D, Benjamin EJ, Go AS, et al. Heart Disease and Stroke Statistics—2015 Update. *Circulation*. 2015;131(4):e29-e39. doi:10.1161/CIR.0000000000000152

71. Sciarretta S, Palano F, Tocci G, Baldini R, Volpe M. Antihypertensive Treatment and Development of Heart Failure in Hypertension: A Bayesian Network Meta-analysis of Studies in Patients With Hypertension and High Cardiovascular Risk. *Arch Intern Med*. 2011;171(5):384-394. doi:10.1001/ARCHINTERNMED.2010.427

72. Program NHBPE. The Seventh Report of the Joint National Committee on Prevention,

Detection, Evaluation, and Treatment of High Blood Pressure. *Seventh Rep Jt Natl Comm Prev Detect Eval Treat High Blood Press*. 2004. https://www.ncbi.nlm.nih.gov/books/NBK9630/. Accessed November 19, 2021.

73. Ferdinand KC, Nasser SA. Management of Essential Hypertension. doi:10.1016/j.ccl.2016.12.005

74. Ogawa R. Mechanobiology and Mechanotherapy in Tissue Engineering. *Situ Tissue Regen Host Cell Recruit Biomater Des*. January 2016:165-181. doi:10.1016/B978-0-12-802225-2.00009-X

75. Samarel AM. Costameres, focal adhesions, and cardiomyocyte mechanotransduction. *Am J Physiol - Hear Circ Physiol*. 2005;289(6 58-6):2291-2301. doi:10.1152/AJPHEART.00749.2005/ASSET/IMAGES/LARGE/ZH40120563640003.JPEG

76. Goult BT, Brown NH, Schwartz MA. Talin in mechanotransduction and mechanomemory at a glance. *J Cell Sci*. 2021;134(20). doi:10.1242/JCS.258749

77. Block MR, Badowski C, Millon-Fremillon A, et al. Podosome-type adhesions and focal adhesions, so alike yet so different. *Eur J Cell Biol*. 2008;87(8-9):491-506. doi:10.1016/J.EJCB.2008.02.012

78. Revach OY, Grosheva I, Geiger B. Biomechanical regulation of focal adhesion and invadopodia formation. *J Cell Sci*. 2020;133(20). doi:10.1242/JCS.244848/226348

79. Zaidel-Bar R, Cohen M, Addadi L, Geiger B. Hierarchical assembly of cell-matrix adhesion complexes. *416 Biochem Soc Trans*. 2004;32. http://portlandpress.com/biochemsoctrans/article-pdf/32/3/416/534276/bst0320416.pdf. Accessed November 8, 2021.

80. Schwartz MA, Ginsberg MH. Networks and crosstalk: integrin signalling spreads. *Nat Cell Biol 2002 44*. 2002;4(4):E65-E68. doi:10.1038/ncb0402-e65

81. Clark EA, Brugge JS. Integrins and Signal Transduction Pathways: the Road Taken. *Science (80-)*. 1995;268(5208):233-239. doi:10.1126/SCIENCE.7716514

82. Hynes RO. Integrins: Bidirectional, Allosteric Signaling Machines. *Cell*. 2002;110(6):673-687. doi:10.1016/S0092-8674(02)00971-6

83. Hynes RO. Integrins: A family of cell surface receptors. *Cell*. 1987;48(4):549-554. doi:10.1016/0092-8674(87)90233-9

84. Giancotti FG, Ruoslahti E. Integrin signaling. *Science (80-)*. 1999;285(5430):1028-1032. doi:10.1126/SCIENCE.285.5430.1028/ASSET/DB7B6FCE-5D55-4DBF-8CD7-FACB4F1228FD/ASSETS/GRAPHIC/SE3097724004.JPEG

85. Takada Y, Ye X, Simon S. The integrins Gene organization and evolutionary history. *Genome Biol*. 2007;8:215. doi:10.1186/gb-2007-8-5-215

86. Calderwood DA, Zent R, Grant R, Rees DJG, Hynes RO, Ginsberg MH. The Talin Head Domain Binds to Integrin β Subunit Cytoplasmic Tails and Regulates Integrin Activation. *J Biol Chem*. 1999;274(40):28071-28074. doi:10.1074/JBC.274.40.28071

87. Calderwood DA. Talin controls integrin activation. *434 Biochem Soc Trans*. 2004;32. http://portlandpress.com/biochemsoctrans/article-pdf/32/3/434/534284/bst0320434.pdf.

Accessed November 8, 2021.

88. Israeli-Rosenberg S, Manso AM, Okada H, Ross RS. Integrins and Integrin-Associated Proteins in the Cardiac Myocyte. doi:10.1161/CIRCRESAHA.114.301275

89. Ross RS, Borg TK. Integrins and the Myocardium. *Circ Res*. 2001;88(11):1112-1119. doi:10.1161/HH1101.091862

90. Ross RS. The extracellular connections: The role of integrins in myocardial remodeling. *J Card Fail*. 2002;8(6):S326-S331. doi:10.1054/JCAF.2002.129263

91. Belkin AM, Retta SF, Pletjushkina OY, et al. Muscle β1D Integrin Reinforces the Cytoskeleton–Matrix Link: Modulation of Integrin Adhesive Function by Alternative Splicing. *J Cell Biol*. 1997;139(6):1583. doi:10.1083/JCB.139.6.1583

92. Krishnamurthy P, Subramanian V, Singh M, Singh K. Deficiency of β1 integrins results in increased myocardial dysfunction after myocardial infarction. *Heart*. 2006;92(9):1309. doi:10.1136/HRT.2005.071001

93. Terracio L, Gullberg D, Rubin K, Craig S, Borg TK. Expression of collagen adhesion proteins and their association with the cytoskeleton in cardiac myocytes. *Anat Rec*. 1989;223(1):62-71. doi:10.1002/AR.1092230110

94. Maitra N, Flink IL, Bahl JJ, Morkin E. Expression of a and b integrins during terminal differentiation of cardiomyocytes. *Cardiovasc Res*. 2000;47:715-725. www.elsevier.com/locate/cardioreswww.elsevier.nl/locate/cardiores. Accessed November 27, 2021.

95. Sun M, Anne Opavsky M, Stewart DJ, et al. Temporal Response and Localization of Integrins 1 and 3 in the Heart After Myocardial Infarction Regulation by Cytokines. 2003. doi:10.1161/01.CIR.0000051363.86009.3C

96. Fan D, Takawale A, Lee J, Kassiri Z. Cardiac fibroblasts, fibrosis and extracellular matrix remodeling in heart disease. doi:10.1186/1755-1536-5-15

97. Burgess ML, Carver WE, Terracio L, Wilson SP, Wilson MA, Borg TK. Integrin-mediated collagen gel contraction by cardiac fibroblasts. Effects of angiotensin II. *Circ Res*. 1994;74(2):291-298. doi:10.1161/01.RES.74.2.291

98. Thibault G, Lacombe M-J, Schnapp LM, Lacasse A, Bouzeghrane F, Lapalme G. Upregulation of α8β1-integrin in cardiac fibroblast by angiotensin II and transforming growth factor-β1. *https://doi.org/101152/ajpcell20012815C1457*. 2001;281(5 50-5). doi:10.1152/AJPCELL.2001.281.5.C1457

99. Bouzeghrane F, Mercure C, Reudelhuber TL, Thibault G. α8β1 integrin is upregulated in myofibroblasts of fibrotic and scarring myocardium. *J Mol Cell Cardiol*. 2004;36(3):343-353. doi:10.1016/J.YJMCC.2003.11.007

100. Critchley DR. Biochemical and Structural Properties of the Integrin- Associated Cytoskeletal Protein Talin. 2009. doi:10.1146/annurev.biophys.050708.133744

101. Klapholz B, Brown NH. Talin – the master of integrin adhesions. *J Cell Sci*. 2017;130(15):2435-2446. doi:10.1242/jcs.190991

102. Dedden D, Schumacher S, Kelley CF, et al. The Architecture of Talin1 Reveals an Autoinhibition Mechanism. *Cell*. 2019;179(1):120-131.e13.

doi:10.1016/J.CELL.2019.08.034

103. Goksoy E, Ma YQ, Wang X, et al. Structural Basis for the Autoinhibition of Talin in Regulating Integrin Activation. *Mol Cell*. 2008;31(1):124-133. doi:10.1016/J.MOLCEL.2008.06.011

104. Goult BT, Xu XP, Gingras AR, et al. Structural studies on full-length talin1 reveal a compact auto-inhibited dimer: Implications for talin activation. *J Struct Biol*. 2013;184(1):21-32. doi:10.1016/J.JSB.2013.05.014

105. Horwitz A, Duggan K, Buck C, Beckerle MC, Burridge K. Interaction of plasma membrane fibronectin receptor with talin - A transmembrane linkage. *Nature*. 1986;320(6062):531-533. doi:10.1038/320531a0

106. Tadokoro S, Shattil SJ, Eto K, et al. Talin Binding to Integrin ß Tails: A Final Common Step in Integrin Activation. *Science (80-)*. 2003;302(5642):103-106. doi:10.1126/SCIENCE.1086652

107. Kim C, Ye F, Ginsberg MH. Regulation of Integrin Activation. 2011. doi:10.1146/annurev-cellbio-100109-104104

108. Mathew S, Palamuttam RJ, Mernaugh G, et al. Talin regulates integrin β1-dependent and -independent cell functions in ureteric bud development. *Dev*. 2017;144(22):4148-4158. doi:10.1242/DEV.149914/VIDEO-4

109. Cram EJ, Clark SG, Schwarzbauer JE. Talin loss-of-function uncovers roles in cell contractility and migration in C. elegans. *J Cell Sci*. 2003;116(19):3871-3878. doi:10.1242/JCS.00705

110. Brown NH, Gregory SL, Rickoll WL, et al. Talin Is Essential for Integrin Function in Drosophila. *Dev Cell*. 2002;3(4):569-579. doi:10.1016/S1534-5807(02)00290-3

111. Monkley SJ, Zhou XH, Kinston SJ, et al. Disruption of the talin gene arrests mouse development at the gastrulation stage. *Dev Dyn*. 2000;219(4):560-574. doi:10.1002/1097-0177(2000)9999:9999<::AID-DVDY1079>3.0.CO;2-Y

112. Atherton P, Stutchbury B, Wang D-Y, et al. Vinculin controls talin engagement with the actomyosin machinery. *Nat Commun*. 2015;6. doi:10.1038/ncomms10038

113. Goult BT, Zacharchenko T, Bate N, et al. RIAM and vinculin binding to talin are mutually exclusive and regulate adhesion assembly and turnover. *J Biol Chem*. 2013;288(12):8238-8249. doi:10.1074/jbc.M112.438119

114. Vigouroux C, Henriot V, Le Clainche C. Talin dissociates from RIAM and associates to vinculin sequentially in response to the actomyosin force. doi:10.1038/s41467-020-16922-1

115. Gingras AR, Ziegler WH, Frank R, et al. Mapping and Consensus Sequence Identification for Multiple Vinculin Binding Sites within the Talin Rod. *J Biol Chem*. 2005;280(44):37217-37224. doi:10.1074/JBC.M508060200

116. Yao M, Goult BT, Chen H, Cong P, Sheetz MP, Yan J. Mechanical activation of vinculin binding to talin locks talin in an unfolded conformation. *Sci Reports 2014 41*. 2014;4(1):1-7. doi:10.1038/srep04610

117. Yao M, Goult BT, Klapholz B, et al. The mechanical response of talin. *Nat Commun 2016*

71. 2016;7(1):1-11. doi:10.1038/ncomms11966

118. Kumar A, Anderson KL, Swift MF, Hanein D, Volkmann N, Schwartz MA. Local Tension on Talin in Focal Adhesions Correlates with F-Actin Alignment at the Nanometer Scale. *Biophys J*. 2018;115(8):1569-1579. doi:10.1016/j.bpj.2018.08.045

119. Senetar MA, Foster SJ, Mccann RO. Intrasteric Inhibition Mediates the Interaction of the I/LWEQ Module Proteins Talin1, Talin2, Hip1, and Hip12 with Actin †. 2004. doi:10.1021/bi0487239

120. Anthis NJ, Wegener KL, Ye F, et al. The structure of an integrin/talin complex reveals the basis of inside-out signal transduction. *EMBO J*. 2009;28:3623-3632. doi:10.1038/emboj.2009.287

121. Anthis NJ, Wegener KL, Critchley DR, Campbell ID. Structural Diversity in Integrin/Talin Interactions. *Structure*. 2010;18(12):1654. doi:10.1016/J.STR.2010.09.018

122. Conti FJ, Monkley SJ, Wood MR, Critchley DR, Muller U. Talin 1 and 2 are required for myoblast fusion, sarcomere assembly and the maintenance of myotendinous junctions. *Development*. 2009;136(21):3597-3606. doi:10.1242/dev.035857

123. Conti FJ, Monkley SJ, Wood MR, Critchley DR, Müller U. Talin 1 and 2 are required for myoblast fusion, sarcomere assembly and the maintenance of myotendinous junctions. *Development*. 2009;136(21):3597. doi:10.1242/DEV.035857

124. Conti FJ, Felder A, Monkley S, et al. Progressive myopathy and defects in the maintenance of myotendinous junctions in mice that lack talin 1 in skeletal muscle. *Development*. 2008;135(11):2043. doi:10.1242/DEV.015818

125. Theodosiou M, Widmaier M, Böttcher RT, et al. Kindlin-2 cooperates with talin to activate integrins and induces cell spreading by directly binding paxillin. *Elife*. 2016;5(JANUARY2016). doi:10.7554/ELIFE.10130

126. Manso AM, Li R, Monkley SJ, et al. Talin1 Has Unique Expression versus Talin 2 in the Heart and Modifies the Hypertrophic Response to Pressure Overload. *J Biol Chem*. 2013;288(6):4252. doi:10.1074/JBC.M112.427484

127. Manso AM, Okada H, Sakamoto FM, et al. Loss of mouse cardiomyocyte talin-1 and talin-2 leads to β-1 integrin reduction, costameric instability, and dilated cardiomyopathy. *Proc Natl Acad Sci*. 2017;114(30):E6250-E6259. doi:10.1073/pnas.1701416114

128. Manso AM, Li R, Monkley SJ, et al. Talini has unique expression versus talin 2 in the heart and modifies the hypertrophic response to pressure overload. *J Biol Chem*. 2013;288(6):4252-4264. doi:10.1074/jbc.M112.427484

129. Uhl EW, Warner NJ. Mouse Models as Predictors of Human Responses: Evolutionary Medicine. 2015. doi:10.1007/s40139-015-0086-y

130. Riehle C, Bauersachs J. Of mice and men: models and mechanisms of diabetic cardiomyopathy. 2019;114(2). doi:10.1007/s00395-018-0711-0

131. Lamb HJ, Beyerbacht HP, Van Der Laarse A, et al. Diastolic dysfunction in hypertensive heart disease is associated with altered myocardial metabolism. *Circulation*. 1999;99(17):2261-2267. doi:10.1161/01.CIR.99.17.2261

132. Berenji K, Drazner MH, Rothermel BA, Hill JA. Does load-induced ventricular hypertrophy

progress to systolic heart failure? *Am J Physiol - Hear Circ Physiol*. 2005;289(1 58-1):8-16. doi:10.1152/ajpheart.01303.2004

133. Hartner A, Cordasic N, Klanke B, Veelken R, Hilgers KF. Strain differences in the development of hypertension and glomerular lesions induced by deoxycorticosterone acetate salt in mice. *Nephrol Dial Transplant*. 2003;18(10):1999-2004. doi:10.1093/ndt/gfg299

134. Karatas A, Hegner B, De Windt LJ, et al. Deoxycorticosterone acetate-salt mice exhibit blood pressure-independent sexual dimorphism. *Hypertension*. 2008;51(4 PART 2 SUPPL.):1177-1183. doi:10.1161/HYPERTENSIONAHA.107.107938

135. Westermann D, Becher PM, Lindner D, et al. Selective PDE5A inhibition with sildenafil rescues left ventricular dysfunction, inflammatory immune response and cardiac remodeling in angiotensin II-induced heart failure in vivo. *Basic Res Cardiol*. 2012;107(6). doi:10.1007/s00395-012-0308-y

136. Kirchhoff F, Krebs C, Abdulhag UN, et al. Rapid development of severe end-organ damage in C57BL/6 mice by combining DOCA salt and angiotensin II. *Kidney Int*. 2008;73(5):643-650. doi:10.1038/sj.ki.5002689

137. Mohammed-Ali Z, Cruz GL, Lu C, et al. Development of a model of chronic kidney disease in the C57BL/6 mouse with properties of progressive human CKD. *Biomed Res Int*. 2015;2015:1-10. doi:10.1155/2015/172302

138. Montani D, Simonneau G. Updated clinical classification of pulmonary hypertension. In: Humber M, Souza R, Simonneau G, eds. *Pulmonary Vascular Disorders*. Vol 41. Karger; 2012:1-13. doi:10.1159/000334959

139. Cappola TP, Felker GM, Kao WHL, Hare JM, Baughman KL, Kasper EK. Pulmonary hypertension and risk of death in cardiomyopathy: Patients with myocarditis are at higher risk. *Circulation*. 2002;105(14):1663-1668. doi:10.1161/01.CIR.0000013771.30198.82

140. Delgado JF, Conde E, Sánchez V, et al. Pulmonary vascular remodeling in pulmonary hypertension due to chronic heart failure. *Eur J Heart Fail*. 2005;7(6):1011-1016. doi:10.1016/j.ejheart.2004.10.021

141. Leung CC, Moondra V, Catherwood E, Andrus BW. Prevalence and risk factors of pulmonary hypertension in patients with elevated pulmonary venous pressure and preserved ejection fraction. *Am J Cardiol*. 2010;106(2):284-286. doi:10.1016/j.amjcard.2010.02.039

142. Meng Q, Lai YC, Kelly NJ, et al. Development of a mouse model of metabolic syndrome, pulmonary hypertension, and heart failure with preserved ejection fraction. *Am J Respir Cell Mol Biol*. 2017;56(4):497-505. doi:10.1165/rcmb.2016-0177OC

143. Garcia MJ, McNamara PM, Gordon T, Kannell WB. Morbidity and mortality in diabetics in the Framingham population. Sixteen year follow up study. *Diabetes*. 1974;23(2):105-111. doi:10.2337/diab.23.2.105

144. Cavaghan MK, Ehrmann DA, Polonsky KS. Interactions between insulin resistance and insulin secretion in the development of glucose intolerance. *J Clin Invest*. 2000;106(3):329-333. doi:10.1172/JCI10761

145. Hayden JM, Reaven PD. Cardiovascular disease in diabetes mellitus type 2: a potential role for novel cardiovascular risk factors. *Curr Opin Lipidol*. 2000;11(5):519-528.

http://www.ncbi.nlm.nih.gov/pubmed/11048895. Accessed October 9, 2019.

146. Semeniuk LM, Kryski AJ, Severson DL. Echocardiographic assessment of cardiac function in diabetic db/db and transgenic db/db-hGLUT4 mice. *Am J Physiol - Hear Circ Physiol*. 2002;283(3 52-3). doi:10.1152/ajpheart.00088.2002

147. Buchanan J, Mazumder PK, Hu P, et al. Reduced cardiac efficiency and altered substrate metabolism precedes the onset of hyperglycemia and contractile dysfunction in two mouse models of insulin resistance and obesity. *Endocrinology*. 2005;146(12):5341-5349. doi:10.1210/en.2005-0938

148. Christoffersen C, Bollano E, Lindegaard MLS, et al. Cardiac lipid accumulation associated with diastolic dysfunction in obese mice. *Endocrinology*. 2003;144(8):3483-3490. doi:10.1210/en.2003-0242

149. Stuckey DJ, Carr CA, Tyler DJ, Aasum E, Clarke K. Novel MRI method to detect altered left ventricular ejection and filling patterns in rodent models of disease. *Magn Reson Med*. 2008;60(3):582-587. doi:10.1002/mrm.21677

150. Senador D, Kanakamedala K, Irigoyen MC, Morris M, Elased KM. Cardiovascular and autonomic phenotype of db/db diabetic mice. *Exp Physiol*. 2009;94(6):648-658. doi:10.1113/expphysiol.2008.046474

151. Kashyap SR, DeFronzo RA. The insulin resistance syndrome: Physiological considerations. *Diabetes Vasc Dis Res*. 2007;4(1):13-19. doi:10.3132/dvdr.2007.001

152. Anstee QM, Goldin RD. Mouse models in non-alcoholic fatty liver disease and steatohepatitis research. *Int J Exp Pathol*. 2006;87(1):1-16. doi:10.1111/j.0959-9673.2006.00465.x

153. Type 1 Diabetes | NIDDK. https://www.niddk.nih.gov/health-information/diabetes/overview/what-is-diabetes/type-1-diabetes#whatis. Accessed November 27, 2021.

154. Liu M, Sun J, Cui J, et al. INS-gene mutations: From genetics and beta cell biology to clinical disease. *Mol Aspects Med*. 2015;42:3-18. doi:10.1016/j.mam.2014.12.001

155. Bugger H, Abel ED. Molecular mechanisms for myocardial mitochondrial dysfunction in the metabolic syndrome. *Clin Sci*. 2008;114(3-4):195-210. doi:10.1042/CS20070166

156. Lu Z, Jiang YP, Xu XH, Ballou LM, Cohen IS, Lin RZ. Decreased L-type Ca2+ current in cardiac myocytes of type 1 diabetic akita mice due to reduced phosphatidylinositol 3-kinase signaling. *Diabetes*. 2007;56(11):2780-2789. doi:10.2337/db06-1629

157. Wang Z, Gleichmann H. GLUT2 in pancreatic islets: Crucial target molecule in diabetes induced with multiple low doses of streptozotocin in mice. *Diabetes*. 1998;47(1):50-56. doi:10.2337/diab.47.1.50

158. Kajstura J, Fiordaliso F, Andreoli AM, et al. IGF-1 0verexpression inhibits the development of diabetic cardiomyopathy and angiotensin II-mediated oxidative stress. *Diabetes*. 2001;50(6):1414-1424. doi:10.2337/diabetes.50.6.1414

159. Lacombe VA, Viatchenko-Karpinski S, Terentyev D, et al. Mechanisms of impaired calcium handling underlying subclinical diastolic dysfunction in diabetes. *Am J Physiol - Regul Integr Comp Physiol*. 2007;293(5):1787-1797. doi:10.1152/ajpregu.00059.2007

160. Epstein PN, Overbeek PA, Means AR. Calmodulin-induced early-onset diabetes in transgenic mice. *Cell*. 1989;58(6):1067-1073. doi:10.1016/0092-8674(89)90505-9

161. Qian LB, Jiang SZ, Tang XQ, et al. Exacerbation of diabetic cardiac hypertrophy in OVE26 mice by angiotensin II is associated with JNK/c-Jun/miR-221-mediated autophagy inhibition. *Oncotarget*. 2017;8(63):106661-106671. doi:10.18632/oncotarget.21302

162. Wang CY, Liao JK. A mouse model of diet-induced obesity and insulin resistance. *Methods Mol Biol*. 2012;821:421-433. doi:10.1007/978-1-61779-430-8_27

163. Wright RJ, Frier BM, Deary IJ. Effects of acute insulin-induced hypoglycemia on spatial abilities in adults with type 1 diabetes. *Diabetes Care*. 2009;32(8):1503-1506. doi:10.2337/dc09-0212

164. Chiang SH, Harrington WW, Luo G, et al. Genetic ablation of CD38 protects against Western diet-induced exercise intolerance and metabolic inflexibility. *PLoS One*. 2015;10(8). doi:10.1371/journal.pone.0134927

165. Cox LS, Mattison JA. Increasing longevity through caloric restriction or rapamycin feeding in mammals: Common mechanisms for common outcomes? *Aging Cell*. 2009;8(5):607-613. doi:10.1111/j.1474-9726.2009.00509.x

166. Agrimi J, Spalletti C, Baroni C, et al. Obese mice exposed to psychosocial stress display cardiac and hippocampal dysfunction associated with local brain-derived neurotrophic factor depletion. 2019. doi:10.1016/j.ebiom.2019.08.042

167. Chen J, Dharmarajan K, Wang Y, Krumholz HM. National Trends in Heart Failure Hospitalization Rates, 2001– 2009. *Jounal Am Coll Cardiol*. 2013;61(10):1078-1088. https://www.ncbi.nlm.nih.gov/pmc/articles/PMC3939721/pdf/nihms497495.pdf. Accessed October 9, 2019.

168. Takeda T, Matsushita T, Kurozumi M, Takemura K, Higuchi K, Hosokawa M. Pathobiology of the Senescence-Accelerated Mouse (SAM). *Exp Gerontol*. 1997;32(1-2):117-127. doi:10.1016/S0531-5565(96)00068-X

169. Reed AL, Tanaka A, Sorescu D, et al. Diastolic dysfunction is associated with cardiac fibrosis in the senescence-accelerated mouse. *Am J Physiol Heart Circ Physiol*. 2011;301(3):H824-31. doi:10.1152/ajpheart.00407.2010

170. Clark TA, Pierce GN. Cardiovascular complications of non-insulin-dependent diabetes: The JCR:LA-cp rat. *J Pharmacol Toxicol Methods*. 2000;43(1):1-10. doi:10.1016/S1056-8719(00)00081-2

171. Muller YD, Golshayan D, Ehirchiou D, et al. Immunosuppressive Effects of Streptozotocin-Induced Diabetes Result in Absolute Lymphopenia and a Relative Increase of T Regulatory Cells. *diabetes.diabetesjournals.org DIABETES*. 2011;60. doi:10.2337/db11-0159

172. Goldfracht I, Efraim Y, Shinnawi R, et al. Engineered heart tissue models from hiPSC-derived cardiomyocytes and cardiac ECM for disease modeling and drug testing applications. *Acta Biomater*. 2019;92:145-159. doi:10.1016/j.actbio.2019.05.016

173. Burridge PW, Li YF, Matsa E, et al. Human Induced Pluripotent Stem Cell-Derived Cardiomyocytes Recapitulate the Predilection of Breast Cancer Patients to Doxorubicin-Induced Cardiotoxicity HHS Public Access Author manuscript. *Nat Med*. 2016;22(5):547-556. doi:10.1038/nm.4087

174. Rockman HA, Ono S, Ross RS, et al. Molecular and physiological alterations in murine ventricular dysfunction. *Proc Natl Acad Sci U S A*. 1994;91(7):2694-2698. doi:10.1073/pnas.91.7.2694

175. Mustonen E, Leskinen H, Aro J, et al. Metoprolol treatment lowers thrombospondin-4 expression in rats with myocardial infarction and left ventricular hypertrophy. *Basic Clin Pharmacol Toxicol*. 2010;107(3):709-717. doi:10.1111/j.1742-7843.2010.00564.x

176. Mohammed SF, Storlie JR, Oehler EA, et al. Variable phenotype in murine transverse aortic constriction. *Cardiovasc Pathol*. 2012;21:188-198. doi:10.1016/j.carpath.2011.05.002

177. Ichinose F, Bloch KD, Wu JC, et al. Pressure overload-induced LV hypertrophy and dysfunction in mice are exacerbated by congenital NOS3 deficiency. *Am J Physiol - Hear Circ Physiol*. 2004;286(3 55-3):1070-1075. doi:10.1152/ajpheart.00940.2003

178. Hu P, Zhang D, Swenson LA, Chakrabarti G, Abel ED, Litwin SE. Minimally invasive aortic banding in mice: Effects of altered cardiomyocyte insulin signaling during pressure overload. *Am J Physiol - Hear Circ Physiol*. 2003;285(3 54-3):1261-1269. doi:10.1152/ajpheart.00108.2003

179. Dealmeida AC, Van Oort RJ, Wehrens XHT. Transverse Aortic Constriction in Mice. *JoVE*. 2010;38. doi:10.3791/1729

180. Merino D, Gil A, Gómez J, et al. Experimental modelling of cardiac pressure overload hypertrophy: Modified technique for precise, reproducible, safe and easy aortic arch banding-debanding in mice. *Sci Rep*. 2018;8(1):3167. doi:10.1038/s41598-018-21548-x

181. Sawall S, Franke D, Kirchherr A, et al. In vivo quantification of myocardial infarction in mice using micro-CT and a novel blood pool agent. *Contrast Media Mol Imaging*. 2017;2017. doi:10.1155/2017/2617047

182. Van Craeyveld E, Jacobs F, Gordts SC, De Geest B. Low-density lipoprotein receptor gene transfer in hypercholesterolemic mice improves cardiac function after myocardial infarction. *Gene Ther*. 2012;19(8):860-871. doi:10.1038/gt.2011.147

183. Swynghedauw B. Molecular mechanisms of myocardial remodeling. *Physiol Rev*. 1999;79(1):215-262. doi:10.1152/physrev.1999.79.1.215

184. Ertl G, Frantz S. Healing after myocardial infarction. *Cardiovasc Res*. 2005;66(1):22-32. doi:10.1016/j.cardiores.2005.01.011

185. Dayeh NR, Tardif JC, Shi Y, Tanguay M, Ledoux J, Dupuis J. Echocardiographic validation of pulmonary hypertension due to heart failure with reduced ejection fraction in mice. *Sci Rep*. 2018;8(1):1363. doi:10.1038/s41598-018-19625-2

186. Go AS, Mozaffarian D, Roger VL, et al. Heart Disease and Stroke Statistics—2013 Update. *Circulation*. 2013;127(1):6-245. doi:10.1161/cir.0b013e31828124ad

187. Xu Z, Alloush J, Beck E, Weisleder N. A murine model of myocardial ischemia-reperfusion injury through ligation of the left anterior descending artery. *J Vis Exp*. 2014;(86):51329. doi:10.3791/51329

188. Rai V, Sharma P, Agrawal S, Agrawal DK. Relevance of mouse models of cardiac fibrosis and hypertrophy in cardiac research. *Mol Cell Biochem*. 2017;424(1-2):123-145. doi:10.1007/s11010-016-2849-0

189. Weinheimer CJ, Lai L, Kelly DP, Kovacs A. Novel mouse model of left ventricular pressure overload and infarction causing predictable ventricular remodelling and progression to heart failure. *Clin Exp Pharmacol Physiol*. 2015;42(1):33-40. doi:10.1111/1440-1681.12318

190. Wang Q, Chen K, Lin H, et al. Induction of Right Ventricular Failure by Pulmonary Artery Constriction and Evaluation of Right Ventricular Function in Mice. *J Vis Exp*. 2019;(147). doi:10.3791/59431

191. Urashima T, Zhao M, Wagner R, et al. Molecular and physiological characterization of RV remodeling in a murine model of pulmonary stenosis. *Am J Physiol - Hear Circ Physiol*. 2008;295(3). doi:10.1152/ajpheart.91526.2007

192. Heywood JT, Fonarow GC, Costanzo MR, Mathur VS, Wigneswaran JR, Wynne J. High Prevalence of Renal Dysfunction and Its Impact on Outcome in 118,465 Patients Hospitalized With Acute Decompensated Heart Failure: A Report From the ADHERE Database. *J Card Fail*. 2007;13(6):422-430. doi:10.1016/j.cardfail.2007.03.011

193. Tsukamoto Y, Mano T, Sakata Y, et al. A novel heart failure mice model of hypertensive heart disease by angiotensin II infusion, nephrectomy, and salt loading. *Am J Physiol Hear Circ Physiol*. 2013;305:1658-1667. doi:10.1152/ajpheart.00349.2013.-Al

194. Chang SC, Ren S, Rau CD, Wang JJ. Isoproterenol-Induced Heart Failure Mouse Model Using Osmotic Pump Implantation. *Methods Mol Biol*. 2018;1816:207-220. doi:10.1007/978-1-4939-8597-5_16

195. Guo R, Ren J. Alcohol dehydrogenase accentuates ethanol-induced myocardial dysfunction and mitochondrial damage in mice: Role of mitochondrial death pathway. *PLoS One*. 2010;5(1). doi:10.1371/journal.pone.0008757

196. Zeiss CJ, Gatti DM, Toro-Salazar O, et al. Doxorubicin-Induced Cardiotoxicity in Collaborative Cross (CC) Mice Recapitulates Individual Cardiotoxicity in Humans. *G3: Genes|Genomes|Genetics*. 2019;9(8):2637-2646. doi:10.1534/g3.119.400232

197. Lymperopoulos A, Rengo G, Koch WJ. Adrenergic nervous system in heart failure: Pathophysiology and therapy. *Circ Res*. 2013;113(6):739-753. doi:10.1161/CIRCRESAHA.113.300308

198. Rau CD, Wang J, Avetisyan R, et al. Mapping genetic contributions to cardiac pathology induced by beta-adrenergic stimulation in mice. *Circ Cardiovasc Genet*. 2015;8(1):40-49. doi:10.1161/CIRCGENETICS.113.000732

199. Peng H, Yang XP, Carretero OA, et al. Angiotensin II-induced dilated cardiomyopathy in Balb/c but not C57BL/6J mice. *Exp Physiol*. 2011;96(8):756-764. doi:10.1113/expphysiol.2011.057612

200. Pan X, Shao Y, Wu F, et al. FGF21 Prevents Angiotensin II-Induced Hypertension and Vascular Dysfunction by Activation of ACE2/Angiotensin-(1–7) Axis in Mice. *Cell Metab*. 2018;27(6):1323-1337.e5. doi:10.1016/j.cmet.2018.04.002

201. Jones WK. A Murine Model of Alcoholic Cardiomyopathy. *Am J Pathol*. 2005;167(2):301-304. doi:10.1016/s0002-9440(10)62975-6

202. Carter SK. Adriamycin. *J Natl Cancer Inst*. 1975;55(6). https://academic.oup.com/jnci/article-abstract/55/6/1265/886353. Accessed October 23,

2019.

203. Bristow MR, Thompson PD, Martin RP, Mason JW, Billingham ME, Harrison DC. Early anthracycline cardiotoxicity. *Am J Med*. 1978;65(5):823-832. doi:10.1016/0002-9343(78)90802-1

204. Ma Y, Zhang X, Bao H, et al. Toll-like receptor (tlr) 2 and tlr4 differentially regulate doxorubicin induced cardiomyopathy in mice. *PLoS One*. 2012;7(7):40763. doi:10.1371/journal.pone.0040763

205. Dellefave L, McNally EM. The genetics of dilated cardiomyopathy. *Curr Opin Cardiol*. 2010;25(3):198-204. doi:10.1097/HCO.0b013e328337ba52

206. Crisp M, Liu Q, Roux K, et al. Coupling of the nucleus and cytoplasm: Role of the LINC complex. *J Cell Biol*. 2006;172(1):41-53. doi:10.1083/jcb.200509124

207. Puckelwartz MJ, Kessler E, Zhang Y, et al. Disruption of nesprin-1 produces an Emery Dreifuss muscular dystrophy-like phenotype in mice. *Hum Mol Genet*. 2009;18(4):607-620. doi:10.1093/hmg/ddn386

208. Puckelwartz MJ, Kessler EJ, Kim G, et al. Nesprin-1 mutations in human and murine cardiomyopathy. *J Mol Cell Cardiol*. 2010;48(4):600-608. doi:10.1016/j.yjmcc.2009.11.006

209. Harris SP, Bartley CR, Hacker TA, et al. Hypertrophic cardiomyopathy in cardiac myosin binding protein-C knockout mice. *Circ Res*. 2002;90(5):594-601. doi:10.1161/01.RES.0000012222.70819.64

210. Barrick CJ, Rojas M, Schoonhoven R, Smyth SS, Threadgill DW. Cardiac response to pressure overload in 129S1/SvImJ and C57BL/6J mice: Temporal- and background-dependent development of concentric left ventricular hypertrophy. *Am J Physiol - Hear Circ Physiol*. 2007;292(5):2119-2130. doi:10.1152/ajpheart.00816.2006

211. Hu J, Zhang Y xue, Wang L, et al. Protective effects of Xinji'erkang on myocardial infarction induced cardiac injury in mice. *BMC Complement Altern Med*. 2017;17(1). doi:10.1186/s12906-017-1846-5

212. Lal H, Ahmad F, Zhou J, et al. Cardiac fibroblast GSK-3β regulates ventricular remodeling and dysfunction in ischemic heart. *Circulation*. 2014;130(5):419-430. doi:10.1161/CIRCULATIONAHA.113.008364

213. Rockman HA, Ross RS, Harris AN, et al. Segregation of atrial-specific and inducible expression of an atrial natriuretic factor transgene in an in vivo murine model of cardiac hypertrophy. 1991;88:8277-8281.

214. Drazner MH. The Progression of Hypertensive Heart Disease. *Circulation*. 2011;123(3):327-334. doi:10.1161/CIRCULATIONAHA.108.845792

215. Segers P, Stergiopulos N, Schreuder JJ, Westerhof BE, Westerhof N. Downloaded from journals.physiology.org/journal/ajpheart. *Am J Physiol Hear Circ Physiol*. 2000;279:1120-1127. http://www.ajpheart.org. Accessed November 5, 2021.

216. Grossman W, Jones D, McLaurin LP. Wall stress and patterns of hypertrophy in the human left ventricle. *J Clin Invest*. 1975;56(1):56. doi:10.1172/JCI108079

217. Noll NA, Lal H, David Merryman W, Merryman D. Mouse Models of Heart Failure with

Preserved or Reduced Ejection Fraction. *Am J Pathol*. 2020. doi:10.1016/j.ajpath.2020.04.006

218. Kanisicak O, Khalil H, Ivey MJ, et al. Genetic lineage tracing defines myofibroblast origin and function in the injured heart. *Nat Commun*. 2016;7:12260. doi:10.1038/ncomms12260

219. Wynn TA, Ramalingam TR. Mechanisms of fibrosis: Therapeutic translation for fibrotic disease. *Nat Med*. 2012;18(7):1028-1040. doi:10.1038/nm.2807

220. Piek A, De Boer • R A, Silljé • H H W. The fibrosis-cell death axis in heart failure. *Heart Fail Rev*. 2016;21. doi:10.1007/s10741-016-9536-9

221. Lips DJ, Dewindt LJ, Van Kraaij DJW, Doevendans PA. Molecular determinants of myocardial hypertrophy and failure: alternative pathways for beneficial and maladaptive hypertrophy. 2003. doi:10.1016/S0195-668X(02)00829-1

222. Bouaouina M, Jani K, Long JY, et al. Zasp regulates integrin activation. *J Cell Sci*. 125:5647-5657. doi:10.1242/jcs.103291

223. Childers RC, Sunyecz I, West TA, Cismowski MJ, Lucchesi PA, Gooch KJ. Role of the cytoskeleton in the development of a hypofibrotic cardiac fibroblast phenotype in volume overload heart failure. *https://doi.org/101152/ajpheart000952018*. 2019;316(3):H596-H608. doi:10.1152/AJPHEART.00095.2018

224. Goult BT, Yan J, Schwartz MA. Talin as a mechanosensitive signaling hub. 2018. doi:10.1083/jcb.201808061

225. Skinner SP, Goult BT, Fogh RH, et al. Biological Crystallography Structure calculation, refinement and validation using CcpNmr Analysis. doi:10.1107/S1399004714026662

226. Monkley SJ, Pritchard CA, Critchley DR. Analysis of the Mammalian Talin2 Gene TLN2. doi:10.1006/bbrc.2001.5497

227. Snider JC, Riley LA, Mallory NT, et al. Targeting 5-HT2B Receptor Signaling Prevents Border Zone Expansion and Improves Microstructural Remodeling After Myocardial Infarction. *Circulation*. 2021;143:1317-1330. doi:10.1161/CIRCULATIONAHA.120.051517

228. Tavakoli R, Nemska S, Jamshidi P, Gassmann M, Frossard N. Technique of Minimally Invasive Transverse Aortic Constriction in Mice for Induction of Left Ventricular Hypertrophy. *J Vis Exp*. 2017;(127):e56231. doi:10.3791/56231

229. Gupte M, Umbarkar P, Singh AP, Zhang Q, Tousif S, Lal H. Deletion of Cardiomyocyte Glycogen Synthase Kinase-3 Beta (GSK-3β) Improves Systemic Glucose Tolerance with Maintained Heart Function in Established Obesity. *Cells*. 2020;9(5). doi:10.3390/CELLS9051120

230. Aghajanian H, Kimura T, Rurik JG, et al. Targeting Cardiac Fibrosis with Engineered T cells. *Nature*. 2019;573(7774):430. doi:10.1038/S41586-019-1546-Z

231. Theodosiou M, Widmaier M, Böttcher RT, et al. Kindlin-2 cooperates with talin to activate integrins and induces cell spreading by directly binding paxillin. *Elife*. 2016;5. doi:10.7554/elife.10130

232. Austen K, Ringer P, Mehlich A, et al. Extracellular rigidity sensing by talin isoform–specific mechanical linkages. *Nat Cell Biol*. 2015;17(12):1597. doi:10.1038/NCB3268

233. Acharya A, Baek ST, Banfi S, Eskiocak B, Tallquist MD. Efficient Inducible Cre-Mediated Recombination in Tcf21 Cell Lineages in the Heart and Kidney. *Genesis*. 2011;49(11):870. doi:10.1002/DVG.20750

234. Gao E, Lei YH, Shang X, et al. A Novel and Efficient Model of Coronary Artery Ligation and Myocardial Infarction in the Mouse. *Circ Res*. 2010;107(12):1445-1453. doi:10.1161/CIRCRESAHA.110.223925

235. Wu L, Dalal R, Cao CD, et al. IL-10–producing B cells are enriched in murine pericardial adipose tissues and ameliorate the outcome of acute myocardial infarction. *Proc Natl Acad Sci U S A*. 2019;116(43):21673-21684. doi:10.1073/pnas.1911464116

236. Lal H, Ahmad F, Zhou J, et al. Cardiac fibroblast glycogen synthase kinase-3β regulates ventricular remodeling and dysfunction in ischemic heart. *Circulation*. 2014;130(5):419-430. doi:10.1161/CIRCULATIONAHA.113.008364

237. Schneider CA, Rasband WS, Eliceiri KW. NIH Image to ImageJ: 25 years of image analysis. 2012. doi:10.1038/nmeth.2089

238. Johnson CL, Riley L, Bersi M, Linton MF, David Merryman W. Impaired macrophage trafficking and increased helper T-cell recruitment with loss of cadherin-11 in atherosclerotic immune response. 2021. doi:10.1152/ajpheart.00263.2021

239. Maezawa Y, Onay T, Scott RP, et al. Loss of the Podocyte-Expressed Transcription Factor Tcf21/Pod1 Results in Podocyte Differentiation Defects and FSGS. *J Am Soc Nephrol*. 2014;25(11):2459. doi:10.1681/ASN.2013121307

240. Nagata M. Podocyte injury and its consequences. *Kidney Int*. 2016;89(6):1221-1230. doi:10.1016/J.KINT.2016.01.012

241. Sachs N, Claessen N, Aten J, et al. Blood pressure influences end-stage renal disease of Cd151 knockout mice. *J Clin Invest*. 2012;122(1):348. doi:10.1172/JCI58878

242. Zhong P, Zeng G, Lei CC, et al. Ciliary neurotrophic factor overexpression protects the heart against pathological remodelling in angiotensin II-infused mice. *Biochem Biophys Res Commun*. 2021;547:15-22. doi:10.1016/J.BBRC.2021.01.111

243. Sklepkiewicz P, Shiomi T, Kaur R, et al. Loss of sFRP-1 Leads to Deterioration of Cardiac Function in Mice and Plays a Role in Human Cardiomyopathy. *Circ Heart Fail*. 2015;8(2):362. doi:10.1161/CIRCHEARTFAILURE.114.001274

244. Kakimoto T, Okada K, Fujitaka K, et al. Quantitative analysis of markers of podocyte injury in the rat puromycin aminonucleoside nephropathy model. *Exp Toxicol Pathol*. 2015;67(2):171-177. doi:10.1016/J.ETP.2014.11.007